ABSTRACT

RECALDE, JUAN JOSE. Estimating Crack Growth in Temperature Damaged Concrete. (Under the direction of Michael L. Leming).

Evaluation of the structural condition of deteriorated concrete infrastructure and evaluation of new sustainable cementitious materials require an understanding of how the material will respond to applied loads and environmental exposures. A fundamental understanding of how microstructural changes in these materials relate to changes in mechanical properties and changes in fluid penetrability is needed. The ability to provide rapid, inexpensive assessment of material characteristics and relevant engineering properties is valuable for decision making and asset management purposes. In this investigation, the effects of changes in dynamic elastic properties with water content and fluid penetrability properties before and after a 300 °C exposure were investigated based on estimates of the crack density parameter from dry and saturated cracked media. The experimental and analytical techniques described in this dissertation allow calculation of a value for the crack density parameter using nondestructive determination of wet and dry dynamic shear modulus of relatively thin disks. The techniques were used to compare a conventional concrete mixture to several mixtures with enhanced sustainability characteristics. The three enhanced sustainable materials investigated were a very high fly ash mixture, a magnesium phosphate cement based mortar, and a magnesium phosphate cement based concrete, and were compared to a conventional concrete mixture. The analysis provided both quantitative assessment of changes with high temperature damage and autogenous healing, and estimates of changes in mean crack trace lengths. The results showed that water interaction, deterioration due to damage, and autogenous healing recovery were different for the magnesium phosphate cement based

mixtures than the portland cement based concrete mixtures. A strong correlation was found between log-transformed Air Permeability Index, dynamic shear modulus, and crack density parameter. The findings imply that the test method and related analysis can be used to evaluate the validity of current standard test methods to new “green” construction materials and therefore be a useful screening tool as well as providing important insight into microstructural changes in concrete under various exposures.

Estimating Crack Growth in Temperature Damaged Concrete

by
Juan José Recalde

A dissertation submitted to the Graduate Faculty of
North Carolina State University
in partial fulfillment of the
requirements for the degree of
Doctor of Philosophy

Civil Engineering

Raleigh, North Carolina

2009

APPROVED BY:

_____	_____
Dr. Michael L. Leming Committee Chair	Dr. James M. Nau
_____	_____
Dr. David W. Johnston	Dr. T. Matthew Evans

DEDICATION

To humankind, for its thirst of knowledge and innovation.

BIOGRAPHY

Juan José Recalde was born in Quito, Ecuador, in 1980. He obtained a B.S. in Construction Management in 2002 and the title of Civil Engineer in 2003 from Universidad San Francisco de Quito. In 2003, as a Fulbright Scholar, he entered the Construction Engineering and Management program at the Department of Civil, Construction, and Environmental Engineering at North Carolina State University and in 2005 earned a M. S. in Civil Engineering. He entered the Ph. D. program in 2005 and achieved doctoral candidacy in 2008.

ACKNOWLEDGMENTS

This dissertation was possible thanks to the guidance of Dr. Michael L. Leming, to whom I am deeply grateful. Contributions by Dr. Matthew Evans and Dr. Christopher Bobko were enlightening for the exploration of geophysics. I extend my gratitude to other members of my committee: Dr. David Johnston, Dr. James Nau, and Dr. Delwayne Bohnenstiehl. Materials and specimens were donated by Thomas Concrete and Ready Mixed Concrete Company; Grancrete™ specimens were provided by Dr. Sami Rizkalla and Dr. Aladdinn Sharkawi. Testing assistance was provided by Isabella, Cristina, Sebastián, Nicolás and Santiago; thanks for the company and unconditional help.

I am very grateful for the financial support provided by the Department of Civil, Construction, and Environmental Engineering at North Carolina State University and by Galo Recalde. I am grateful to all members of the faculty with whom I had the pleasure to work, especially Mr. Roberto Núñez. I thank my parents and sisters for their support and encouragement, and also thank my extended family and friends.

TABLE OF CONTENTS

LIST OF TABLES

LIST OF FIGURES

CHAPTER 1. INTRODUCTION

1.1 Background

Two areas of vital concern in construction engineering are sustainability and asset, or infrastructure, management. These issues are related in that agencies owning or charged with oversight of infrastructure elements may be interested in using sustainable construction materials in the repair or retrofit of existing structures, or to build new structures.

The use of portland cement concrete is generally considered a sustainable material since it is recyclable, environmentally benign in service, and produced primarily using local materials, and can, for example, help attain points toward LEED™ certification (U. S. Green Building Council 2008). Concerns have been expressed over the CO_2 emissions associated with the production of portland cement, however. Portland cement production was reported to contribute over 3% of the global CO_2 emissions from fossil fuel combustion and cement production in 2000 (Hanle *et al.* 2004). Others have reported even higher percentages. Mehta and Monteiro (2006) reported that about 7 percent of the total CO_2 produced globally was due to portland cement production. Increased use of alternative cements or concrete mixtures with reduced portland cement content has been suggested as a way to improve the sustainability of concrete. One of the most common ways to reduce portland cement content is the use of supplementary cementitious materials, sometimes called mineral admixtures, such as fly ash, slag, or silica fume.

Considerable potential exists for use of sustainable concrete in infrastructure applications. The U.S. Census Bureau (2008) reports that over $20.5 trillion (in constant 1996 dollars)

worth of total construction was put into service between 1964 and 2002 in the United States. New construction continues to add to this total, with about $5.5 trillion put in place between 2003 and 2007 (U. S. Census Bureau 2009c), and seasonally adjusted annual rates slightly above $1 trillion for new construction were reported during 2008 (U. S. Census Bureau 2009a) and above $900 billion in 2009 (U. S. Census Bureau 2009b). The current economic stimulus plans could create over $160 billion in construction-related spending for public works (Ichniowsky 2009).

ASCE (2009) reported a general rating of "D" for much of the infrastructure, implying considerable work is needed to repair, rehabilitate, upgrade, replace or expand many of the structures. The use of sustainable concrete for any significant part of this construction could have far-reaching consequences on CO_2 reductions. There are currently several limitations with specifying concrete with enhanced sustainability characteristics, however.

The successful use of any construction material, including conventional concrete and concrete with enhanced sustainability, requires that the material respond to both applied loads and environmental exposures over time without excessive loss of serviceability. Acceptance and approval of proposed concrete mixtures requires documentation that the materials have adequate structural properties, typically strength and stiffness, and appropriate durability to anticipated environmental exposures. The current level of understanding of durability, deterioration mechanisms and effects in concrete relies heavily on experiential observations. Experience in long-term exposures in service of many of the new cementitious materials or concrete mixtures with very low portland cement contents is extremely limited or non-existent.

The means and methods required to obtain appropriate levels of durability of concrete mixtures and structures exposed to a variety of environments has developed largely as a result of failures of structures in practice. The current state of knowledge of concrete durability can be said to result from well over a hundred years of "trial and error" construction using construction materials based predominantly on moderate strength, portland cement concrete mixtures. Frost attack, external sulfate attack, and the effects of alkali-silica reaction and heat of hydration were all first identified in structures then in service, often years after construction. Clearly the use of the built environment as a large scale testing program for concretes claiming to have enhanced sustainability is not economically viable.

The existing state of knowledge is largely empirically based and cannot necessarily be applied directly to all concrete mixtures. The use of products that reduce portland cement content can negatively affect performance. The Building Code limits the use of fly ash in slabs exposed to deicing salts (ACI-318 2008), for example. Evaluation based on test methods originally developed for moderate strength portland cement based concretes may not be sufficient for materials with significantly different microstructures. The extension of standards and specifications to high strength concrete is known to be inappropriate for frost exposures (ACI-318 2008; Zia *et al.* 1993) and the behavior of high strength concrete is significantly different than moderate strength concrete exposed to high temperatures (Phan and Carino 1998; Recalde and Leming 2009), for example.

Many of the test methods used to evaluate durability of portland cement concretes are at least semi-empirically based, with acceptance criteria and specifications often strongly

affected by comparison of test data to performance in service or long term testing in severe exposures. The applicability of existing, often accelerated durability related test methods to new materials has not, in general, been established. Limited data exists on the durability of many cementitious products other than portland cement. A need exists to identify potential limitations or restrictions of materials with limited service records such that new or sustainable materials can be used appropriately. Simple determination of mechanical properties and behavior in standard durability tests is not necessarily sufficient.

Additional studies examining the behavior of all concrete mixtures, but particularly recently developed or modified, enhanced sustainability materials, are needed at the fundamental, microstructural level to improve the understanding of deterioration mechanisms and rates, and relationships between changes in different material characteristics of concrete mixtures exposed to damaging or aggressive environments. These studies could increase the use of concretes with enhanced sustainability by improving the ability of the Engineer of Record (EOR) to intelligently specify these types of mixtures, and may improve the ability of the EOR to select or specify conventional concrete mixtures with significantly reduced portland cement content. These studies could also provide the asset manager with useful analytical and forensic tools for evaluation of existing structures. An improved understanding of deterioration mechanisms at the microstructural level, based on fundamental principles, would have important applications to sustainable construction, to infrastructure management, and to development of design and specification codes.

1.2 Changes in Microstructure and Relationships between Durability and Mechanical Properties

Hsu, Slate, Sturman and Winter (1963), and Carrasquillo, Nilson, and Slate (1981) conclusively established that microcracking in concrete exposed to compressive loads primarily results in minor extension of pre-existing, transition zone cracks up to stresses of 40 to 50 percent of the ultimate strength as measured using conventional testing methods, and that additional cracking occurs primarily through extension of those cracks up to approximately 70 percent of ultimate strength before significant formation of new cracks. Their results were based on visual assessment of cracks, which is time consuming and expensive, as well as being semi-quantitative. Dilek, Leming, and Guth (2004) demonstrated that uniaxial compressive loads of 80 percent of ultimate strength maintained for four hours resulted in a significant reduction in elastic modulus and a significant increase in permeability.

An increase in permeability can reduce the durability of an element to aggressive environments; a reduction in stiffness or strength can compromise load carrying capacity. Real structures are exposed to a combination of environmental conditions while simultaneously under stress from applied loads. Dilek, Leming, and Guth (2004) found that a linear relationship existed between changes in elastic modulus and the logarithm of the Air Permeability Index for different strength mixtures containing otherwise similar materials and proportions. This relationship was also reported by Dilek, Leming, and Sharpe (2003), Dilek and Leming (2007a; 2008) and Recalde and Leming (2009). These studies did not, however, include any fundamental assessment of changes in microstructure. Testing and related

analytical methodologies are needed to combine the quantitative assessment of changes in important properties and changes in fundamental microstructural properties to better understand the behavior of concrete elements exposed to both loads and aggressive environments. Investigations of the relationship between changes in elastic modulus and permeability, and changes in the microstructure of construction materials claiming enhanced sustainability have not been previously reported.

The evaluation of concrete cores taken from members can provide information regarding the existing structural capacity, extent of deterioration and presence or absence of contributing factors and indicators such as entrained air, alkali, chloride, or ettringite contents. Evaluation of sections of core samples to simultaneously determine the dynamic elastic Young's modulus of concrete and various permeability measures at approximately 20 to 25 mm (about 1 in.) depths, thereby providing not only important engineering properties, but information on possible damage gradients in existing structures, has been reported (Dilek *et al.* 2003; Dilek and Leming 2007a; Dilek and Leming 2008). The lack of long term experience with many concrete mixtures claiming to enhance sustainability significantly complicates similar forensic analysis.

1.3 General Problem Statement

Additional studies to establish a quantitative relationship between changes in the microstructure of various concretes and changes in both durability and the ability to carry load would be useful in several applications. A better understanding of how changes in the microstructure resulting from damaging exposures affect both the permeability, a key factor in many durability-related processes, and selected mechanical properties of concrete, based

on fundamental principles, may improve design and construction capabilities permitting development of infrastructure elements with longer service lives. The ability to quantitatively describe the crack density, the shear and elastic (dynamic) moduli, and permeability of specimens taken from existing concrete elements may also improve the analysis of existing conditions of infrastructure assets.

A promising and critically needed potential application for the experimental and analytical techniques developed in this study is the evaluation of the potential use of cementitious materials claiming to enhance sustainability. It is hypothesized that materials showing the same general changes in crack density characteristics as conventional portland cement based concretes, when both are exposed to similar damaging conditions, would behave similarly in service. A similarity in crack density changes would also imply that the testing methodology used for assessment is appropriate for classifying and characterizing new, sustainable concretes, and that design principles developed for portland cement concretes are appropriate. This further implies that the test methods and analytical procedures developed in the study can be used to provide preliminary evaluation or "screening" of new concrete materials.

1.4 Overview of the Study

The study described in this dissertation was intended to expand the state of knowledge of the relationship between changes in mechanical properties and permeability, and, more importantly, how these changes in material properties are related to changes in the microstructure of concrete exposed to a damaging environment. This dissertation describes the development and extension of testing protocols and analytical methods to quantitatively

estimate the changes in crack density parameter of concrete specimens before and after moderate damage caused by relatively short exposure to temperatures of 300 °C. This dissertation also describes the application of these methods to initial evaluation of concrete mixtures with enhanced sustainability based on their similarity or dissimilarity to the responses of conventional concrete.

The testing protocols are based on previous work (Recalde and Leming 2009; Recalde 2005) comparing conventional strength and high strength concretes to elevated temperatures, using procedures adapted from those developed by Leming, Nau, and Fukuda (1998). The analytical methods are an extension of the methods described by O'Connell and Budiansky (1974), modified and adapted for use with concrete disks, to determine the crack density parameter or changes in the crack density parameter based on differences in shear modulus due to the presence of water filling the cracks in the concrete.

The findings of the study have important implications to both asset management and sustainable construction. The ability to provide rapid, economical assessment of concrete characteristics and relevant engineering properties of existing structures is valuable in managing these vast resources. The use of simple, inexpensive and portable tests to classify changes in engineering properties and changes in microstructure based on fundamental analytical principles should improve the ability of the researcher and practicing engineering in examining a multitude of specimens under a variety of conditions. The factors may also have important implications in developing countries with extensive infrastructure needs but limited testing or research budgets.

This study was intended to:

(1) provide improvement and further development of a simple test methodology to quantitatively evaluate the relationship between changes in permeability and shear modulus of concrete exposed to moderately high temperatures, due to changes in microstructure, by estimating the crack density parameter under various conditions of concrete disks, which requires

(2) development of the testing and analytical protocols required to estimate the crack density parameter, such that

(3) the test and analytical methodology can be used as a simple screening test to compare conventional concrete mixtures to concrete mixtures that may provide enhanced sustainability, and should

(4) provide useful insight into the crack propagation characteristics of these concretes with exposure to high temperatures.

CHAPTER 2. LITERATURE REVIEW

2.1 Background

2.1.1 Evaluation of Damaged Concrete

Evaluating the condition of an existing concrete structure by the engineer after a visual inspection (see, for example, ACI-201 2008), requires either testing the structural condition of the concrete with load tests or assessment of the member by inspection of the concrete quality and location of the reinforcing steel. Testing concrete structural members by load testing, such as the method specified in Chapter 20 of the ACI-318 Building Code (2008), can be a costly and time-consuming operation with elevated risk due to safety concerns. Assessment of the member through evaluation of the concrete quality can be done using in-place nondestructive methods, or through extraction of core samples. Often nondestructive methods allow identification of affected concrete locations for later core extraction. Nondestructive methods to estimate concrete strength can be found in ACI 228 Committee Report 228.1R-03 (2003) and nondestructive evaluation of concrete in structures in Report 228.2R-98 (1998). ACI 214 Committee Report 214.4R-03 (2003) provides a guide for obtaining cores and interpreting results. Analysis of the compressive strength of cores is typically considered to be adequate for evaluating the overall quality of the concrete, such as concerns about the quality of the concrete batch used during construction.

Damage gradients can be created by environmental exposures such as fire. Compressive strength of cylindrical cores might therefore not be representative of the concrete quality in case of damage gradients with a limited depth compared to the length of the cylinder. Dilek,

Caldwell, Sharpe and Leming (2003) present results of a forensic investigation of pre-stressed double-tees damaged by fire, comparing results of nondestructive evaluation techniques to testing of concrete cores and load testing, where damage gradients where identified by using disk specimens sawed from cores. Dilek, Leming and Sharpe (2003) also identified damage gradients in concrete elements damaged by exposure to a cryogenic fluid. Assessments of damage gradients were done by measuring the dynamic Young's modulus of elasticity of disks at 25 mm (1 in.) increments from the exposure surface. This technique was successfully implemented in other forensic investigations (Dilek and Leming 2007a; Dilek and Leming 2008; Dilek 2005; Dilek 2006).

The dynamic elastic Young's modulus of elasticity (E_d) of relatively thin concrete disks sawed from cores or cylinders can be determined with a simple, lightweight, easily transported, and relatively low cost apparatus, using a technique developed by Leming, Nau and Fukuda (1998). The resonant frequency of the disk is used to calculate E_d, which is typically determined from analysis of the signal provided by an accelerometer attached to a disk in free-free vibration; further comments are provided in section 2.5.2, and a detailed description of the test method is given in Chapter 3. This technique is minimally invasive and often done to complement and calibrate more extensive nondestructive evaluation on site, and provide information not readily available with impact-echo or pulse velocity (Dilek and Leming 2007a). Variations of properties with depth are not only identified, they are quantified using relevant engineering values.

The technique to determine E_d has also been used in laboratory based research investigations. Dilek, Leming and Guth (2004) studied the relationship between E_d and air

permeability using specimens damaged by static load fatigue, fire, and cryogenic exposure. Dilek and Leming (2007b) studied the de-icer salt scaling resistance of concrete containing manufactured sands. Recalde and Leming (2009) studied the changes in E_d with high temperature damage, and compared results to fluid penetrability properties.

2.1.2 Moisture Considerations

The dynamic modulus can be determined within minutes of obtaining a concrete disk, if desired, allowing rapid evaluation and analysis on site. These characteristics can make the technique very useful in forensic analysis of damaged concrete, particularly in remote locations. Since cores are typically obtained using water-cooled, hollow-core bits, and disks are sawed from cores or cylinders using water-cooled blades, the moisture content is high for most disk specimens immediately after fabrication. The effects of changes in the measured dynamic modulus due to moisture content must be understood so that the analysis and conclusions of the practicing engineer are based on consistent estimates of the mechanical properties of the concrete.

Recalde (2005) studied the signal characteristics of concrete disks in free-free vibration before and after high temperature exposures, and observed that the signals from specimens following the exposure had low damping compared to the signals obtained from the same specimens prior to damage. It was not clear if these differences were caused by damage or by low moisture contents in the damaged specimens since signals were obtained as soon as specimens reached ambient temperature. This investigation (Chapter 4) included analysis of properties and signal characteristics at various moisture conditions of the disks before and after damage by exposure to high temperature. The differences in results found between wet

and dry samples appeared to provide information on the microstructure not otherwise available, or at least not easily available. Additional study to develop a more theoretical basis for these observations was conducted, which is presented in Chapter 5 of this dissertation, and which includes a literature review pertinent to the fields of investigation explored.

The effects of moisture on the mechanical properties of concrete can be significant. The compressive strength of concrete cylinders in a dry condition is typically higher than in wet conditions (Popovics 1986). Standard curing of concrete cylinders fabricated according to ASTM Standard C 31-09 (2009) require specimens to be stored in water or moist rooms, and are tested for compressive strength immediately after removal from such moist condition (ASTM-C39 2008); this procedure is intended for reproducibility. Popovics (1986) suggests that the higher compressive strength in dry concrete is caused by a confining effect by the drying shrinkage of the outer core.

Bartlett and MacGregor (1994) reported that compressive strength of cores tested in dry conditions was about 15 percent higher than cores tested in wet conditions. ASTM Standard C 42 (2004) requires allowing surface moisture evaporation within an hour after drilling the cores, and then storing specimens in sealed plastic bags for at least 5 days prior to testing. This standard was changed largely due to work by Fiorato, Burg and Gaynor (2000).

In contrast, the modulus of rupture of concrete beams when tested in wet conditions is higher than when measured in dry conditions (Galloway *et al.* 1979). Similarly, the static elastic Young's modulus of concrete cylinders is higher when measured in wet conditions than when measured in dry conditions (Mehta and Monteiro 2006; Guo and Waldron 2001).

Ultrasonic pulse velocities can be up to 5 percent higher when measured in wet concrete than in dry concrete (Bungey 1989; ASTM-C597 2003).

2.1.3 Changes in Properties with Damage

Changes in microstructure clearly affect both mechanical properties, that is, the ability to resist applied loads, and durability the ability to resist environmental loads. Concrete durability is fundamentally related to fluid transport characteristics (Mehta and Monteiro 2006; Neville 1995). The general relationship between mechanical properties and fluid transport characteristics of concrete have long been established, largely through the correlation of both with water cement (w/c) ratio, but quantitative relationships between changes in these properties due to damage of the concrete have not been well established (Dilek *et al.* 2004; Dilek and Leming 2007a).

The relationship between the dynamic modulus and fluid transport characteristics as measured by the air permeability index (API) has been studied in both forensic analysis and laboratory testing. Changes in E_d and API due to damage caused by loading, fire, or frost attack have been found to be similar for a wide variety of concretes. A linear relationship between E_d and log(API) was reported for concrete with moderate damage by Dilek, Leming and Guth (2004), and analyzed in subsequent investigations (Dilek and Leming 2008; Dilek and Leming 2007b). Recalde and Leming (2009) report a correlation between changes in E_d and changes in fluid transport as measured by the API and by sorptivity for concrete exposed to high temperatures (150 °C and 300 °C). Test methods are discussed in more detail in Chapter 3, but, briefly, the API can be determined by measuring the time for a change in vacuum pressure from air flow through concrete (Schonlin and Hilsdorf 1988) and sorptivity

is determined by measuring the mass of water taken up over time due to capillary suction (Hall 1989; DeSouza *et al.* 1997; ASTM-C1585 2004).

Recalde and Leming (2009) also report a non-linear relationship between E_d and log(API) for high strength concrete specimens with significant, cumulative damage, indicating a difference in behavior between conventional and high strength concrete. This difference has been reported by others as well (Phan and Carino 1998), but direct quantitative evaluation using other, more conventional methods is costly and time consuming. The ability to easily identify differences in response to damage between different concrete mixtures has important implications in the development of new construction materials, such as sustainable cementitious materials, with limited exposure in service.

2.2 Microstructure of Concrete

Concrete is a heterogeneous material composed of aggregate, hydrated cement paste and an interfacial transition zone between them. The hydrated cement paste consists of calcium silicate hydrate (C-S-H) (50 to 60 percent of the solids volume), portlandite (calcium hydroxide crystals, $Ca(OH)_2$, 20 to 25 percent by volume), and calcium aluminate hydrates (15 to 20 percent by volume). Unhydrated cement particles also exist. The morphology of the C-S-H is irregular, modeled as a layered structure, with solid-to-solid distance of 0.18 nm according to the Powers-Brunauer model (1958), and between 0.05 and 0.25 nm according to the Feldman-Sereda model (1970), and accounts for a 28 percent porosity of the C-S-H. A model of a hydrated cement paste is given in Figure 2.1, where aggregation of C-S-H particles are of at least 1 to 100 nm, crystalline products (calcium hydroxide and calcium sulfoaluminate hydrates) are typically 1 μm wide, and capillary pores at locations that were

not filled by hydration products of the cement are of irregular shape and may range between 10 to 50 nm in low water-cement ratio pastes, and up to 5 μm in high water-cement ratio pastes. Entrained air voids are generally spherical and are typically 50 to 200 μm, and entrapped air voids may be as large as 3 mm. A comparison of scales of each of the paste constituents is presented in Figure 2.2.

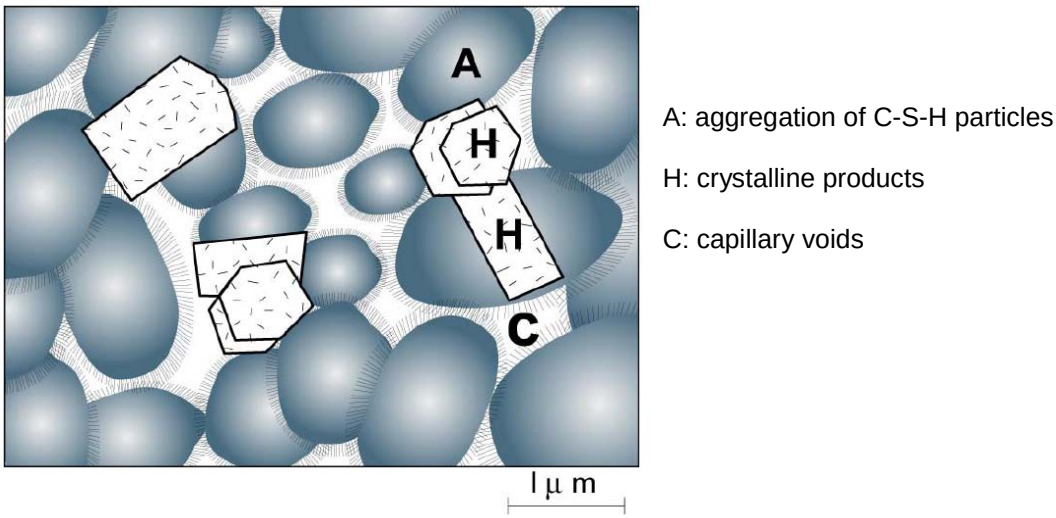

Figure 2.1 - Model of a Well-Hydrated Portland Cement Paste (Mehta and Monteiro 2006)

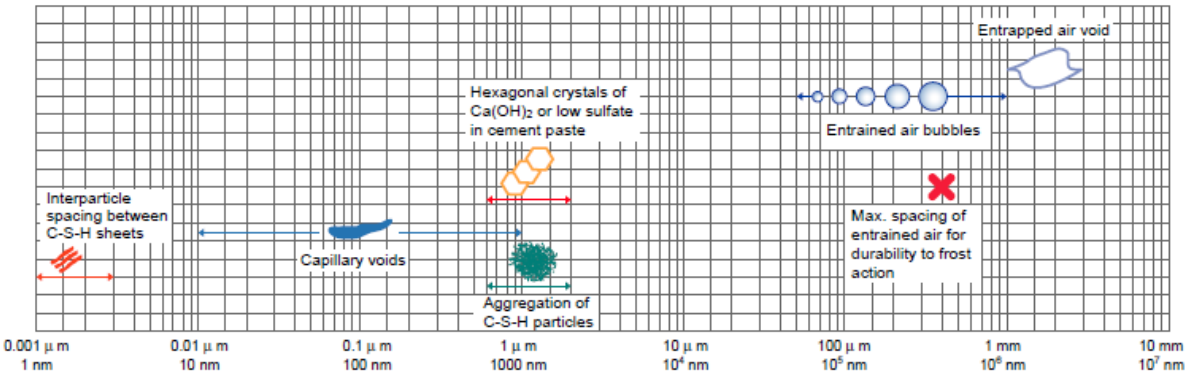

Figure 2.2 - Dimensional Ranges of Solids and Pores in a Hydrated Portland Cement Paste (Mehta and Monteiro 2006)

The interfacial transition zone between large aggregates and hydrated cement paste has a different microstructure and is therefore typically treated as a different phase in microstructural evaluation. Aggregates in fresh cement will have a layer of water which creates zones of paste with higher water-cement ratio surrounding the aggregate and therefore larger capillary voids. A similar and more detrimental situation is created with bleeding water of fresh concrete. The transition zone consists of a hydrated paste layer around 50 µm thick, with large $Ca(OH)_2$ crystals and little or no unhydrated cement, with a 0.5 µm layer of oriented $Ca(OH)_2$ crystals surrounding the aggregate (Larbi 1993). Larbi's (1993) findings support earlier work by Scrivener and Gartner (1988) who reported porosity gradients in hydrated cement paste, with porosities decreasing from 30 to about 10 percent within the first 30 µm from the surface of the aggregate.

2.3 Microcracking in Concrete

Slate and Hover (1984) used the term 'microcrack' for cracks up to 100 μm in thickness, which could be traced using the x-ray methodology developed by Slate and Olsefsky (1963) Hsu, Slate, Sturman and Winter (1963) showed that drying and shrinkage produced microcracks at the interfacial transition zone, prior to application of any stress. Pre-existing microcracks have also been observed in wet-cured concrete (Jornet *et al.* 1993).

Hsu, *et al.* (1963) determined that at 30 percent of the ultimate strength, using short-term loading on conventional strength concrete, microcracks at the transition zone begin to increase in trace length, trace width and number with increasing strain, and the stress-strain curve begins to deviate from a linear elastic behavior. At about 70 to 90 percent of the ultimate strength, microcracks begin to increase noticeably and start to interconnect, with a significant deviation in the stress-strain curve and indicative of impending failure. Carrasquillo, Slate and Nilson (1981) extended the study for concrete mixtures of compressive strengths above 55 MPa (8000 psi), and confirmed that cracks start to interconnect in conventional strength concrete at about 70 percent of the ultimate strength, and that in high strength concrete, cracks start to interconnect at about 90 percent of the ultimate strength. Less microcracking was observed in high strength concrete than normal strength concrete at all strain levels, and the sudden failure characteristic of high strength concrete had fewer planes of failure, resembling the behavior of a homogeneous brittle material. This behavior has been largely ascribed to the improved transition zone in high strength concrete and the smaller difference in the elastic modulus of the paste and aggregates.

2.4 Effect of High Temperature Exposure on Concrete Properties

Figure 2.3 presents the elastic behavior of concrete at high temperatures, as obtained by Cruz (1966) (ACI-216 1989), where a decrease in Young's modulus and shear modulus is observed. Similar results were obtained by Philleo (1958) using dynamic methods up to about 370 °C (700 °F) with higher values at higher temperatures. Dias, Khoury and Sullivan (1990) report a linear decrease of the residual dynamic Young's modulus, with around 0.6 of the original unexposed modulus after a single exposure to 300 °C.

Phan and Carino (2002) measured the static Young's modulus of high strength concrete cylinders at high temperatures for unstressed and stressed (40 percent of the ultimate strength) conditions, and also measured the residual modulus at room temperature. The Young's modulus at 300 °C was between 0.4 and 0.6 of the unexposed modulus for the cylinders tested at high temperature, and between 0.3 and 0.5 for the residual modulus measured at room temperature. Phan and Carino (2002) observed that explosive spalling of cylinders occurred at temperatures between 200 °C and 325 °C, coinciding with a time at which a high temperature difference existed between the surface and the center of the cylinder.

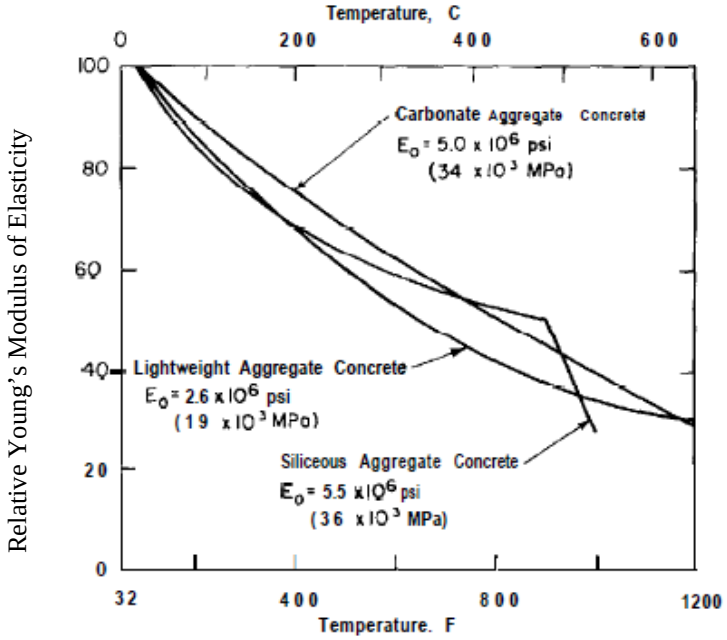

(a)

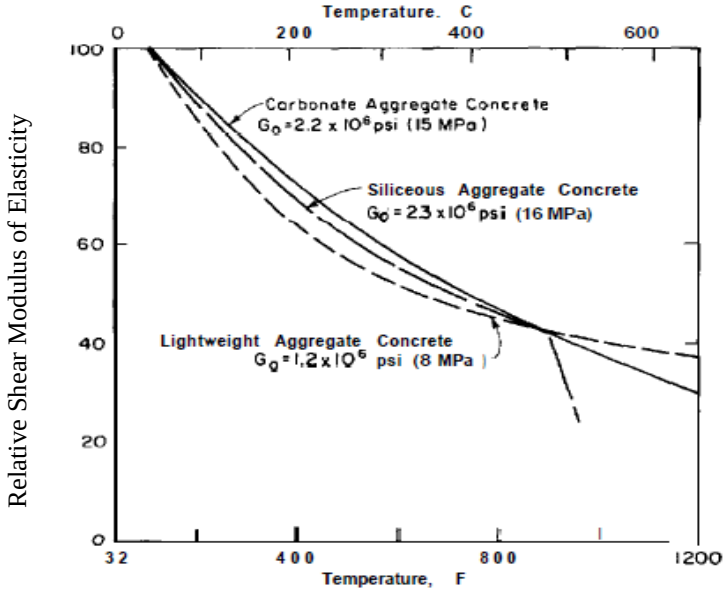

(b)

Figure 2.3 - Modulus of Elasticity at High Temperatures (Cruz 1966; ACI-216 1989): (a) Young's Modulus, (b) Shear Modulus

Cruz (1966) observed that on conventional strength concrete, for three different types of aggregate, the elastic modulus decreased more rapidly than compressive strength as exposure temperature was increased. This may be due to transition zone microcracking, which will affect the elastic modulus and flexural strength more than compressive strength (Mehta and Monteiro 2006). Phan and Carino (1998) provide a review of high strength concrete properties at high temperature. They identified differences in residual compressive strength behavior for temperatures above and below 200 °C. Phan and Carino (2002) therefore considered the range between 100 °C and 350 °C as an intermediate zone in their proposed strength-temperature relationship.

The amount of moisture and the degree of hydration of the cement paste affect the damaged induced by high temperature (ACI-216 1989). Besides the adsorbed water in concrete, free water is retained in pores and capillaries, which, in the presence of high temperature, will escape through the capillary network as water vapor. If a high rate of heating occurs and permeability is low, large amounts of free water may cause spalling of the concrete surface, speculated to be due to a higher increase rate of vapor pressure to that of pressure relief through the pore system (Mehta and Monteiro 2006; Phan and Carino 2002). When the temperature reaches approximately 300 °C, the interlayer water in the calcium silicate hydrate (C-S-H) and some of the chemically bonded water are lost, at 400 °C calcium hydroxide starts to decompose (Lea 1970), and between 600 and 900 °C, the C-S-H decomposes (Mehta and Monteiro 2006). Concretes made with siliceous or limestone aggregate show a permanent change in color after exposure to high temperature, becoming

pink or red between 300 and 600 °C, grey up to about 900 °C, and buff at higher temperatures (Zoldners 1960).

2.5 Elastic Considerations for Concrete Evaluation

2.5.1 Effective Media

The heterogeneous nature of concrete can be approximated using elastic models for composite materials. Figure 2.4 shows five two-phase models that have been used to predict the elastic moduli of concrete from volumetric proportions of aggregate and mortar. Hirsch (1962) proposed a model relating the elastic moduli of concrete to the elastic moduli of the aggregate and mortar matrix, using volume fractions and an empirical constant relating the relative contributions of equivalent layers in parallel and series arrangements. Hansen (1965), based on the formulation by Hashin (1962), proposed a model using spherical aggregate inside spheres of mortar matrix. Counto (1964) considered an aggregate prism inside the center of a prism of mortar matrix of similar height-to-area proportions. Upper and lower limits of these two-phase composite elastic models are given by the parallel model and the series model, respectively (Hill 1952).

The two-phase models have the limitation that interfacial transition zones are neglected. Also, void content is incorporated as a constant effect in the mortar matrix, and changes in void content, such as inclusion of entrained air voids or presence of existing microcracks cannot be modeled. Review of the limitations of the two-phase models is provided by Nilsen and Monteiro (1993). A three-phase model was proposed by Hashin and Monteiro (2002), modeling aggregate as a sphere surrounded by a soft concentric spherical shell representing

the transition zone, embedded in a mortar matrix medium, and obtained estimates of elastic properties of the interphase.

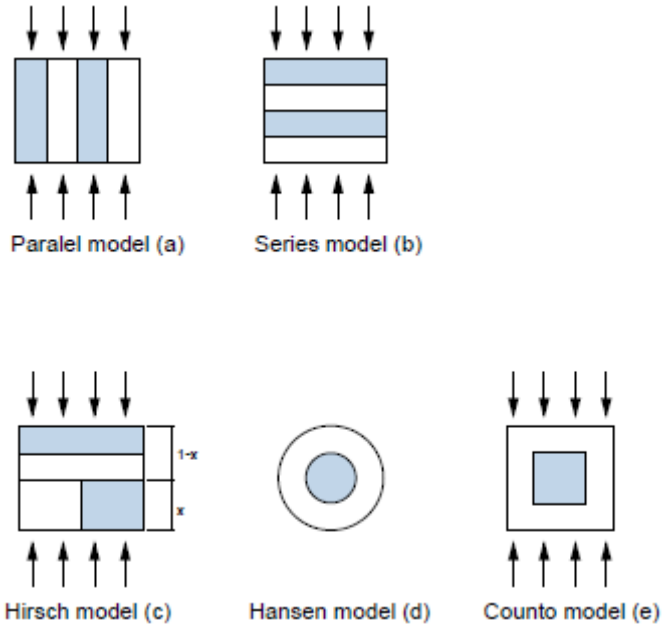

Figure 2.4 - Two-Phase Elastic Models for Concrete (Mehta and Monteiro 2006)

For the effects of pores and cracks, volume fractions and geometry need to be considered. The Mori-Tanaka (1973) method allows estimating decreases in elastic moduli with inclusions of spherical or flat circular shaped voids. For spherical pores, volumetric proportions can be used. For flat circular inclusions, the crack density parameter (ε) is used, defined for circular cracks as $\varepsilon = (N/V)\sum a^3 = N\langle a^3 \rangle$, where N is the number of cracks, and $\langle a^3 \rangle$ is a measure of the mean crack radius a per unit volume V (Walsh 1965).

O'Connell and Budiansky (1974) considered randomly distributed flat ellipsoidal cracks with and without a fluid, using a self-consistent energy method (see also Budiansky and

O'Connell 1976). The crack density parameter for ellipsoidal cracks is defined as $\varepsilon = (2N/\pi)\langle A^2/P \rangle$, where $\langle A^2/P \rangle$ is the mean squared area to perimeter ratio of the cracks per unit volume. The mathematical models relating elastic moduli and ε are discussed in detail in Chapter 5 of this dissertation.

O'Connell and Budiansky (1977) extended their analysis for viscoelastic properties of fluid-saturated cracks, considering the cases of saturated isolated cracks and saturated isobaric cracks, and compared it to the case of saturated relaxed cracks. The saturated isolated case corresponds to cracks that are not interconnected and therefore no fluid pressure interaction between cracks, the saturated isobaric case corresponds to a system of interconnected cracks at constant fluid pressure but at different pressure than the fluid surrounding the solid, and the saturated relaxed cracks correspond to the condition in which the fluid in cracks is in contact with the fluid surrounding the solid and therefore effectively behaving as a dry case with empty cracks. O'Connell and Budiansky (1979) also provide an extension to seismic wave propagation with viscoelastic behavior for all frequencies.

2.5.2 Dynamic Elastic Modulus of Concrete Disks

The method to determine E_d by measuring the resonant frequency is described by Leming, Nau and Fukuda (1998) which is based on the theory developed by Hutchinson (1979), based on evaluation of the shear modulus of a standing shear wave in a thick, free circular plate. A complete description of the test method is given in Chapter 3 of this dissertation and Hutchinson's solution is given in Appendix A. It may be shown that the dynamic elastic modulus of a disk under free-free vibration is related to the natural frequency of vibration by

$$E_d = 2(1+\upsilon)\rho\left(\frac{\pi f d}{\Omega_0}\right)^2 \tag{2.1}$$

where

E_d = dynamic Young's modulus of elasticity, Pa,

υ = Poisson's ratio,

ρ = mass density of the disk, kg/m^3,

f = frequency, Hz,

d = diameter of the disk, m, and

Ω_0 = dimensionless frequency parameter associated with the first mode of vibration.

Recalde (2005) used time domain analysis to measure frequency and damping from the acceleration signals of resonant disks. Time-domain analysis was preferred over frequency-domain techniques due to concerns in frequency resolution and small bandwidth for determining damping ratios. The mathematical model of the response of a simple single-degree-of-freedom linear elastic system with viscous damping was used. A representation of such system is given in Figure 2.5, whose governing equation of motion is $m\ddot{u} + c\dot{u} + ku = 0$, where u is displacement (m), dot ($\dot{u}, \ddot{u}$) denotes derivation with respect to time, m is mass (kg), k is the stiffness (kN/m), and c is the damping coefficient (kN·s/m). A non-trivial solution is given by Eq. 2.2, where ξ is the damping ratio, t is time (s), ω is the natural frequency of the system (rad/s), ω_d is the damped natural frequency (rad/s), v_0 is the initial velocity (m/s), and u_0 is the initial displacement (m). Natural frequency and damping ratio are related to the system stiffness and damping coefficient by the relations in Equations 2.3 to

2.5. Equations 2.1 and 2.3 relate the effects of stiffness and mass on the measured frequency of vibration of the corresponding systems. Recalde (2005) reported differences in damping ratio before and after damage, but results were not conclusive, and values for E_d from measurement of the frequency were more informative.

$$u(t) = e^{-\xi\omega t}\left(u_0 \cos(\omega_d t) + \frac{v_0 + \xi\omega u_0}{\omega_d} \sin(\omega_d t) \right) \tag{2.2}$$

$$\omega = \sqrt{\frac{k}{m}} \tag{2.3}$$

$$\xi = \frac{c}{2m\omega} \tag{2.4}$$

$$\omega_d = \omega\sqrt{1-\xi^2} \tag{2.5}$$

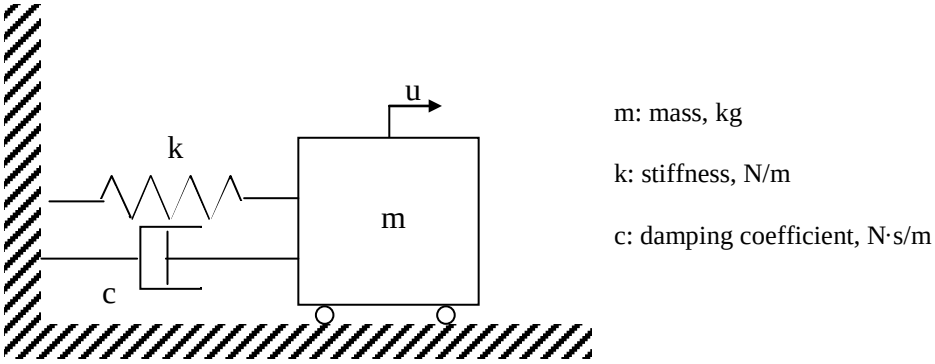

Figure 2.5 - Example of a Single-Degree-of-Freedom (SDOF) System

2.5.3 Quantification of Distributed Damage using Impact-Echo Techniques

Analysis of signal decay in impact-echo analysis of slab specimens with distributed damage was studied by Kesner, Sansalone and Poston (2004). The decay of the stress wave signal in the time domain was obtained by fitting an exponential curve through the peaks

after filtering the signal. The values for the decay constant were compared to modeled and real data to assess the amount of damage in the concrete member. The investigators concluded that this technique has significant potential in detecting and qualitatively assessing distributed damage. This technique expands the benefits of impact-echo testing, but is unable to detect localized damage. Dilek and Leming (2007a) observed that ultrasonic techniques in general do not provide reliable estimates of mechanical properties in the presence of damage gradients, such as those observed on surface deterioration due to exposures to fire.

2.5.4 Remarks

The dynamic Young's modulus (E_d) of concrete, and the damping of the pulse wave in the Kesner *et al.* (2004) method, will depend on the degree of crack density in the concrete. The use of a cracked media model for concrete to measure extent of damage from measurements of the dynamic elastic moduli is the essence of Chapter 5, therefore relevant models studied for effective elastic media and stress wave propagation characteristics are reviewed in that chapter. Fundamentals of stress wave propagation in continuous media are provided in Appendix B. Fundamentals of stress wave propagation in granular media can be found in Santamarina, Klein and Fam (2001).

CHAPTER 3. RESEARCH METHODOLOGY

3.1 Overview of the Test Program

This investigation was conducted in three phases. In Phase I, the effects of moisture content on vibration characteristics of thin concrete disks in free-free vibration was examined. The purpose of this part of the investigation was to evaluate signal characteristics that may provide information about the condition of the concrete microstructure, as related to mechanical and fluid penetrability properties, to refine the experimental and analytical techniques described by Recalde and Leming (2009), Dilek and Leming (2007a; 2008), and Leming, Nau and Fukuda (1998). Changes in the microstructure were attained by exposing the disks to a temperature of 300 °C. In Phase II, the results from Phase I were used to develop a model to characterize the microstructure based on pore and crack systems, using the resonant behavior of thick circular plates. In Phase III, the model was validated experimentally using a control concrete mixture, two mixtures reported to enhance sustainability and a mortar sample produced using a cementitious material other than portland cement. The characterization methodology was calibrated, and changes in the microstructure, fluid penetrability and mechanical properties by high temperature exposure were studied. The samples were analyzed for changes in mechanical properties as measured by dynamic moduli of elasticity and for changes in fluid penetrability as measured by the rate of absorption of water and by air permeability. Phase III was also considered to be a valuable “proof-of-concept” evaluation of the potential for using these test and analytical

methods to establish the general utility on types of mixtures other than conventional, portland cement based concrete.

3.2 Materials and Specimens

Two traditional concrete mixtures were used for Phase I, a low strength (mixture L) and a conventional moderate strength concrete mixture (mixture N) with average compressive strengths of 16 MPa (2.3 ksi) and 26 MPa (3.8 ksi) respectively. In Phase III, three sustainable cementitious materials were investigated: a very high volume fly ash (VHFA) concrete with 70% cement replacement by weight of a class F fly ash (mixture F), a magnesium phosphate cement mortar (mixture M), and a magnesium phosphate cement concrete (mixture G). The mixture proportions for the traditional concrete mixtures used in Phase I are given in Table 3.1. The mixture proportions of the control and VHFA concrete mixtures used for Phase III are given in Table 3.2. The mixtures based on magnesium phosphate cement were cast using Grancrete™, a proprietary, high early strength cement mixture by Grancrete, Inc. The mixture proportions by weight, of the Grancrete™ mortar (M) and concrete (G) mixtures were 1 : 0.5 : 0.23 (Grancrete™ : sand : water) for mortar and 1 : 1 : 1.5 : 0.3 (Grancrete™ : sand : coarse aggregate : water) for concrete using a nominal maximum sized aggregate of 9.5 mm (3/8 in).

Table 3.1 - Characteristics of Traditional Concrete Mixtures Used in Phase I

Property	Low Strength (L)	Moderate Strength (N)
Nominal strength	21 MPa (3 ksi)	32 MPa (4.5 ksi)
Coarse aggregate (19 mm NMSA, size # 67)	1088 kg/m^3 (1834 pcy)	1082 kg/m^3 (1824 pcy)
Fine aggregate	631 kg/m^3 (1063 pcy)	627 kg/m^3 (1057 pcy)
Cement Type I	286 kg/m^3 (482 pcy)	402 kg/m^3 (677 pcy)
Fly Ash	86 kg/m^3 (145 pcy)	0 kg/m^3 (0 pcy)
Water	166 kg/m^3 (279 pcy)	170 kg/m^3 (287 pcy)
Air entraining agent	145 mL/100 kg (2.2 fl oz/cwt)	24 mL/100 kg (0.4 fl oz/cwt)
Water reducing admixture	191 mL/100 kg (2.9 fl oz/cwt)	173 mL/ 100 kg (2.7 fl oz/cwt)
w/c	0.45	0.42
Slump	100 mm (4.0 in)	115 mm (4.5 in)
Air content	6.0 %	6.5 %
28-day compressive strength	15.8 MPa (2300 psi)	26.5 MPa (3840 psi)

NMSA: nominal maximum sized aggregate; w/c: water-to-cementitious-materials ratio; cwt: 100 lb of cementitious materials; “pcy” is pounds per cubic yard; “pcf” is pounds per cubic foot, “psi” is pounds per square inch

Table 3.2 - Characteristics of Concrete Mixtures Used in Phase III

Property	Control Mixture (C)	Very High Fly Ash (F)
Nominal strength	35 MPa (5 ksi)	70% fly ash replacement
Coarse aggregate (19 mm NMSA, size #67)	1068 kg/m^3 (1800 pcy)	1068 kg/m^3 (1800 pcy)
Fine aggregate	772 kg/m^3 (1302 pcy)	697 kg/m^3 (1174 pcy)
Cement Type I	306 kg/m^3 (515 pcy)	71 kg/m^3 (120 pcy)
Fly Ash	71 kg/m^3 (120 pcy)	306 kg/m^3 (515 pcy)
Water	168 kg/m^3 (283 pcy)	168 kg/m^3 (283 pcy)
Air content	1.5 %	1.5%
Water reducing admixture	255 mL/100 kg (4.0 oz/cwt)	255 mL/100 kg (4.0 oz/cwt)
w/c	0.45	0.45
Density	2340 kg/m^3 (146.0 pcf)	2305 kg/m^3 (143.9 pcf)
Slump	10 cm (4.0 in)	10 cm (4.0 in)
28-day compressive strength	39.7 MPa (5760 psi)	6.3 MPa (920 psi)
56-day compressive strength	45.5 MPa (6600 psi)	9.44 MPa (1370 psi)

NMSA: nominal maximum sized aggregate; w/c: water-to-cementitious-materials ratio; cwt: 100 lb of cementitious materials; “pcy” is pounds per cubic yard; “pcf” is pounds per cubic foot, “psi” is pounds per square inch

In Phase I, eight cylinders, 100 by 200 mm (4 by 8 in.) each, were fabricated from mixtures L and N and cured in accordance with ASTM Standard C 31 (2009) "Standard Practice for Making and Curing Concrete Test Specimens in the Field." Two cylinders from each batch were used to measure the compressive strength in accordance with ASTM Standard C 39 (2008) "Standard Test Method for Compressive Strength of Cylindrical Concrete Specimens." At an age not earlier than 28 days, six disks, 25±3 mm thick, and six disks, 50±3 mm thick, were obtained from each mixture by saw cutting the cylinders using a water-cooled saw with a diamond impregnated blade.

Figure 3.1 shows the locations from which disks were obtained, where the 25 mm thick disks were located between 30 and 55 mm from one of the faces of the cylinder, and the 50 mm thick disks were located between 60 and 110 mm of the face, allowing a 5 mm space for the blade cut. The disk at the face of the cylinder was discarded because of concerns in different mortar content and an irregular surface from the finishing operation during fabrication.

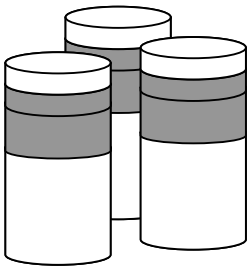

Figure 3.1 - Location of Disk Specimens Sawn from 100 by 200 mm Concrete Cylinders

In Phase III, cylinders for mixtures C and F were fabricated as in Phase I and disk specimens were obtained from the same locations shown in Figure 3.1. Curing conditions and age at which disk specimens were obtained varied. Cylindrical specimens for mixture F were cured for 7 days in the moist room and then cured in water at 50±3 °C to promote strength gain, until the age of 14 days, age at which disk specimens were obtained (compressive strength of 17.4 MPa = 2520 psi). This was necessary due to the very low early strengths of the mixture. For mixture C, disks were sawn at an age of 7 days immediately after removing cylinders from the moist room, then disks were cured in water at 23±3 °C until the age of 14 days (compressive strength of 37.0 MPa = 5370 psi).

Cylindrical specimens for mixtures G and M were cast using the method described by Montesdeoca (2008). Cylinders were allowed to cure in laboratory air at 23±3 °C. Disk specimens for mixtures G and M were obtained from three cylindrical specimens, requiring two 50 mm thick disk specimens and two 25 mm thick disk specimens to be obtained from each cylinder. Considering that more than 50% of the compressive strength was expected for the Grancrete™ materials within the first day (Montesdeoca 2008), disk specimens for mixture M were saw cut at an age of 7 days and disk specimens for mixtures G and M were sawn at an age between 3 and 7 days.

The labeling system used to identify each specimen consists of three characters. The first character describes the mixture (L, N, C, F, M, or G), the second character describes the specimen thickness (“1” for 25 mm or 1 in., “2” for 50 mm or 2 in.) and the third character identifies the individual specimen. For mixtures L, N, C and F, the third character paired the 25 mm and 50 mm specimens to a same cylinder permitting paired statistical analysis if

needed. The six specimens per mixture, per specimen thickness, were divided into two groups. Group T (disks 1, 2 and 3) was treated with exposure to high temperature and Group U (disks 4, 5 and 6) was a control group that remained undamaged, or unexposed, throughout the experimental program.

3.3 Experimental Program

3.3.1 Test Matrix

Table 3.3 shows the test matrix used for Phase I of this investigation. The sequence of testing was selected to measure the dynamic modulus of elasticity (E_d) and air permeability index (API) in both desorption and sorption. Descriptions of the test methods are given in section 3.4. Table 3.4 shows the sample conditioning methods used in Phase I. Two disk thicknesses were investigated to allow comparison of test measurements since E_d and API results were previously reported using 25 mm disks only, whereas standard fluid penetrability tests use the 50 mm disks. Similarly, Table 3.5 shows the test matrix and sequence of testing used in Phase III of this investigation, and Table 3.6 describes the moisture conditioning methods used in this phase.

Table 3.3 - Phase I Test Matrix

Step	ID	Description	Tests for Mixtures L and N			
			25 mm thick specimens		50 mm thick specimens	
			Group T	Group U	Group T	Group U
1	SKD	Soaked	E_d*	E_d*	E_d*	E_d*
2	CND	Conditioned in desorption	E_d, API	E_d, API	E_d, API	E_d, API
3	DRY	Dry in desorption	E_d, API	E_d, API	E_d, API	E_d, API
4	DMG	Dry in sorption	E_d, API	---	E_d, API	---
5	CND'	Conditioned in sorption	E_d, API	E_d, API	E_d, API	E_d, API
6	C1585	Sorptivity**	*S*	*S*	*S*	*S*
7	SKD'	Soaked in sorption	E_d*	E_d*	E_d*	E_d*

"E_d" is dynamic modulus of elasticity (Young's modulus for this Phase), "API" is air permeability index, "*S*" is rate of absorption of water, "---" means "not-applicable" since the dry in the sorption phase was the same as dry in the desorption phase for undamaged disks; the dry in the sorption phase began after cooling the disks in lab air for 24 to 48 hours after exposure to 300 °C.

* API and Sorptivity tests not possible due to moisture content

** Sorptivity testing requires a specific conditioning regime, as described in ASTM Standard C 1585 (2004)

Table 3.4 - Phase I Moisture Conditioning Methods for Disk Specimens

State	Condition	Specimen Conditioning
Soaked	SKD, SKD'	At least 3 days submerged in water, or moist room at 100% RH
Conditioned	CND, CND'	3 days at 50±2 °C and 80% RH, then at least 1 day sealed at 23±2 °C
Dry	DRY	1 day at 40±2 °C, then at least 1 day sealed at 23±2 °C
Damage	DMG	Air dried specimens at 23±2 °C exposed to 300 ± 20 °C (25 mm disks for 30±2 min and 50 mm disks for 60±2 min) , then sealed and tested at 23±2 °C within 24 hours
Sorptivity	C1585	Conditioning and testing according to ASTM Standard C 1585 (2004)

Note: during the "sealed" stage, specimens were stored separately in sealable containers, similar to the conditioning requirements of ASTM C 1585 (2004)

Table 3.5 - Phase III Test Matrix

Step	ID	Description	Tests for Mixtures C, F, M and G			
			25 mm thick specimens		50 mm thick specimens	
			Group T	Group U	Group T	Group U
1	SKD	Soaked	E_d	E_d	E_d	E_d
2	CND	Conditioned in desorption	E_d, API	E_d, API	E_d, API	E_d, API
3	DRY1	Dry in desorption	E_d, API	E_d, API	E_d, API	E_d, API
4	DMG	Dry after damage	E_d, API	---	E_d, API	---
5	CND'	Conditioned in sorption	E_d, API	E_d, API	E_d, API	E_d, API
6	C1585	Sorptivity	*S*	*S*	*S*	*S*
7	SKD'	Soaked in sorption	E_d	E_d	E_d	E_d
8	SAT	Saturated	E_d	E_d	---	---
9	ALC	Soaked in alcohol	---	---	---	---
10	DRY2	Dry in desorption	E_d, API	E_d, API	---	---

"E_d" is dynamic modulus of elasticity (shear modulus for this Phase), "API" is air permeability index, "*S*" is rate of absorption of water, "---" means that properties were not measured. Note: Alcohol soaking was used to stop any hydration after vacuum saturation.

Table 3.6 - Phase III Moisture Conditioning Methods

State	Condition	Specimen Conditioning
Soaked	SKD, SKD'	In water for 1 day with one face exposed to ambient air, then at least 1 day submerged in water or moist room at 100 % RH and tested immediately after removal from water.
Conditioned	CND, CND'	3 days at 50±2 °C and 80% RH, then at least 1 day sealed at 23±2 °C
Dry	DRY1, DRY2	Oven dried at 40±2 °C (RH = 25±5 %) for 2 days then sealed and tested within 18 hours
Damaged	DMG	Air dried specimens at 23 ± 2 °C exposed to 300 ± 20 °C for 60 ± 1 min, then sealed and tested at 23 ± 2 °C within 24 hours
Sorptivity	C1585	Conditioning and testing according to ASTM Standard C 1585 (2004)
Saturated	SAT	Oven dried at 40 ± 2 °C for 2 days, then vacuum saturated in general accordance with ASTM Standard C1202 (2009)
Alcohol soaked	ALC	1 day standing in 70% isopropyl alcohol (one face immersed, one face exposed to the atmosphere), then at least 1 day submerged.

Note: Alcohol soaking was used to stop any hydration after vacuum saturation.

A typical testing sequence of a set of disks started with soaked disks, usually kept in water after saw cutting, and tested for dynamic elastic properties (condition SKD). Then soaked disks were conditioned by storing at 50 °C and 80% relative humidity (RH) for three days after which the specimens were stored in sealed containers at 23±2 °C. The dynamic elastic properties and API were then measured (condition CND). The 80% RH and 50 °C conditioning was selected since that is specified in ASTM Standard C 1585 (2004). Disks were then air dried at 40 °C in an oven and tested for dynamic elastic properties and API (condition DRY). Disks of groups "T" were then exposed to high temperature, allowed to cool to room temperature and stored in sealed containers prior to testing for dynamic elastic properties and API (condition DMG). Disks from both groups were then conditioned for three days by storing at 50 °C and 80% RH, then kept in a sealed container for at least fifteen days before testing for dynamic elastic properties and API (condition CND'). Disks were then sealed around the edges and top face and tested for sorptivity (eight days). Side sealing was removed and specimens were then submerged in water for at least one day and tested for dynamic elastic properties (condition SKD'). For Phase III, specimens were then dried for two days and then vacuum saturated and tested for dynamic elastic properties (condition SAT). Specimens were then air dried followed by soaking in alcohol (dynamic elastic properties were measured on the first sets, but were not found to be useful), then re-dried and tested for dynamic elastic properties and API (condition DRY2). It was anticipated that testing at various moisture conditions would permit evaluation of the characteristics of microcracks with different nominal diameters since moisture is held in different diameters at

different humidities. This was not found to be useful, however. The findings are discussed in detail in section 4.2.

3.3.2 Microstructural Damage

Damage to selected specimens was attained by exposure to 300±20 °C in a muffle furnace; specimens were then allowed to cool to a temperature of 23±2 °C in laboratory air before further testing. This exposure has been shown to induce mechanical damage by thermal expansion of the different constituents and gas pressure of entrapped vapor inside the specimens without causing chemical degradation (Phan and Carino 1998; Recalde and Leming 2009; ACI-216 1989). The exposure time used in Phase I was 30±2 min for 25 mm thick specimens and 60±2 min for 50 mm thick specimens. The exposure time used in Phase III was 60±1 min for specimens of both thicknesses. The 30 min exposure for 25 mm thick disks during Phase I was selected to permit direct comparison to the results by Recalde (2005) and Recalde and Leming (2009). The exposure time used for Phase III was based on the results of Phase I.

3.4 Test Methods

3.4.1 Early Age Properties

The early age properties of concrete mixtures were measured in accordance with the standards given in Table 3.7. Compressive strength was measured on 100 by 200 mm cylindrical specimens in accordance with ASTM Standard C 39 (2008) “Standard Test Method for Compressive Strength of Cylindrical Concrete Specimens”.

Table 3.7 - Standard Methods Used to Test Fresh Properties of Concrete Mixtures

Property	ASTM Standard
Slump	C 143 (2009) "Standard Test Method for Slump of Hydraulic-Cement Concrete
Temperature	C 1064 (2008) "Standard Test Method for Temperature of Freshly Mixed Hydraulic-Cement Concrete"
Unit Weight	C 138 (2009) "Standard Test Method for Density (Unit Weight), Yield, and Air Content (Gravimetric) of Concrete
Air Content	C 231 (2009) "Standard Test Method for Air Content of Freshly Mixed Concrete by the Pressure Method"

3.4.2 Resonant Characteristics of Concrete Disks

The acceleration of the disk in vibration was obtained using a small, piezoelectric accelerometer connected to one side of the specimen with a soft, adhesive wax with good acoustical properties. Figure 3.2 shows the test setup. The disk was excited by striking it with a small steel sphere (20 mm diameter and a mass of 28.3 g in this investigation). Free-free vibration was attained by suspending the disk vertically with a thin, flexible line (Recalde, 2005). The signal from the accelerometer was captured at a sampling rate of 400 kHz; sample filtering was not used. For Phase I, a minimum of 1088 data points were acquired per signal; for Phase III, 2500 data points were acquired. Signal analysis was done using R™ (R Development Core Team 2008), a software environment for statistical computing.

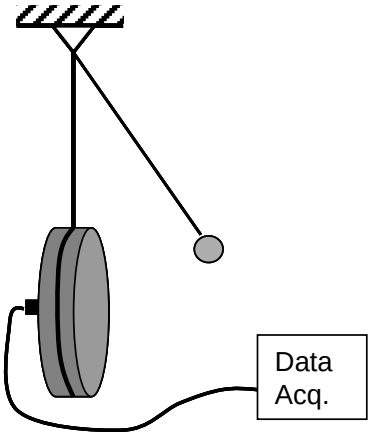

Figure 3.2 - Test Setup for Vibration Signal Acquisition of Concrete Disks

For purposes of obtaining the frequency and damping, the signal was analyzed by removing the portion of the signal at and immediately after the impact and selecting an initial acceleration maximum after which all other amplitudes in the signal were lower in value. This method of filtering has been shown to reduce spurious signals in the resonant frequency analysis reported in previous studies (Recalde and Leming 2009; Dilek *et al.* 2004; Dilek and Leming 2008). A sample size of 512 data points were used for each analysis in Phase I, whereas for Phase III the number of data points used for analysis varied in order to account for most of the steady-state signal depending on the frequency and damping exhibited. Fewer data points were used in the analysis when the signal damped very rapidly. The resonant frequency was identified by applying a nonlinear regression method on the signal in the time domain using the mathematical model presented in Eq. 3.1, which is mathematically equivalent to Eq. 2.2. This harmonic function with exponential decay corresponds to the dynamic response of a single-degree of freedom, elastic system with linear viscous damping,

a response that has been used to analyze free resonant attenuation of porous materials (Recalde 2005; Qiu and Fox 2006).

$$a(t) = e^{-\xi\omega t}\left[A\cos\left(\omega_d t\right) + B\sin\left(\omega_d t\right)\right] + C \tag{3.1}$$

where:

ξ = damping ratio,

ω = natural frequency, rad/s,

t = time, s,

ω_d = damped natural frequency, rad/s,

$$\omega_d = \omega\sqrt{1-\xi^2} \tag{3.2}$$

C = constant bias resulting from a base voltage not exactly equal to zero, V, and

A and B are constants to account for initial amplitude and slope.

The bias observed (Recalde 2005) is an artifact of charge accumulation prior to signal acquisition due to the very high electrical impedance of the test device.

The natural frequency ω can be transformed to frequency f, in Hz, using Eq. 3.3. Values for A_0, B, ξ, ϕ, and ω were obtained from the results of the nonlinear regression that minimized the square of the residuals.

$$f = \frac{\omega}{2\pi} \tag{3.3}$$

The method to obtain the dynamic Young's modulus of elasticity from free resonance of concrete disks is discussed in detail by Leming, Nau, and Fukuda (1998), which is based on the theory developed by Hutchinson (1979) assuming axisymmetric flexural vibration of a

thick, free, circular plate, including shear and rotary inertia effects. The dynamic elastic modulus of a disk under free-free vibration is given by Eq. 2.1.

$$E_d = 2(1+\upsilon)\rho\left(\frac{\pi fd}{\Omega_0}\right)^2 \tag{2.1}$$

where:

E_d = dynamic Young's modulus of elasticity, Pa,

υ = Poisson's ratio,

ρ = mass density of the disk, kg/m^3,

f = fundamental cyclic natural frequency, Hz,

d = diameter of the disk, m, and

Ω_0 = dimensionless frequency parameter.

Ω_0 is associated with the first mode of vibration according to Eq. 3.4

$$\Omega_0 = \frac{\omega r}{v_s} = \frac{\pi fd}{v_s} \tag{3.4}$$

where:

v_s = shear wave speed, m/s, and

r = disk radius, m.

The dynamic Young's modulus of elasticity was determined by measuring f, d, and ρ, estimating υ, and obtaining Ω_0 from an iterative solution easily implemented in a spreadsheet with Bessel function evaluation capabilities. A description of the analytical procedure to obtain Ω_0 using Hutchinson's (1979) solution is provided in Appendix A.

The thickness and the diameter were the average of at least four measurements taken at approximately equal spacing around the perimeter, measured to the nearest 0.1 mm. The bulk mass density of the concrete disk was determined by dividing the mass of the disk by an equivalent cylindrical volume.

$$\rho = \frac{M}{AL} \tag{3.5}$$

where:

M = mass of disk, kg

L = thickness of the disk, m

A = cross sectional area of the disk, m^2

$$A = \frac{\pi d^2}{4} \tag{3.6}$$

Density was not measured using the weight in air and the weight submerged in water, as is commonly done, due to moisture conditioning constraints.

For Phase I, E_d was measured assuming υ = 1/6, an estimate that has been used in previous investigations (Recalde and Leming 2009; Dilek *et al.* 2004; Dilek and Leming 2007a; Recalde 2005). Recalde and Leming (2009) report that estimates of E_d with υ = 0.25 instead of υ = 0.15 result in a reduction of less than 7% in calculated value of Ed for concrete disks, and differences less than 5% in relative residual E_d calculated for concrete disks using υ = 1/6 and υ = 1/4 undergoing high temperature damage. Other investigations have reported values of 0.20 to as high as 0.25 for Poisson's ratio when determined using dynamic tests (Weiss 2006). This issue is discussed further in section 5.4.

For Phase III, υ was estimated from the relationship to the stress wave velocities ratio in an elastic continuum given in Eq. 3.7 where v_p is the P-wave or compression wave velocity. The P-wave velocity was determined by measuring the length of transit time of longitudinal waves across the disk diameter in accordance with ASTM Standard C 597 (2003) "Standard Test Method for Pulse Velocity Through Concrete." The average of three measurements taken along three different diameter locations spaced approximately equally around the specimen perimeter was used as a representative v_p for each specimen at each moisture condition. The relatively small dimension (100 mm) of the disk and the resolution of the testing device, a commercially available device commonly used in field and forensic studies with 54 kHz transducers, limited the accuracy of the calculated v_p. Averaging the three measurements, and discarding those that were clearly too high or too low, appeared to provide acceptable results but future studies using this size of test specimen should consider using a device with better resolution. Further discussion using measured data is provided in section 5.4.

$$\left(\frac{v_p}{v_s}\right)^2 = \frac{2(1-\upsilon)}{1-2\upsilon} \tag{3.7}$$

The shear wave velocity was obtained using an iterative process to solve for Ω_0 and υ simultaneously using Hutchinson's solution, Eq. 3.4 and Eq. 3.7. An estimate of the dynamic shear modulus (G_d), instead of E_d, was obtained from the relationship given in Eq. 3.8 in order to reduce the dependence on υ for measuring elastic material constants.

$$v_s^2 = \frac{G_d}{\rho} \tag{3.8}$$

Adhesive wax was effective for attaching the accelerometer to dry concrete, but difficulties were found when attaching the accelerometer to wet concrete. Once attached, measurements of frequency were possible without significant variability. For mixture M, nuts were attached to the specimen using epoxy in order to screw in the accelerometer, but most of them came lose after the high temperature exposure, and even the nut was often lost after the wetting and drying cycles. The bonding failure occurred between the epoxy and the nut, but it was also observed that the bonding of the epoxy to the Grancrete™ mortar was weak since the epoxy was easily removed with the use of a screw driver. For attenuation measurements in future research, a better coupling mechanism should be found to improve accuracy and reduce variability of damping factors.

3.4.3 Air Permeability Index

The air permeability index of the concrete disks was obtained using the method described by Schonlin and Hilsdorf (1988). Schonlin and Hilsdorf refer to this parameter as a permeability "index" to avoid confusion with permeability coefficients. The Schonlin and Hilsdorf methodology is essentially a falling head, gas permeameter. The time is measured for a given pressure drop to occur between opposite faces of the disk as air permeates through it. The equation for the air permeability index was developed on the basis of the Boyle-Marriotte law assuming the concrete disk is a homogeneous porous material. API is calculated as given in Eq. 3.9.

$$API = \frac{(p_1 - p_0)V_s}{(t_1 - t_0)\left(p_a - \frac{p_0 + p_1}{2}\right)}\frac{L}{A} \tag{3.9}$$

where:

API = air permeability index, m^2/s,

p_0 = pressure inside the vacuum chamber at the beginning of measurement, Pa,

p_1 = pressure inside the vacuum chamber at the end of measurement, Pa,

p_a = atmospheric pressure, Pa,

$t_1 - t_0$ = duration of measurement, s,

V_s = volume of vacuum chamber, m^3,

L = thickness of the disk, m, and

A = cross section of specimen, m^2

The apparatus for the air permeability index test is shown in Figure 3.3. The vacuum chamber was metallic with a volume of 435 cm^3. The disk was sealed on the side with the use of removable impervious material to allow air transport only through the faces of the disk. A seal between the disk and the chamber is provided with the use of a thin strip of soft clay, a method that has been successfully used in other studies (Recalde and Leming 2009; Dilek *et al.* 2004; Dilek and Leming 2007a; Recalde 2005). Air from the chamber was evacuated using a vacuum pump; the vacuum also firmly seated the specimen. The valve to the vacuum pump was closed when the vacuum reached a constant level of about 725 mm Hg (28.5 in. Hg). The time for the absolute pressure inside the chamber to increase by any selected amount from the lowest achievable pressure was measured to the nearest 0.01 s.

To seal the sides of the test specimens, duct tape was used during Phase I, a method used in other investigations (Recalde and Leming 2009; Dilek *et al.* 2004; Dilek and Leming 2007a; Recalde 2005). During Phase III, soft adhesive clay was preferred for sealing the

sides since it was observed that duct tape did not have proper adhesion to the concrete at locations where the coupling agent used for pulse velocity measurements had been absorbed.

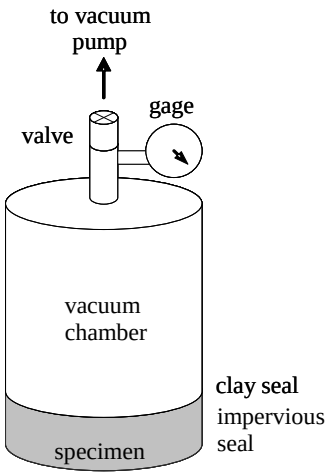

Figure 3.3- Test Apparatus for Measurement of the Air Permeability Index

3.4.4 Rates of Absorption of Water

The Rates of Absorption of Water (sorptivity) were measured in accordance with ASTM Standard C 1585 (2004) "Standard Test Method for Measurement of Rate of Absorption of Water by Hydraulic-Cement Concretes." Companion 25 mm disk specimens were used for comparison to the standard 50 mm disks. Figure 3.4 shows the setup as used in this investigation, where the plastic sheet was secured with an elastic band and adhesive tape in order to prevent accidental removal of the sheet during testing.

Figure 3.4 - Test Setup for Measurement of the Rates of Absorption of Water

CHAPTER 4.

CHANGES IN PROPERTIES WITH MOISTURE CONDITIONING AND HIGH TEMPERATURE DAMAGE (PHASE I)

4.1 Introduction

Free-free vibration signals, dynamic modulus of elasticity, air permeability index and sorptivity measurements were obtained for disks from mixtures L and N. First, the effect of moisture presence before and after microstructural damage by high temperature on signal characteristics of concrete disks in free-free vibration was studied. Then, E_d calculated from the measured resonant frequency and density was analyzed to determine the overall effect of water held in the capillary pores and cracks on this property. Companion API measurements were taken for each non-soaked condition to analyze the sensibility of the test and observe any interaction in the E_d-API relationship. Finally, sorptivity (*S*) measurements for 25 mm (1 in.) and 50 mm (2 in.) thick disks were measured to relate API measurements to a standard fluid penetrability test, to compare the rates of absorption of water on 25 mm (1 in.) thick disks to the standard 50 mm (2 in.) thick disks, and to compare the relationships between E_d and API to those between E_d and *S*.

4.2 Differences in Signal Characteristics

Signal characteristics for soaked, conditioned and dry states were obtained using LabVIEW™ software by National Instruments (2008). The code used to read, plot and fit the nonlinear model given in Eq. 3.1 by a method of least squares using R™ software (2008) is:

```
# read the signal from the *.txt file obtained using LabView:
s311skd1=read.table("C:/file_directory/.../311-01(filename)",
    skip=5)
a311skd1=S311SKD1[,3]

#plot the measured signal
t=(1:1088)*2.5E-6
plot(t*1000, a311skd1 type="p", xlab="t, ms", ylim=c(-10,10),
    pch=20, cex=0.5)

#fit the nonlinear model by least squares:
nls311skd1=nls(a311skd1~B0+exp(-X*W*t)*(A*cos(W*sqrt(abs(1-
    X^2))*t)+B*sin(W*sqrt(abs(1-X^2))*t)),   start=list(B0=0.14,
    X=0.03, W=64000, A=5, B=10), trace=TRUE, subset=(50:1088))

#display the results of the nonlinear fit:
summary(nls311skd1)

#plot the fitted equation over the previously plotted measured
    signal:
lines(t[50:1088]*1000, predict(nls311skd1), type="l", col=2)
```

Table 4.1 provides the mean measured frequency (ω) and damping ratio (ζ) for each disk at each condition. Table 4.2 provides the sample standard deviations of these measurements. Coefficients of variation, were around 0.13%, with a maximum of 0.82% for ω_{SKD} of specimen N23 which had a standard deviation of of 822 rad/s (131 Hz). At a sampling rate of 400 kHz and 1024 data points, the frequency resolution using a Fast Fourier Transform (FFT) would be about 391 Hz. The time domain analysis therefore allowed a higher frequency resolution at the selected sampling rate. Higher resolution from FFT techniques can be achieved by reducing the sampling frequency but care is needed in order to have enough data points for high frequency signals. Frequencies are given to the nearest 10 rad/sec to use four significant figures. Figure 4.1 shows the average resonant frequency and damping ratio by experimental group. Figure 4.2 shows representative signals of disks N11 and N14 showing the general behavior observed during Phase I.

Table 4.1 - Mean Resonant Frequency and Damping Ratio of Concrete Disks of Two Thicknesses and Two Mixtures for Different Moisture Conditioning Methods and a High Temperature Exposure

Group	Spe-cimen	Resonant Frequency, rad/s						Damping Ratio, %					
		SKD	CND	DRY	DMG	CND'	SKD'	SKD	CND	DRY	DMG	CND'	SKD'
L1T 25 mm	L11	63,010	60,960	60,490	*55,240*	*54,430*	*58,980*	2.7	2.6	0.7	*0.8*	*0.8*	*3.5*
	L12	62,430	59,700	59,370	*53,390*	*53,250*	*58,940*	2.5	1.6	0.8	*0.6*	*0.5*	*3.1*
	L13	64,030	62,080	61,030	*53,620*	*53,500*	*60,400*	2.6	1.3	0.7	*0.4*	*0.6*	*2.8*
L1U 25 mm	L14	61,760	59,120	58,730	—	57,880	60,740	2.8	1.7	0.8	—	0.8	2.9
	L15	63,810	61,260	60,980	—	60,130	62,100	2.4	1.3	0.8	—	0.9	3.1
	L16	64,490	60,390	59,960	—	59,300	62,410	2.7	1.1	0.7	—	0.5	3.6
N1T 25 mm	N11	68,020	65,350	65,050	*58,130*	*57,570*	*62,530*	2.3	1.6	1.0	*0.7*	*0.6*	*4.0*
	N12	69,780	67,940	67,020	*61,420*	*62,510*	*64,590*	2.2	1.8	0.9	*0.7*	*0.7*	*3.8*
	N13	69,400	65,580	65,430	*59,420*	*58,820*	*63,580*	2.6	1.4	0.7	*0.5*	*0.9*	*4.4*
N1U 25 mm	N14	70,430	66,880	66,940	—	66,450	67,860	2.9	1.8	0.9	—	0.9	3.6
	N15	71,900	67,010	67,730	—	67,290	68,570	3.4	1.7	0.9	—	0.7	4.2
	N16	68,920	66,950	66,970	—	66,400	67,590	2.4	1.4	0.8	—	0.9	3.7
L2T 50 mm	L21	93,360	91,880	88,690	*67,580*	*70,090*	*85,310*	2.8	2.0	0.6	*0.4*	*0.5*	*3.8*
	L22	93,510	89,760	88,980	*71,890*	*73,240*	*87,050*	2.6	1.0	0.7	*0.3*	*0.5*	*3.6*
	L23	92,910	90,860	88,830	*69,310*	*71,120*	*85,290*	2.6	2.3	0.6	*0.3*	*0.5*	*4.0*
L2U 50 mm	L24	94,930	96,060	90,020	—	89,420	92,680	3.1	2.9	1.0	—	0.7	3.7
	L25	97,250	91,020	90,250	—	89,440	93,520	2.9	1.0	0.6	—	0.6	3.9
	L26	91,590	91,800	85,560	—	84,960	89,130	3.1	2.4	0.5	—	0.7	3.4
N2T 50 mm	N21	100,300	95,260	94,220	*79,810*	*80,660*	*88,270*	2.8	1.5	0.6	*0.3*	*0.4*	*4.2*
	N22	101,020	96,410	95,190	*82,780*	*83,130*	*89,710*	2.5	2.2	0.7	*0.4*	*0.5*	*4.1*
	N23	100,760	95,740	94,830	*81,960*	*82,420*	*90,130*	2.6	1.6	0.6	*0.4*	*0.6*	*3.9*
N2U 50 mm	N24	103,610	97,190	96,940	—	96,950	96,380	3.0	0.9	0.6	—	0.7	5.0
	N25	102,780	95,500	94,820	—	95,000	97,030	2.8	0.9	0.6	—	0.6	4.5
	N26	102,910	94,650	93,360	—	93,580	93,430	2.8	2.1	0.7	—	0.6	4.9

"L": low strength mixture; "N": moderate strength mixture. *Values in italic* represent conditions after damage to high temperature (300 °C); "SKD" and "SKD'": at least 3 days submerged in water, or moist room at 100% RH; "CND" and "CND'": 3 days at 50±2 °C and 80% RH, then at least 1 day sealed at 23±2 °C; "DRY": 1 day at 40±2 °C, then at least 1 day sealed at 23±2 °C; "DMG": air dried specimens at 23±2 °C exposed to 300 ± 20 °C (25 mm disks for 30±2 min and 50 mm disks for 60±2 min) , then sealed and tested at 23±2 °C within 24 hours ; "T" is high temperature treated group, "U" is untreated group. "—" is data not taken (no exposure). 2π rad/s = 1 Hz

Table 4.2 - Sample Standard Deviation of Resonant Frequency and Damping Ratio Measurements of Concrete Disks of Two Thicknesses and Two Mixtures for Different Moisture Conditioning Methods and a High Temperature Exposure (3 tests per disk)

Group	Spe-cimen	Resonant Frequency standard deviation, rad/s						Damping Ratio standard deviation, %					
		SKD	**CND**	**DRY**	**DMG**	**CND'**	**SKD'**	**SKD**	**CND**	**DRY**	**DMG**	**CND'**	**SKD'**
L1T 25 mm	L11	255	464	30	*34*	*61*	*49*	0.11	0.26	0.01	*0.11*	*0.01*	*0.04*
	L12	25	17	27	*21*	*43*	*117*	0.04	0.01	0.15	*0.02*	*0.06*	*0.07*
	L13	160	124	2	*25*	*201*	*17*	0.03	0.24	0.01	*0.02*	*0.08*	*0.01*
L1U 25 mm	L14	244	110	28	—	58	27	0.37	0.36	0.09	—	0.10	0.01
	L15	52	51	17	—	16	18	0.00	0.12	0.02	—	0.16	0.03
	L16	29	24	4	—	4	36	0.02	0.03	0.02	—	0.00	0.29
N1T 25 mm	N11	71	76	60	*15*	*23*	*17*	0.00	0.13	0.03	*0.02*	*0.01*	*0.04*
	N12	13	39	9	*24*	*25*	*7*	0.01	0.01	0.02	*0.01*	*0.02*	*0.03*
	N13	28	99	10	*24*	*41*	*131*	0.05	0.02	0.01	*0.00*	*0.02*	*0.10*
N1U 25 mm	N14	15	48	33	—	46	31	0.12	0.11	0.01	—	0.01	0.01
	N15	199	47	22	—	21	14	0.61	0.04	0.01	—	0.01	0.05
	N16	34	118	9	—	43	34	0.03	0.05	0.02	—	0.09	0.12
L2T 50 mm	L21	191	92	27	*44*	*182*	*166*	0.07	0.02	0.01	*0.01*	*0.07*	*0.13*
	L22	66	41	7	*17*	*29*	*368*	0.28	0.04	0.01	*0.00*	*0.01*	*0.05*
	L23	99	126	30	*46*	*179*	*365*	0.06	0.08	0.00	*0.02*	*0.05*	*0.51*
L2U 50 mm	L24	290	216	28	—	7	368	0.26	0.14	0.03	—	0.02	0.19
	L25	376	119	44	—	57	301	0.22	0.07	0.03	—	0.01	0.16
	L26	154	125	23	—	165	162	0.15	0.14	0.01	—	0.08	0.27
N2T 50 mm	N21	168	11	5	*45*	*13*	*115*	0.27	0.05	0.01	*0.02*	*0.02*	*0.06*
	N22	101	28	17	*22*	*80*	*352*	0.04	0.10	0.03	*0.06*	*0.03*	*0.20*
	N23	822	72	56	*83*	*135*	*331*	0.15	0.01	0.00	*0.03*	*0.10*	*0.38*
N2U 50 mm	N24	56	225	11	—	30	584	0.10	0.02	0.00	—	0.03	0.03
	N25	289	20	28	—	39	248	0.36	0.09	0.01	—	0.04	0.15
	N26	415	109	12	—	39	334	0.25	0.12	0.01	—	0.01	0.19

"L": low strength mixture; "N": moderate strength mixture. *Values in italic* represent conditions after damage to high temperature (300 °C); "SKD" and SKD'": at least 3 days submerged in water, or moist room at 100% RH; "CND" and "CND'": 3 days at 50±2 °C and 80% RH, then at least 1 day sealed at 23±2 °C; "DRY": 1 day at 40±2 °C, then at least 1 day sealed at 23±2 °C; "DMG": air dried specimens at 23±2 °C exposed to 300 ± 20 °C (25 mm disks for 30±2 min and 50 mm disks for 60±2 min) , then sealed and tested at 23±2 °C within 24 hours ; "T" is high temperature treated group, "U" is untreated group. "—" is data not taken (no exposure). 2π rad/s = 1 Hz

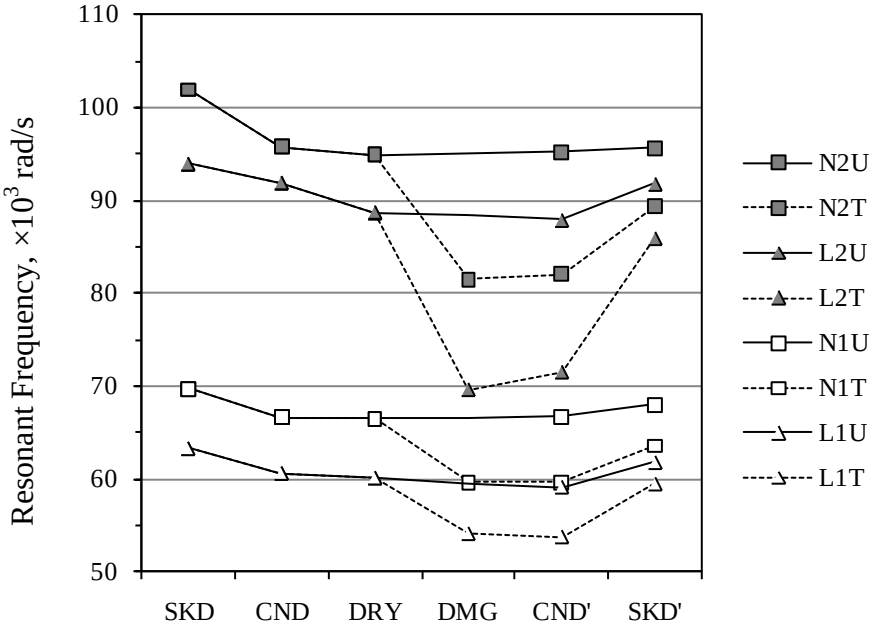

(a)

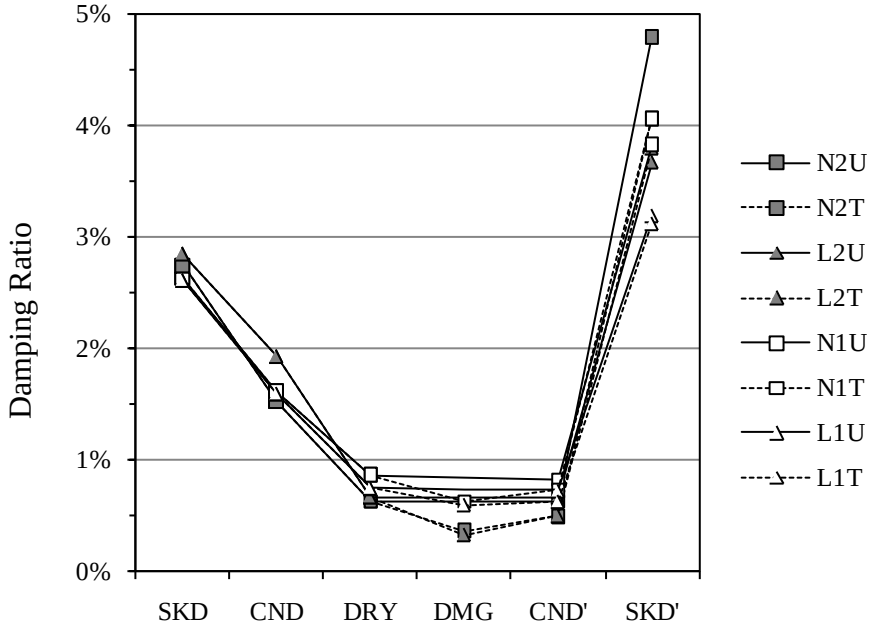

(b)

Figure 4.1 - Average Signal Characteristics for a Low (L) and a Moderate (N) Strength Mixture After Different Moisture Conditioning Methods, High temperature Damage, and Two Specimen Thicknesses: (a) Resonant Frequency, (b) Damping Ratio

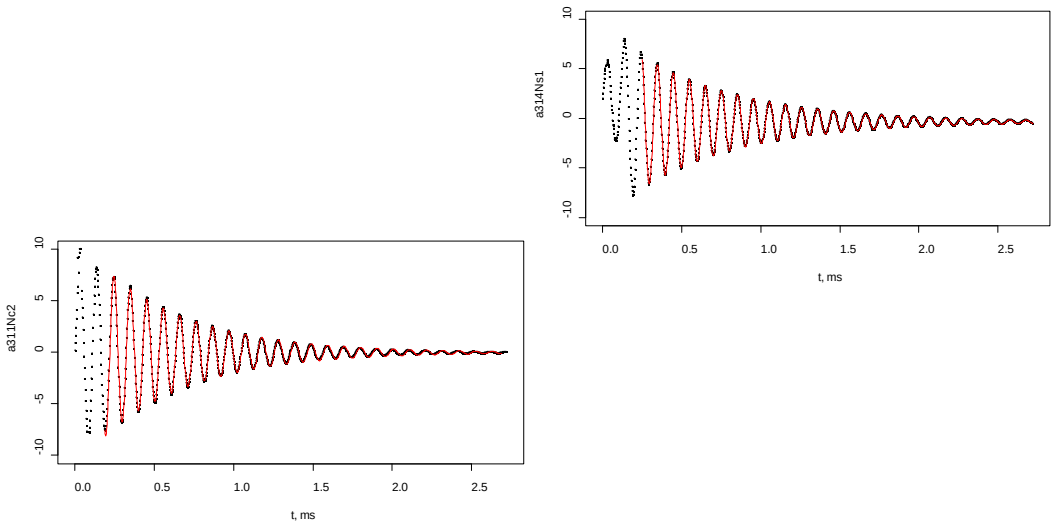

Figure 4.2 - Representative Signals from Disks of a Moderate Strength Mixture at Different Moisture Conditions and High Temperature Damage (disk N11 was exposed at state DMG, disk N14 remained undamaged)

Differences in frequencies were expected between specimens due to geometry, mixture characteristics, and inertial effects of water mass in the system. In general, water presence in the specimen when soaked resulted in a higher measured resonant frequency, especially in desorption, that is, $\omega_{SKD} > \omega_{DRY}$, for undamaged specimens. The largest increase in frequency was observed on treated groups after high temperature damage, that is, $\omega_{CND'}$ to $\omega_{SKD'}$, with mixture L showing a larger increase than mixture N for both specimen thicknesses. The extent of damage on both types of specimens was expected to be different due to different exposure times, capillary pore and microcrack interconnectivity, internal moisture content at time of exposure, and time for heat penetration.

All groups except N1U showed a slight decrease in resonant frequency from condition CND to DRY, with ranges between 100 to 1000 rad/s (0.02 to 0.16 Hz) for 25 mm (1 in.) specimens and between 200 and 6000 rad/s (0.03 and 0.95 kHz) for 50 mm (2 in.) thick specimens. A decrease in measured frequency between ω_{DRY} and ω_{CND} was observed for specimens of groups U, except for group N2U. Although it was intended that CND' conditioning would provide a higher moisture content in the specimens, density measurements revealed that undamaged groups had a lower density at condition CND' than at condition DRY meaning that the specimens lost internal moisture between or during the test conditioning procedures. Specimens from groups U were left at laboratory air conditions after testing for condition DRY and remained in laboratory air while groups T were exposed to high temperature. This observation is consistent with the decrease in frequency between these two states.

In general, for each 25 mm (1 in.) thick disk, differences in measured frequency at non-soaked conditions (CND, DRY, CND') without damage were within 1,000 rad/sec (160 Hz). More variability was observed for 50 mm (2 in.) thick disks, but it also was observed that the difference in measured frequency between ω_{DRY} and $\omega_{CND'}$ for undamaged specimens was also within 1,000 rad/sec (0.16 kHz). These differences are low compared to changes from ω_{SKD} to ω_{DRY} (desorption) with ranges between 2,000 and 4500 rad/sec (0.32 and 0.72 kHz) for 25 mm (1 in.) thick disks and between 4,000 and 10,000 rad/sec (0.64 and 1.59 kHz) for 50 mm (2 in.) thick disks between ω_{SKD} and ω_{DRY} (desorption).

In sorption, undamaged specimens exhibited increases ($\omega_{CND'}$ to $\omega_{SKD'}$) between 2,000 and 3,000 rad/sec (0.32 and 0.48 kHz) for group L1U, 1,200 to 1,400 rad/sec (0.19 to 0.22 kHz) for group N1U, 3,300 to 4,200 rad/sec (0.53 to 0.67 kHz) for group L2U, and no statistically significant increase was found for group N2U. Changes in frequency after damage seem more significant with water sorption conditioning, but it was later identified in Phase III that this change was a combined effect of water presence and autogenous healing and therefore no further analysis is presented in this section regarding changes in signal characteristics after damage.

Damping ratios exhibited coefficients of variation of up to 21% for individual disks, with sample standard deviations based on three measurements. An average coefficient of variation of 4.8% was found for all measurements. This high variability indicates that measuring damping ratios at various moisture conditions with the methodology used in this investigation cannot be used to identify the extent of damage in disks exposed to thermal stress. The findings of Kesner, Sansalone and Poston (2004) were not adaptable to the

testing methodology in this study. Improvement of the methodology for determining damping factor may be useful if further precision is required, but the use of damping ratio to assess differences in damage of a disk at resonant frequency in free-free vibration does not appear promising. The significant effect of moisture content on damping ratio is clear, however.

Average measurements indicate a higher damping ratio when soaked, compared to drier states. For dry, undamaged conditions (DRY and CND'), damping ratios were very similar in value. In many cases, no statistically significant differences were found. Damping of dry specimens was less than in soaked conditions (SKD and SKD') for all specimens. Water therefore effectively acts as a viscous damping mechanism in the free-free vibration of concrete disks.

The damping ratio at non-soaked conditions is expected to be associated with the material's energy dissipation capabilities and the increase in damping with water presence is the hydraulic damping which dissipates energy mostly through viscous shear (Qiu and Fox 2006). Figure 4.1(b) shows that the group averages are basically independent of concrete mixture and damage, and, for mixtures of similar constituents, is more dependent on the content of free water within its void system.

Comparison of the observed phenomena to the linearly elastic single degree of freedom (SDOF) system provides insight into the effect of water presence in the larger capillaries and pores (see section 2.6). In the SDOF model, the addition of mass without modifying the system's stiffness should result in a lower natural frequency, as stated in the relationship $\omega = \sqrt{k/m}$ (Eq. 2.3) where ω is the natural frequency, *k* is the system stiffness and *m* is the

mass of the body (see Figure 2.5). The observed increase in frequency in concrete disks when soaked is therefore associated with an increase in stiffness due to the presence of water, which is predominant over the increase in mass in the system, in other words, the difference due to the presence of water held in the larger pores and capillaries therefore has a stiffening effect in the resonant behavior of concrete disks.

Similarly, the increase in damping ratio with water in the larger pores, regardless of mixture or damage, is consistent with the observations by Qiu and Fox (2006) for granular material, in which the total damping ratio is a combination of the material's attenuation properties plus damping due to viscous flow of water in the capillaries. Dry concrete damping ratios (ξ_{DRY}, ξ_{DMG} and $\xi_{CND'}$), associated with the attenuation of the material, were between 0.3% and 1.0 % for mixtures L and N, both of which possessed similar constituents. Damping ratios for wet conditions, which combine material attenuation and water interaction, were between 1% and 3% at condition ξ_{CND} (desorption), and between 2 and 5 % for soaked conditions (ξ_{SKD} and $\xi_{SKD'}$).

4.3 Differences in Dynamic Modulus of Elasticity

The calculated dynamic (Young's) modulus of elasticity for each disk at each moisture condition is given in Table 4.3. These values consider the measured resonant frequency (Table 4.1), measured density, and assumes a Poisson's ratio (υ) of 1/6 and a shear coefficient K of $\pi^2/12$. Figure 4.3 shows the group averages for each moisture condition.

Table 4.3 - Dynamic Young's Modulus of Elasticity of Concrete Disks of Two Thicknesses, Two Mixtures for Different Moisture Conditioning Methods and a High Temperature Exposure

		Dynamic Modulus of Elasticity, GPa (Mpsi)					
Group	**Specimen**	**SKD**	**CND**	**DRY**	**DMG**	**CND'**	**SKD**
	L11	22.5 (3.27)	20.5 (2.98)	19.9 (2.88)	*16.1 (2.34)*	*15.8 (2.29)*	*19.4 (2.82)*
L1T	L12	21.2 (3.07)	19.1 (2.77)	18.5 (2.69)	*14.5 (2.11)*	*14.6 (2.12)*	*18.9 (2.74)*
25 mm	L13	22.1 (3.21)	20.1 (2.91)	19.0 (2.75)	*14.1 (2.05)*	*14.3 (2.07)*	*19.2 (2.78)*
	L14	22.1 (3.21)	19.9 (2.89)	19.3 (2.80)	—	18.6 (2.70)	21.3 (3.09)
L1U	L15	22.9 (3.32)	20.5 (2.97)	19.9 (2.89)	—	19.2 (2.79)	21.2 (3.08)
25 mm	L16	22.0 (3.19)	18.5 (2.68)	17.9 (2.59)	—	17.4 (2.53)	20.0 (2.90)
	N11	28.2 (4.09)	25.6 (3.71)	24.9 (3.61)	*19.1 (2.77)*	*19.0 (2.76)*	*23.5 (3.41)*
N1T	N12	28.3 (4.11)	26.5 (3.84)	25.2 (3.66)	*20.8 (3.02)*	*21.6 (3.14)*	*24.0 (3.48)*
25 mm	N13	29.4 (4.26)	25.7 (3.73)	25.2 (3.66)	*20.1 (2.91)*	*19.9 (2.89)*	*24.3 (3.53)*
	N14	28.1 (4.07)	25.2 (3.66)	24.8 (3.60)	—	24.4 (3.54)	26.1 (3.79)
N1U	N15	29.0 (4.20)	24.6 (3.57)	24.8 (3.59)	—	24.4 (3.54)	26.0 (3.77)
25 mm	N16	25.9 (3.76)	23.5 (3.41)	23.2 (3.36)	—	22.7 (3.29)	24.1 (3.50)
	L21	24.4 (3.54)	23.5 (3.41)	21.5 (3.12)	*12.0 (1.74)*	*13.2 (1.91)*	*20.4 (2.96)*
L2T	L22	24.4 (3.54)	22.3 (3.23)	21.6 (3.13)	*13.5 (1.96)*	*14.2 (2.06)*	*21.2 (3.07)*
50 mm	L23	24.1 (3.49)	22.8 (3.31)	21.4 (3.11)	*12.5 (1.82)*	*13.4 (1.95)*	*20.3 (2.94)*
	L24	25.1 (3.64)	25.6 (3.71)	22.0 (3.19)	—	21.6 (3.14)	23.9 (3.46)
L2U	L25	26.5 (3.85)	23.0 (3.33)	22.3 (3.23)	—	21.9 (3.18)	24.5 (3.56)
50 mm	L26	24.0 (3.48)	24.1 (3.49)	20.4 (2.96)	—	20.1 (2.92)	22.8 (3.30)
	N21	28.8 (4.17)	25.7 (3.73)	24.8 (3.60)	*17.0 (2.47)*	*17.6 (2.55)*	*22.3 (3.23)*
N2T	N22	29.4 (4.26)	26.6 (3.86)	25.5 (3.70)	*18.5 (2.69)*	*18.9 (2.74)*	*23.1 (3.35)*
50 mm	N23	29.7 (4.31)	26.7 (3.87)	25.7 (3.73)	*18.4 (2.67)*	*18.8 (2.73)*	*23.7 (3.44)*
	N24	31.6 (4.59)	27.6 (4.00)	27.1 (3.93)	—	27.0 (3.92)	27.4 (3.97)
N2U	N25	30.8 (4.47)	26.3 (3.82)	25.7 (3.73)	—	25.8 (3.74)	27.5 (3.99)
50 mm	N26	31.2 (4.52)	26.2 (3.80)	25.1 (3.64)	—	25.2 (3.65)	25.6 (3.72)

"L": low strength mixture; "N": moderate strength mixture. *Values in italic* represent conditions after damage to high temperature (300 °C); "SKD" and "SKD'": at least 3 days submerged in water, or moist room at 100% RH; "CND" and "CND'": 3 days at 50±2 °C and 80% RH, then at least 1 day sealed at 23±2 °C; "DRY": 1 day at 40±2 °C, then at least 1 day sealed at 23±2 °C; "DMG": air dried specimens at 23±2 °C exposed to 300 ± 20 °C (25 mm disks for 30±2 min and 50 mm disks for 60±2 min) , then sealed and tested at 23±2 °C within 24 hours ; "T" is high temperature treated group, "U" is untreated group. "—" is data not taken (no exposure)

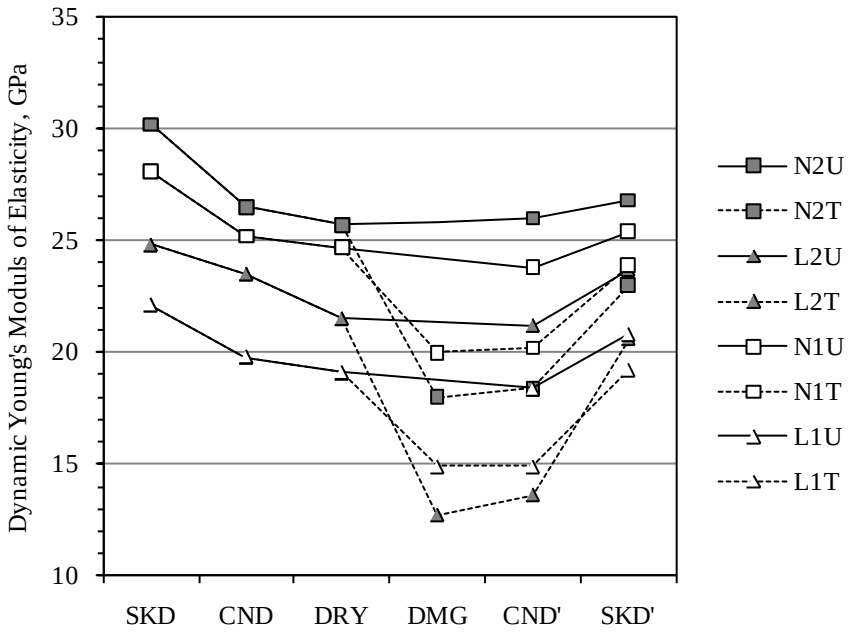

Figure 4.3 - Average Dynamic Young's Modulus of Elasticity of a Low (L) and a Moderate (N) Strength Concrete Mixtures for Two Specimen Thicknesses and Different Moisture Conditioning Methods (1 Mpsi = 6.895 GPa)

The test method is effective in discriminating between concrete mixtures according to their expected characteristics, that is, the average E_d of mixture N was higher than the average E_d of mixture L, the lower strength mixture, at each condition for a same specimen geometry. Specimen geometry seems to have an effect on the measured E_d, since a higher average E_d was measured for the 50 mm (2 in.) thick specimens than 25 mm (1 in.) companion specimens at the same undamaged conditions; t-tests for means of two paired samples, paired by cylinder, were statistically significantly different at a 95 % confidence level for each moisture condition and mixture. It is not clear if the difference in measured E_d due to specimen geometry is caused by model assumptions and limitations such as the value

for shear coefficient *K* (discussed in detail by Hutchinson, 1979), by damage imparted by the saw cutting operation, or any fluid interaction due to an extended network of interconnected voids. Additional research is recommended for future investigations.

The dynamic Young's modulus of elasticity takes into account the density of the specimen after moisture conditioning and the measured resonant frequency. It is clear from Eq. 2.1 that the calculated E_d is more sensitive to a change in frequency (squared relationship) than a change in density (linear); an increase in density of 100 kg/m^3 (6.25 pcf) results in an increase in calculated E_d of around 1.0 GPa (0.15 Mpsi), maintaining all other characteristics and assumptions constant using representative values from each mixture and geometry.

The stiffening effect from the presence of water held in the capillary pores and microcracks is more clearly seen in Figure 4.4 where paired differences in changes in E_d and changes in density based on $E_{d\text{-}DRY}$ are presented. For undamaged conditions, the changes in density are a result of water content alone. The microstructure was modified by exposure to damaging temperature and characteristics from Groups T after damage (DMG, CND' and SKD') were expected to be different than for undamaged conditions.

The extent of damage in the 50 mm (2 in.) thick specimens appears to be different from that in the 25 mm (1 in.) thick specimens. This is consistent with the exposure time and geometry. For undamaged conditions, the 25 mm (2 in.) specimens exhibited a linear trend of increase in E_d with an increase in density due to water content and a higher increase in density due to water absorption, compared to the 50 mm (2 in.) thick companion specimens.

The 50 mm (2 in.) thick specimens had clusters of data by moisture condition, even at similar densities, which implies the possible presence of moisture gradients.

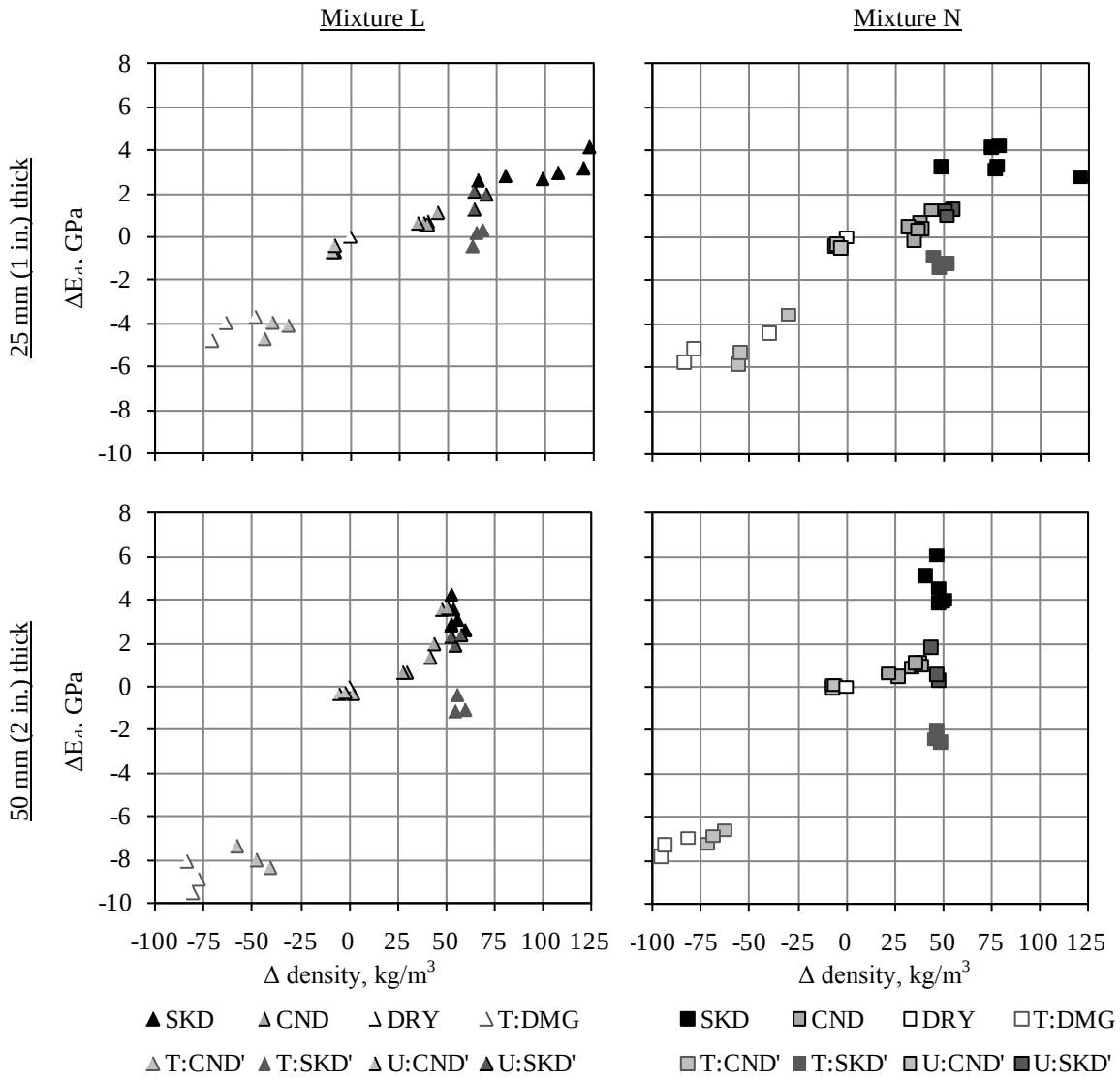

Figure 4.4 - Changes in Dynamic Young's Modulus with Changes in Density Due to Water Content and High Temperature (300 °C) Damage of Concrete Disks of Two Thicknesses from a Low (L) and a Moderate (N) Strength Mixture (1 Mpsi = 6.895 GPa; 1 kg/m^3 = 0.625 pcf)

Similar behavior is observed between mixtures L and N with moisture content by specimen type. A higher moisture content is associated with a higher E_d associated primarily with an increase in measured frequency (see section 4.2). Differences in measured E_d for non-soaked conditions (DRY, CND') are within 2 GPa (0.3 Mpsi), which are minor compared to differences of up to 4 GPa (0.6 Mpsi) between $E_{d\text{-}SKD}$ and $E_{d\text{-}DRY}$ in desorption for 25 mm (1 in.) thick disks and up to 6 GPa (0.9 Mpsi) for 50 mm (2 in.) thick disks observed in mixture N (specimen N26).

Damaged groups (groups T) had similar density recovery after soaking (condition SKD') compared to the undamaged companion specimens (groups U) with a lower average E_d due to damage, as expected. Densities at condition SKD were generally higher in value than at condition SKD' for 25 mm (1 in.) thick disks after going through a desorption-sorption cycle. Interestingly, the soaked E_d after damage recovered back to an E_d similar in value to the undamaged E_d measured in dry conditions.

The higher E_d for condition SKD than for condition CND' of the 50 mm (2 in.) specimens from mixture N at similar densities, imply either test variability (density most likely) or that since soaked condition is not a saturated state, the different distribution of water at same water contents had a different effect on the resonant behavior of the disks, consistent with moisture gradients in condition SKD' which was soaked in sorption. The purpose for testing the 50 mm (2 in.) thick disks was to be able to compare results between sorptivity (using 50 mm thick specimens) and E_d and API (using 25 mm thick specimens), but findings also indicate that results are more informative, in general, for the 25 mm specimens.

Due to the difference observed in E_d deterioration for different exposure times and disk thicknesses, and due to temperature variability of the muffle furnace, it was decided for the next phases of this investigation to use a single 60 minute exposure. It was also decided to use only the 25 mm (1 in.) thick specimens to be exposed to high temperature, and use the 50 mm (2 in.) thick specimens as companion specimens for measurements of undamaged conditions. The 25 mm (1 in.) thick disks were preferred because of the ease in handling and obtaining vibration signals, lower dependence of E_d on the value of *K*, and because of its applicability in forensic investigations (see, for example, Dilek 2008).

4.4 Differences in Fluid Penetrability Properties

Fluid penetrability properties, as measured by Air Permeability Index (API) and Rates of Absorption of Water (*S*) (ASTM-C1585 2004) for specimens from mixtures L and N are presented in Table 4.4 and shown in Figure 4.5. Previous studies found little difference in API for undamaged concrete with moderate to high strengths; it was speculated (Dilek *et al.* 2004; Dilek and Leming 2007a) that API was sensitive to the presence of interconnected microcracks since sound concrete, with few cracks other than those in the transition zone and even fewer that were interconnected (Carrasquillo *et al.* 1981), would permit only a small amount of air to flow through the specimen. The relative insensitivity of the API for sound concrete was confirmed in this part of the study, even for a relatively low strength concrete.

Table 4.4 - Air Permeability Index and Rates of Absorption of Water of Concrete Disks from Two Mixtures for Different Moisture Conditioning Methods, a High Temperature Exposure, and Two Specimen Thicknesses

Group	Specimen	Air Permeability Index, m^2/s				Initial Rate of Absorption of Water, $\times 10^{-4}$ mm/sec$^{0.5}$
		CND	DRY	DMG	CND'	
	L11	2.5E-07	5.0E-07	*6.3E-07*	*6.8E-07*	*43.5*
L1T	L12	4.5E-07	4.8E-07	*1.1E-06*	*9.9E-07*	*40.3*
25 mm	L13	1.5E-06	3.4E-07	*1.4E-06*	*9.1E-07*	*
	L14	5.2E-07	3.5E-07	—	4.0E-07	31.8
L1U	L15	3.5E-07	5.8E-07	—	2.9E-07	29.3
25 mm	L16	1.9E-06	5.9E-07	—	4.4E-07	*
	N11	1.8E-08	5.3E-07	*3.4E-07*	*2.4E-07*	*69.3*
N1T	N12	1.7E-07	7.5E-08	*1.6E-07*	*1.6E-07*	*48.7*
25 mm	N13	4.3E-08	1.0E-07	*3.8E-07*	*2.5E-07*	*
	N14	3.8E-08	4.7E-08	—	9.8E-08	30.4
N1U	N15	2.3E-07	8.9E-08	—	6.4E-08	31.1
25 mm	N16	3.0E-08	4.8E-08	—	1.0E-07	*
	L21	1.4E-07	1.9E-07	*1.5E-06*	*1.2E-06*	*
L2T	L22	2.3E-07	3.0E-07	*1.8E-06*	*1.3E-06*	*37.5*
50 mm	L23	6.5E-07	3.3E-07	*1.7E-06*	*1.2E-06*	*48.1*
	L24	1.0E-07	2.1E-07	—	4.0E-07	26.6
L2U	L25	3.6E-07	2.7E-07	—	2.6E-07	31.3
50 mm	L26	3.3E-07	4.5E-07	—	4.4E-07	*
	N21	3.9E-08	4.3E-08	*7.6E-07*	*8.5E-07*	*48.0*
N2T	N22	1.9E-07	1.3E-07	*4.3E-07*	*7.6E-07*	*53.4*
50 mm	N23	1.9E-07	1.3E-07	*8.3E-07*	*9.4E-07*	*
	N24	2.5E-08	3.5E-08	—	1.4E-07	30.6
N2U	N25	4.0E-07	1.8E-07	—	3.2E-07	26.6
50 mm	N26	1.5E-08	1.4E-07	—	1.3E-07	*

"L": low strength mixture; "N": moderate strength mixture. *Values in italic* represent conditions after damage to high temperature (300 °C); "—": data not-taken (no exposure); "*" data not taken (sorptivity measured on two disks only); "N/A": non-available ($r<0.98$)

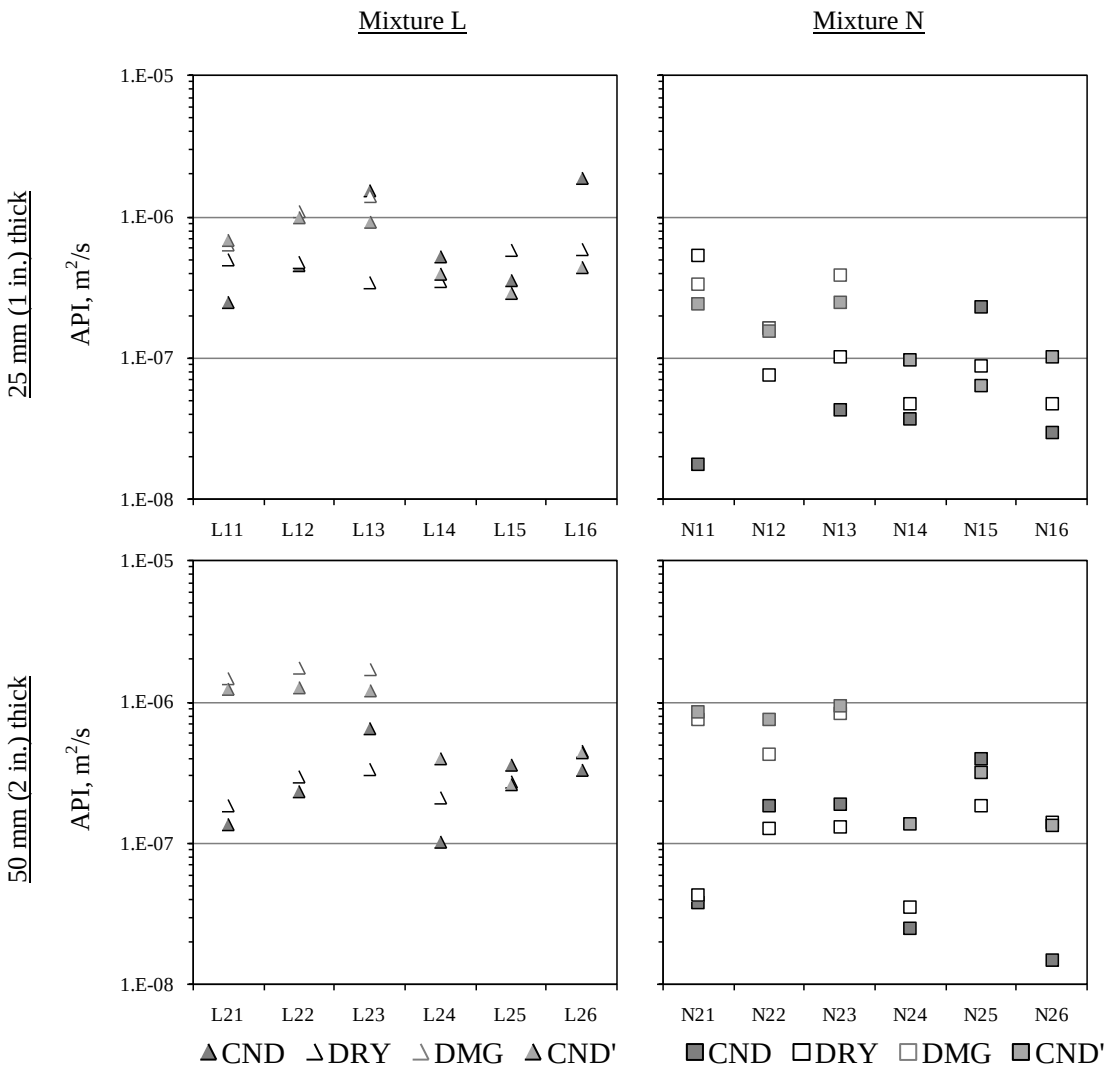

Figure 4.5 - Measured Air Permeability Index of Concrete Specimens of Two Thicknesses from a Low (L) and a Nominal (N) Strength Mixture, at Different Moisture Conditioning Methods and High Temperature Damage

Measurements after high temperature damage seemed to provide more reproducible results than for undamaged specimens. It is not clear if this variability is due to the logarithmic scale transformation for low permeability values, or an artifact of limitations of the test method procedure, such as small leaks which would influence measurements of low permeability to a higher extent than measurements of specimens with high permeability, but both seem likely contributing factors. Despite the variability for measurements of low permeability, the average of log(API) of these measurements provides some insight into changes with damage, as shown in Figure 4.6. The general trends observed with E_d are also captured by API, such as an increase in air permeability after deterioration of the microstructure by high temperature damage, and lower API for mixture N compared to API of mixture L for similar conditions.

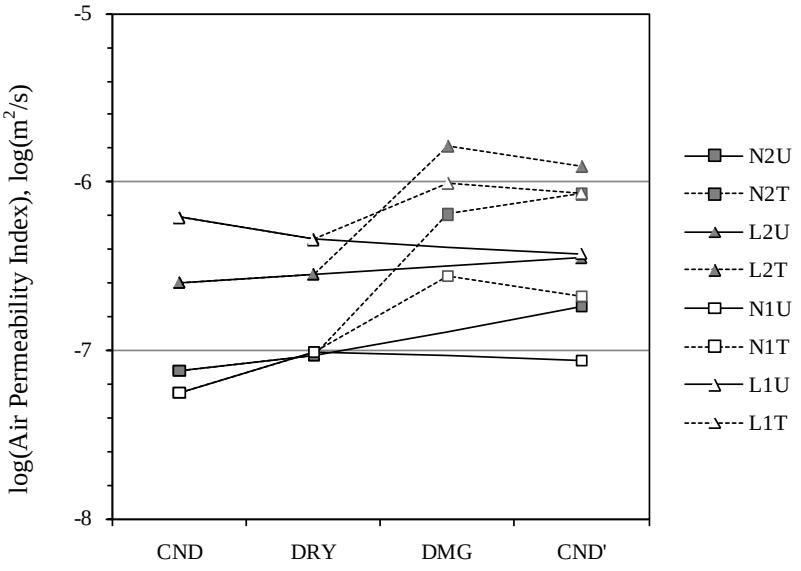

Figure 4.6 - Average Log-Transformed Air Permeability Index for a Low (L) and a Moderate (N) Strength Mixture, Two Disk Thicknesses and Different Moisture Conditioning Methods

Differences in Rates of Absorption of Water are presented in Figure 4.7 where plots of the absorption versus square root of time for each set of disks are presented. The corresponding initial and secondary rates of water absorption were given in Table 4.4. Disks damaged by high temperature exposure had higher Initial Rates of Absorption of Water (S_i) than undamaged disks for both mixtures. No significant difference was observed between S_i of 25 mm (1 in.) thick disks compared to the standard 50 mm (2 in.) disks. Estimating S_i using 25 mm (1 in.) thick disks would be advantageous for forensic investigations in order to improve the resolution in determining the depth of damage when gradients are present. The Secondary Rates of Absorption of Water (S_s) characteristics were different for different disk thicknesses, although determining a rate in most cases was not possible since the correlation coefficient (r) was less than 0.98. The secondary sorptivity characteristics for the 50 mm (2 in.) thick disks were higher than the 25 mm (1 in.) disks. It was observed that the low secondary rates of the 25 mm (1 in.) thick disk specimens occurred when water had reached the upper face of the specimen during the test. The only S_s with r higher than 0.98 were 3.7 and 4.0 $\times 10^{-4}$ mm/sec$^{0.5}$ for specimens N11 and N12, and 15.2 and 15.6 $\times 10^{-4}$ mm/sec$^{0.5}$ for specimens L24 and L25.

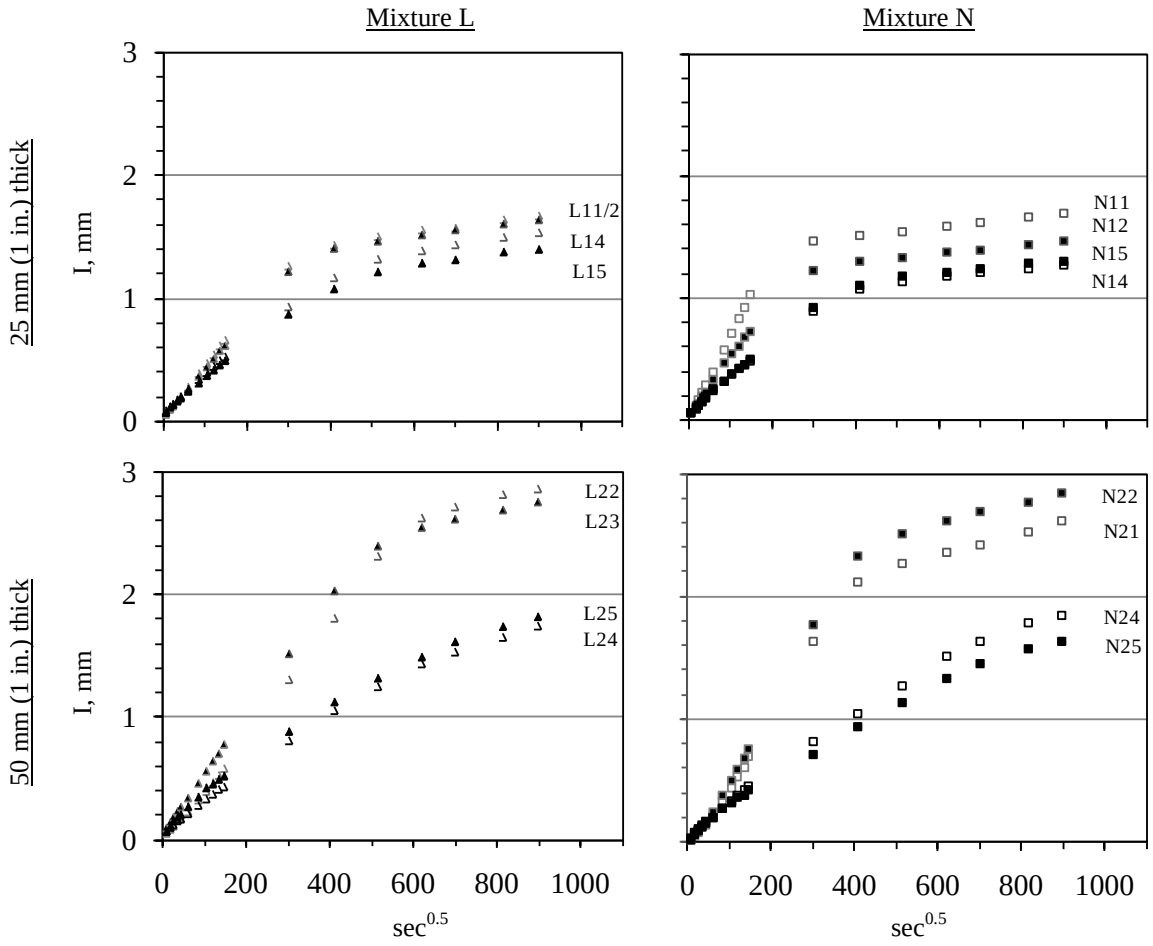

Figure 4.7 - Absorption of Water With Time for Two Disk Thicknesses, Two Mixtures and High Temperature (300 °C) Damage

4.5 Relationships Between Measured Properties

Differences in E_d and API after moisture conditioning are of interest since these measurements have been successfully used in forensic investigations (Dilek and Leming 2007a; Dilek *et al*. 2003; Dilek 2008), exploratory research (Recalde and Leming 2009; Recalde 2005; Dilek and Leming 2007b), and more importantly because the inverse semi-log relationship might provide insight into fundamental changes in microstructure with

differences in strength due to damage (Recalde and Leming 2009; Dilek *et al.* 2004). Figure 4.8(a) shows E_d and API measurements by condition, mixture and specimen thickness. The data tend to cluster by damage condition, that is, clusters for undamaged conditions (CND, DRY and CND' of Group U) at high E_d and low API, and damaged conditions (DMG and CND' of Group T) creates a cluster at low E_d and high API.

Figure 4.8(b) shows the complete data set for E_d and API on two different scales for API. The data are generally consistent with previously reported findings of an inverse relationship between E_d and log(API). A violation of the assumption of constant variance of the residuals was found, however, consistent with the observation by Recalde and Leming (2009). There is only a moderate correlation (R^2 of 0.64) for the data, due scatter from random variability and possible measurement errors more likely from sensitivity of API measurement to air leaks. This finding is consistent with the relative insensitivity of the test with sound concrete.

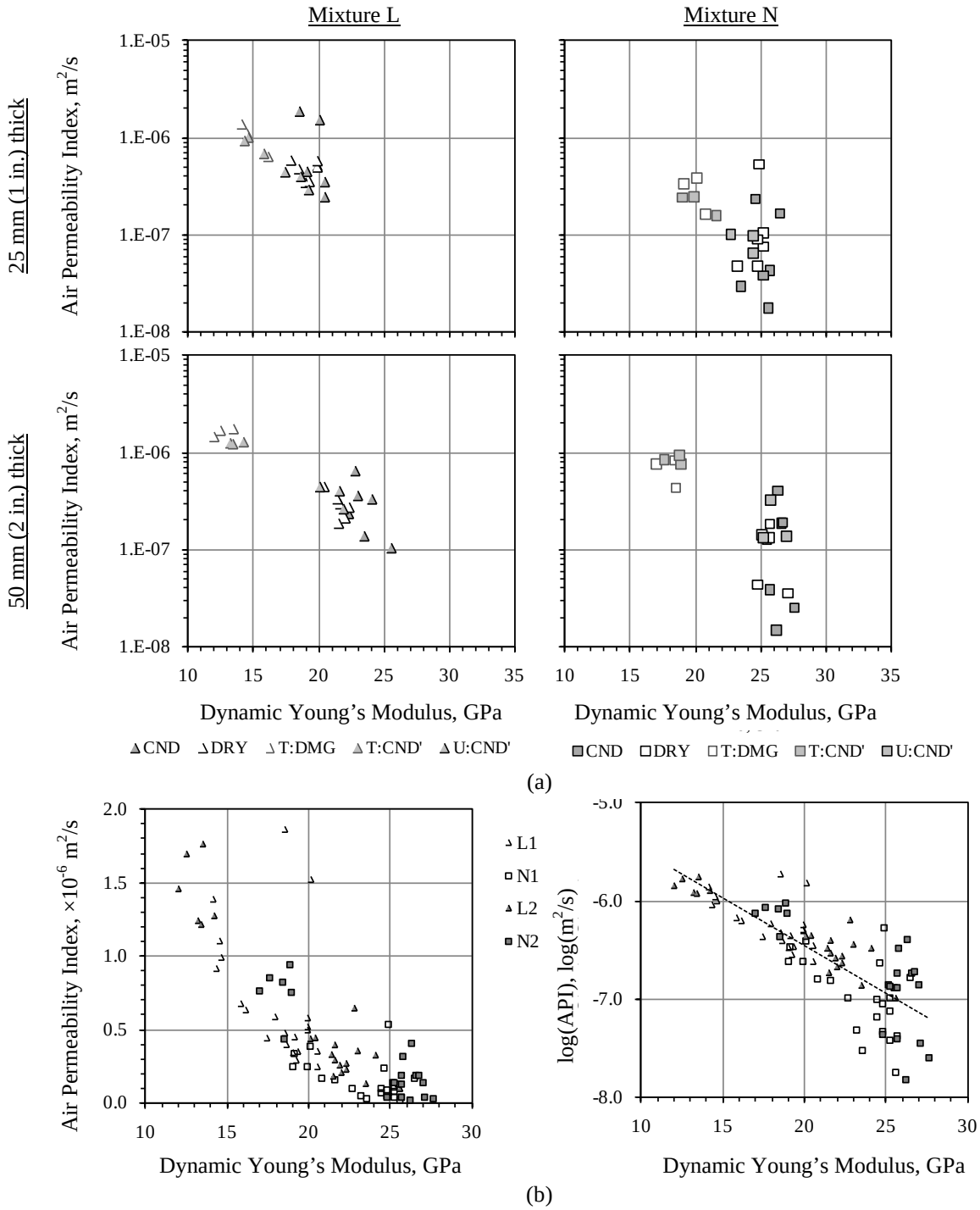

Figure 4.8 - Relationship Between E_d and API: (a) E_d versus API for Two Mixtures, Different Moisture Conditioning Methods and Specimen Thickness, (b) E_d versus API Relationship for All Measurements (two mixtures and two disk thicknesses)

The relationship between fluid penetrability properties, if any, is presented in Figure 4.9. An increase in fluid penetrability with damage is observed for each particular group (mixture and thickness), but appear to be weakly dependent at most. Figure 4.10 shows the individual measurements for E_d and Initial Rate of Absorption of Water for each disk. While an increase in fluid penetrability was found to be related to a decrease in E_d, the scatter in the data is also relatively high and limits the value of any regression analysis. Values for $E_{d\text{-}CND}$, and API_{CND}, were used to pair sorptivity measurements with E_d and API in Figure 4.9 and Figure 4.10, since this was the condition prior to the sorptivity measurement. Both API and S_i were found to be useful in characterizing damage, and the dynamic Young's modulus of elasticity of relatively dry specimens was found to provide a reliable indicator of damage regardless of disk thickness. Values for sorptivity are low compared to results by Recalde and Leming (2009).

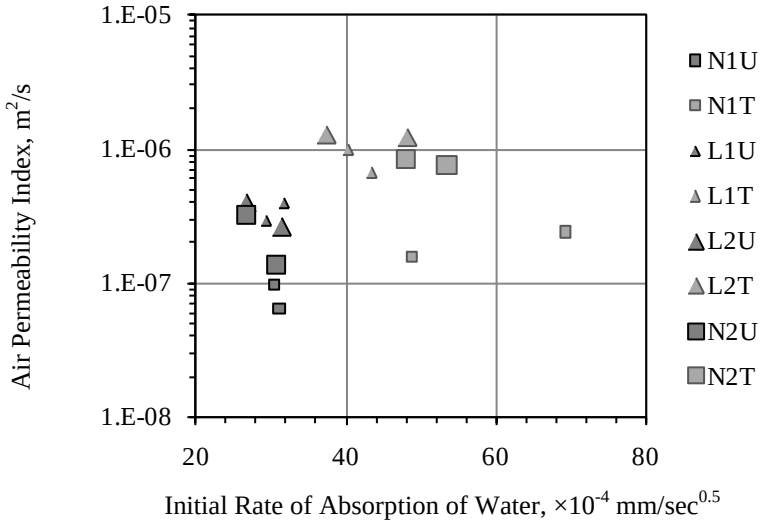

Figure 4.9 - Relationship Between Initial Rate of Absorption of Water and Air Permeability Index of Concrete Disks of Two Thicknesses from a Low (L) and a Moderate (N) Strength Mixture

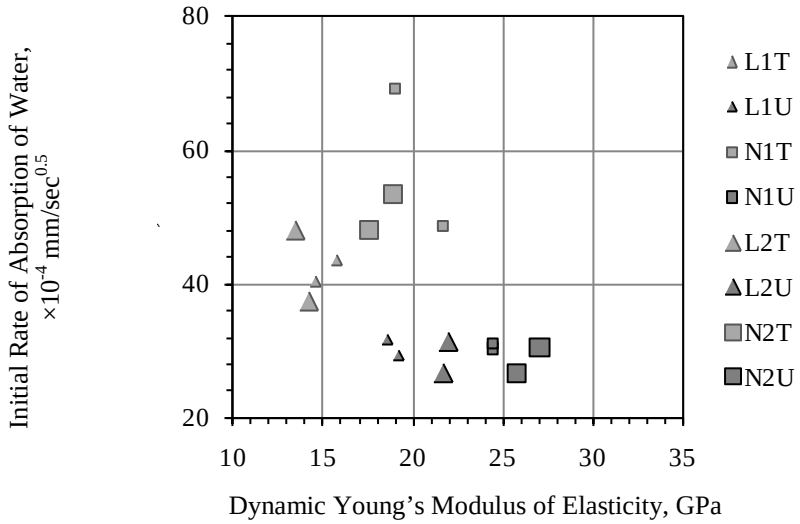

Figure 4.10 - Relationship Between Dynamic Young's Modulus of Elasticity and Initial Rate of Absorption of Water of Concrete Disks of Two Thicknesses from a Low (L) and a Moderate (N) Strength Mixture

4.6 Summary

Phase I of this investigation provided insight into important characteristics of the test methodologies used, the effects of moisture content on measured values, and relationships between changes in mechanical and fluid penetrability properties. The following is a list of conclusions obtained from the first phase of the investigation:

- Water held in large capillaries has a stiffening effect in the measured E_d, with higher values when the concrete disk is soaked than when non-soaked (either dry or with slight moisture content). This increase in E_d is associated mostly by an increase in the resonant frequency of the disk to a larger extent than the increase in density of the test specimen.
- The presence of adsorbed water in concrete disks increases the viscous damping of free-free resonant vibrations. Damping ratio is more sensitive to water presence than concrete mixture, specimen geometry, or extent of damage. Large coefficients of variation in damping ratios reduce the precision of its measurement.
- Initial Rates of Absorption of Water for 25 mm (1 in.) disks were similar to those measured using standard 50 mm (2 in.) disks. Secondary rates of absorption of water were different.
- Variability in API measurements possibly due to the presence of a few but large voids, measurement errors, or both, was not conclusive of a linear relationship between E_d and log(API).
- The direct relationship between changes in API and sorptivity with damage were different by mixture and specimen thickness, whereas the inverse relationship

between changes in E_d and sorptivity were different by mixture only, regardless of disk geometry.

The following is a list of recommendations:

- E_d measured in a non-soaked condition provides a more representative measure of the mechanical properties of the concrete structure without the compounding effects of moisture.
- An analytical method to describe the increase in E_d in resonant testing when the concrete is soaked is needed. This theoretical frame should provide insight into the microstructural void system of the material.
- Variability in API testing suggests using care when sealing the specimen.
- Additional analysis of the inverse relationship between elastic properties and air permeability of concrete disks is also needed, especially for materials of low API and high E_d.

CHAPTER 5.

DEVELOPMENT OF AN ANALYTICAL TECHNIQUE FOR THE MICROSTRUCTURAL CHARACTERIZATION OF CONCRETE (PHASE II)

5.1 Introduction

This chapter presents the results of Phase II of this investigation. The purpose was to identify a theoretical framework or model to adequately describe the stiffening effect of "free" water in a concrete disk vibrating in free resonance. This model should ideally provide insight into the microstructure, specifically the pore/crack system, that is quantifiable using easily measurable material properties, and that could be used to quantify degradation of the microstructure with damage. In this chapter, the problem is defined, and the results of a search for a physical model are presented. The model is then identified and adjusted to resonant testing of concrete disks, and finally validated using a control concrete mixture. Concrete mixtures used in Phase I are then re-analyzed using the analytical technique developed.

5.2 Problem Description

A small, concrete circular plate with absorbed water in free-free vibration has several different mechanisms acting on it. Concrete is a heterogeneous material, often treated as a three-phase media composed of coarse aggregate, mortar matrix, and a soft transition zone between them (see, for example, Hashin and Monteiro 2002) where each of the constituent phases are porous materials themselves and poroelastic properties can be estimated using upscale homogenization techniques (see, for example, Ulm *et al.* 2004). Alternatively,

capillary pores and microcracks can be modeled as inclusions in a solid, creating an effective cracked media (see section 2.5.1).

The interconnected void system is filled with a combination of fluids, air and water, whose volumetric proportions depend on the matric suction at dry conditions, and the water content when soaked. For the test method presented in section 3.4.2 and used in Phase I, the observed difference in resonant characteristics between soaked conditions and non-soaked conditions are due to the presence of the free water. When soaked, water held in the interconnected pore/crack system during resonance is held by a combination of capillary adsorptive forces, therefore pore fluid pressure is exerted onto the concrete skeleton walls at rest. During vibration, flexural and shear strains at high frequencies, in the order of 10 kHz, create a hydraulic interaction between solids and fluids through viscous flow. At low strain rates, in which the time for load application is much higher than the time for fluid pressure diffusion, isobaric conditions in the liquid are achieved and liquid would not restrict the solid skeleton deformation. This condition is known as 'drained' condition in the soil mechanics literature, and as 'relaxed' in the geophysics literature. With a harmonic oscillation, 'undrained' or 'unrelaxed' conditions are achieved (Santamarina *et al.* 2001), in which the time for pressure diffusion of liquid is much higher than the time of loading, creating liquid pressure distributions in the capillary pores.

The inertial effects due to relative movement between solids and liquid are different than when there is no relative movement between them. Tortuosity and quasi-random distribution of the voids and microcracks in the circular, concrete plate will create different effects in the relative movement of liquids and solids. Movement parallel to the capillary longitudinal axis

and movement perpendicular to this axis will result in different stiffening effects from water interaction.

The random distribution, size, and volumetric proportions of each of the constituents in different concrete mixtures with different degrees of damage complicate modeling an individual specimen, but in general, the differences in resonant behavior are an overall effect of water in the interconnected void system of each specimen. Variability of the orientation and distribution of these systems between specimens is expected by mixture, but mean characteristics between mixtures or materials should provide insight into the primary microstructural differences.

5.3 Model Identification

5.3.1 Fields Examined

The problem requires a multidisciplinary understanding of the effects of each constituent and their interactions during free-free resonant vibration. Different areas were explored, such as solid mechanics and vibrations to understand the behavior at the macroscale, fluid mechanics and tribology to understand viscous liquid interaction, and geophysics and poroelasticity to understand the effect of the presence of cracks and fluid-filled pores in the macroscopic behavior of elastic porous media.

Simple fluid mechanics models were not found to provide an accurate description of behavior, apparently due to the very high strain rate of the fluid. Several potential models from tribology and nano-tribology were also examined without success. Models, including the squeeze effect of two parallel plates in harmonic motion in a fluid, a discontinuous oil wedge, and meniscus force at contacting interfaces, did not provide a useful way of

discriminating between different types of concrete. Detailed examination of the models and the test results indicated this is likely related to the very low strain in the concrete disks at resonance in free-free vibration.

Successful models for most of the research observations were found in the area of stress wave propagation. Stress wave propagation in an elastic continuum, cracked media, porous media and particulate media provided insight into the observed behavior and an understanding of the fluid-solid interaction with harmonic strains at high frequencies. In most cases, the theories and models either consider dry media or saturated media. The unsaturated case is approached in different ways, such as a saturation ratio of filled-to-dry cracks, menisci surrounding contact points in particulate media, or saturation with an equivalent fluid. A common method to find an equivalent fluid bulk modulus is using the Reuss average of the liquid and gas compressibilities (inverse of the harmonic mean) as given in Eq. 5.1, where K_{fl-h} is the equivalent homogeneous bulk modulus of the fluid, K_i is the bulk modulus of each of the phases and s_i is the volumetric saturation of each phase. This approximation is thought to be valid only when the fluids are mixed at fine scales (Mavko *et al.* 2003), such as fluid in menisci in particulate media (Santamarina *et al.* 2001). The Voigt average (arithmetic mean) defined in Eq. 5.2, can be used to approximate the bulk modulus of an equivalent fluid for spatially variable saturation, most commonly known as 'patchy' saturation, where K_{fl-p} is the equivalent patchy bulk modulus of the fluid. Equations 5.1 and 5.2 provide lower and upper bounds, respectively, for the composite media.

$$\frac{1}{K_{fl-h}} = \sum \frac{s_i}{K_i} \tag{5.1}$$

$$K_{fl-p} = \sum s_i K_i \tag{5.2}$$

5.3.2 Model Selection

The following subsections briefly describe the different physical models and theories analyzed that describe higher measured elastic moduli when the specimen is soaked than when it is air dry. Since this phenomenon is due to the presence of free water in the interconnected void system, the objective of this search was to find a parameter that could characterize the microstructure and could be quantifiable from the simple measurements described in Chapter 3. In the following sections, the relation between stress waves and free-free resonance of circular plates is explained and then the different models are briefly presented and discussed relative to the applicability to the circular plate resonance test.

Specimens such as cylinders, rods and circular plates are excited at resonance by the presence of a standing wave that coincides with their first mode of vibration. For the particular case of a thick circular plate, using Hutchinson's (1979) thick plate theory, the first mode of vibration is induced by the presence of a standing shear wave. The equation to obtain the dynamic shear modulus (G_d) of concrete disks is given in Eq. 5.3, which combines the expressions for shear wave velocity and shear modulus given in Eq. 3.4 and Eq. 3.8, respectively. For resonant testing of materials with high hydraulic conductivity such as gravels and sands, Qiu and Fox (2006) recommend calculating G_d using the dry density

instead, consistent with a void system in which the skeleton vibrates independently from the fluid without major inertial interaction.

$$G_d = \rho v_s^2 = \rho\left(\frac{\omega r}{\Omega_0}\right)^2 = \rho\left(\frac{\pi f d}{\Omega_0}\right)^2 \tag{5.3}$$

In order to fully describe the elastic body, another elastic parameter such as Poisson's ratio, bulk modulus, Young's modulus or Lamé's constants are needed. For this purpose, measurement of the ultrasonic pulse velocity (ASTM-C597 2003) was used, as described in Section 3.4.2.

Gassmann's (1951) relations, which predict an increase in bulk modulus when a porous material is saturated, are given in Eq. 5.4 and Eq. 5.5. Gassmann's relations may be used to predict the bulk modulus of a saturated porous material from the dry bulk modulus. Gassmann's relations are valid for drained/relaxed conditions for a quasi-static analysis such as low frequency propagation of seismic waves (Berryman 1999).

$$\frac{K_{sat}}{K_0 - K_{sat}} = \frac{K_{dry}}{K_0 - K_{dry}} + \frac{K_{fl}}{\phi\left(K_0 - K_{fl}\right)} \tag{5.4}$$

$$G_{dry} = G_{sat} \tag{5.5}$$

where

K_{sat} = effective bulk modulus of the porous material saturated with pore fluid, Pa

K_0 = effective bulk modulus of the solid, Pa

K_{dry} = effective bulk modulus of the dry porous material, Pa

K_{fl} = effective bulk modulus of the pore fluid, Pa

ϕ = porosity

G_{dry} = effective shear modulus of the dry porous material, Pa

G_{sat} = effective shear modulus of the porous material saturated with pore fluid, Pa

Gassmann's equation predicts the stiffening effect of water held in the pores, as given by the second term on the right hand side of Eq. 5.4, which accounts for the stiffness contribution of the saturated porous system. Applications and other derived relations are discussed in detail by Mavko, Mukerji and Dvorkin (2003).

In order to calculate any one parameter, the four other parameters need to be measured or estimated. Ideally, determining porosity nondestructively would be beneficial, but this did not seem applicable to the resonant testing of disks because conceptually there is no K_0 in concrete since it is a heterogeneous material, K_{fl} is not the bulk modulus of water unless the test was conducted saturated and submerged in de-aired water, and more importantly, it is not clear if the frequencies of vibration are at the lower limits for which Gassmann's relations are valid. Since Gassmann's relations predict the same shear modulus for dry and saturated material, and measurements from Phase I show that $G_{wet} > G_{dry}$, Gassmann's relations were not considered as an appropriate approach.

Biot's (1956a; 1956b) theory of stress wave propagation in a porous material describes the viscoelastic, dynamic interaction between a pore fluid and the solid skeleton of a porous material. The theory assumes a saturated porous material that is macroscopically isotropic and homogeneous, all pores are interconnected and of uniform size, and the relative motion

between solids and the Newtonian fluid is described by Poiseuille flow satisfying Darcy's law. A discussion of uses, assumptions and limitations of Biot's theory, including the system of equations that describe the frequency dependence of stress waves, can be found in Mavko *et al.* (2003), and discussion on the application to soils can be found in Santamarina *et al.* (2001).

The frequency dependence of the shear wave is obtained from the root of the dispersion relation given in Eq. 5.6. The complex root is given in Eq. 5.7, where the real and imaginary parts give the velocity and attenuation, respectively. The low frequency limit of Biot's theory coincides with Gassmann's relations.

$$\begin{vmatrix} \rho - \dfrac{G_{sk}}{v_s^2} & \rho_{fl} \\ \rho_{fl} & q \end{vmatrix} = 0 \tag{5.6}$$

$$v_s{}^2 = \frac{qG_{sk}}{q\rho - \rho_{fl}{}^2} = \frac{G^*}{\rho} \tag{5.7}$$

where

$$q = \frac{\alpha\rho_{fl}}{\phi} - \frac{i\eta F_\zeta}{\omega\kappa}$$

$$F_\zeta = \frac{\zeta T_\zeta}{4\left(1 + 2iT_\zeta/\zeta\right)}$$

$$T_\zeta = \frac{e^{i3\pi/4} J_1\left(\zeta e^{-i\pi/4}\right)}{J_0\left(\zeta e^{-i\pi/4}\right)}$$

$$\zeta = \sqrt{\frac{\omega a^2 \rho_{fl}}{\eta}}$$

i = $\sqrt{-1}$

ρ_{fl} = fluid density, kg/m^3

α = tortuosity factor

ϕ = porosity

η = fluid viscosity, Pa·s

ω = angular frequency of the wave, rad/s

κ = absolute permeability of the material, m^2

J_n = Bessel function of order n

a = pore size parameter

G^* = complex shear modulus, Pa

G_{sk} = shear modulus of the skeleton, Pa

Descriptors of the microstructure can include the tortuosity factor and the pore size parameter, for which porosity and permeability would need to be assumed or measured separately. Some of the assumptions used to develop Eq. 5.6 and Eq. 5.7 are not applicable to concrete, such as complete saturation, all solid constituents having the same shear modulus, and a uniform interconnected pore system of same pore size. Another assumption of concern is that Biot's theory only considers fluid flow parallel to the direction of propagation of the stress wave, which can be inaccurate if dispersion from perpendicular fluid flow is neglected (Mavko and Jizba 1991; Dvorkin and Nur 1993). Applying the solution for shear wave speed from Biot's theory to the resonant testing of concrete disks was therefore not considered appropriate for the purpose of this investigation.

Mavko and Jizba (1991) derived formulae to predict the moduli of saturated rocks at high frequencies incorporating the concept of a fluid 'squirt', or local flow perpendicular to the direction of stress wave propagation, created during the propagation of high frequency seismic waves. Their formulae can be used to predict high frequency seismic velocities in a saturated porous material from the pressure dependence of the dry material (Mavko *et al*. 2003), as given in Eq. 5.8 and Eq. 5.9. These unrelaxed moduli can then be used in Gassman's or Biot's relations.

$$\frac{1}{K_{uf}} \approx \frac{1}{K_{dry-hiP}} + \left(\frac{1}{K_{fl}} - \frac{1}{K_0} \right) \phi_{soft} \tag{5.8}$$

$$\frac{1}{G_{uf}} - \frac{1}{G_{dry}} = \frac{4}{15} \left(\frac{1}{K_{uf}} - \frac{1}{K_{dry}} \right) \tag{5.9}$$

where

K_{uf} = unrelaxed high frequency wet frame bulk modulus, Pa

$K_{dry-hiP}$ = dry bulk modulus at very high pressure, Pa

K_{fl} = bulk modulus of the pore fluid, Pa

K_0 = bulk modulus of the solid, Pa

ϕ_{soft} = soft porosity (porosity that closes at high pressure), Pa

G_{uf} = unrelaxed high frequency wet frame shear modulus, Pa

G_{dry} = dry shear modulus, Pa

An extension of the model was developed by Dvorkin, Mavko and Nur (1995) to calculate the elastic moduli at intermediate frequencies using the squirt relations. This extended model incorporates the parameter $Z = \sqrt{R^2/K_s}$, where R is a characteristic squirt-flow length and K_s is the diffusivity of the soft (pore and crack) space, which determines the frequency scale of the dispersion, characterizing the microstructure of the material. A step-by-step procedure of the solution of this extension is given in detail by Mavko *et al.* (2003).

The squirt model was promising in the application for resonant testing of concrete disks since it predicts a higher shear modulus when wet than when dry, the extension to all frequencies allows prediction of moduli and attenuation at a particular frequency, and a measurement of Z could be used to characterize the microstructure. Unfortunately, $K_{dry-hiP}$ and ϕ_{soft} would be difficult to measure, and for the frequency extension, an estimate of K_0, and ϕ is required. Further, the model considers the saturated case only, either saturated with air or saturated with water, and unsaturated cases would require assuming or measuring a composite fluid bulk modulus.

The unified Biot-Squirt (BISQ) model developed by Dvorkin and Nur (1993) and Dvorkin, Nolen-Hoeksema and Nur (1994) incorporates the fluid squirt mechanism presented in section 5.3.2.4 into Biot's theory, presented in section 5.3.2.3, for a prediction of seismic velocities and attenuation for the entire frequency spectrum with any fluid of known viscosity. As in the Mavko-Jizba relations, the characteristic squirt-flow length R could characterize the pore structure of the material. The limitations of the two previous models

subsist in the BISQ model, that is, limitations in measuring or estimating κ, K_0, ϕ, α, a, and assuming complete saturation. The ability to apply this model to concrete in future research would be helpful since it predicts seismic velocities and attenuation at all frequencies for saturated concrete, and the microstructure could be characterized by κ, R, or both.

O'Connell and Budiansky (1974; 1977) developed sets of equations to predict the elastic moduli of solids permeated with flat ellipsoidal cracks. They considered the following cases: dry and saturated circular cracks, dry and saturated elliptical cracks, partial saturation, soft-fluid saturation, saturated isolated cracks, isobaric saturated cracks, and viscoelastic properties for all frequencies. The model is based on thin cracks randomly distributed in a homogeneous, isotropic elastic solid under constant stress, using a 'self-consistent' approximation based on the change in energy obtained by the inclusion of an isolated crack in an infinite medium (O'Connell and Budiansky 1977).

The O'Connell and Budiansky models describe the changes in Poisson's ratio, bulk modulus, shear modulus and Young's modulus with crack concentration in the solid, as measured by the crack density parameter (ε) defined in Eq. 5.10 for circular cracks and Eq. 5.11 for elliptical cracks. The crack density parameter ε is a function of the number of cracks and their geometry, that is, radius for circular cracks and squared area to perimeter ratio for elliptical cracks.

$$\varepsilon_c \equiv \frac{1}{V}\sum a^3 \tag{5.10}$$

$$\varepsilon_e = \frac{2N}{\pi V}\sum \frac{A_c^2}{P_c} \tag{5.11}$$

where

V = volume of the solid, m^3

a = long elliptical radius, m

N = number of cracks

A_c = crack area, m^2

P_c = crack perimeter, m

Two scenarios were of interest to this investigation: soft-fluid saturation and partial saturation. The expressions describing the effective moduli for a solid permeated with thin cracks, for the case of saturation with a soft fluid and the case of partial saturation, have the same mathematical structure, given by the set of equations Eq. 5.12 to Eq. 5.15.

$$\frac{K}{K_0} = 1 - \frac{16}{9}\frac{\left(1-\upsilon^2\right)}{\left(1-2\upsilon\right)} D\varepsilon \tag{5.12}$$

$$\frac{E}{E_0} = 1 - \frac{16}{45}\left(1-\upsilon^2\right)\left[3D + \frac{4}{\left(2-\upsilon\right)}\right]\varepsilon \tag{5.13}$$

$$\frac{G}{G_0} = 1 - \frac{32}{45}\left(1-\upsilon\right)\left[D + \frac{3}{\left(2-\upsilon\right)}\right]\varepsilon \tag{5.14}$$

where

$$\varepsilon = \frac{45}{16}\frac{\left(\upsilon_0 - \upsilon\right)}{\left(1-\upsilon^2\right)}\frac{\left(2-\upsilon\right)}{\left[D\left(1+3\upsilon_0\right)\left(2-\upsilon\right) - 2\left(1-2\upsilon_0\right)\right]} \tag{5.15}$$

K = effective bulk modulus, Pa

K_0 = bulk modulus of the uncracked solid, Pa

υ = effective Poisson's ratio

υ_0 = Poisson's ratio of the uncracked solid

G = effective shear modulus, Pa

G_0 = shear modulus of the uncracked solid, Pa

a = long elliptical radius, m

c = crack thickness, m

K_{fl} = bulk modulus of the fluid, Pa

and D depends on the degree of saturation. For cracks saturated with a soft-fluid,

$$D_{sf} = \left[1 + \frac{4}{3\pi} \frac{\left(1-\upsilon^2\right)}{\left(1-2\upsilon\right)} \frac{K_0}{K} \omega_{OB} \right]^{-1} \tag{5.16}$$

where

$$\omega_{OB} = \frac{a}{c} \frac{K_{fl}}{K_0} \quad , \tag{5.17}$$

and for the case of partial saturation,

$$D_{ps} = 1 - \xi_{OB} \tag{5.18}$$

where ξ_{OB} is the level of saturation, defined as the ratio of saturated cracks to the total number of cracks in the solid.

The effect of ε on the effective moduli for both cases are given in Figure 5.1 for a solid with circular cracks and $\upsilon_0 = ¼$. Differences in predicted moduli between circular cracks and elliptical cracks were found to be practically negligible for $\varepsilon < 0.5$ (O'Connell and Budiansky

1974). For the case of saturation with a soft fluid, partial saturation could be modeled using the Reuss average of the bulk modulus of air and water (Mavko *et al.* 2003). Of applicability to this investigation is the second quadrant of Figure 5.1(a) and Figure 5.1(b) which describe a higher shear modulus for a cracked material when cracks are filled with a fluid than when cracks are empty. The models also predict a higher difference in shear modulus with an increase in crack density, which could be tested on a same specimen after high temperature damage. These models may be used for high frequency seismic analysis but might not be appropriate for relaxed conditions if cracks are interconnected (Mavko *et al.* 2003).

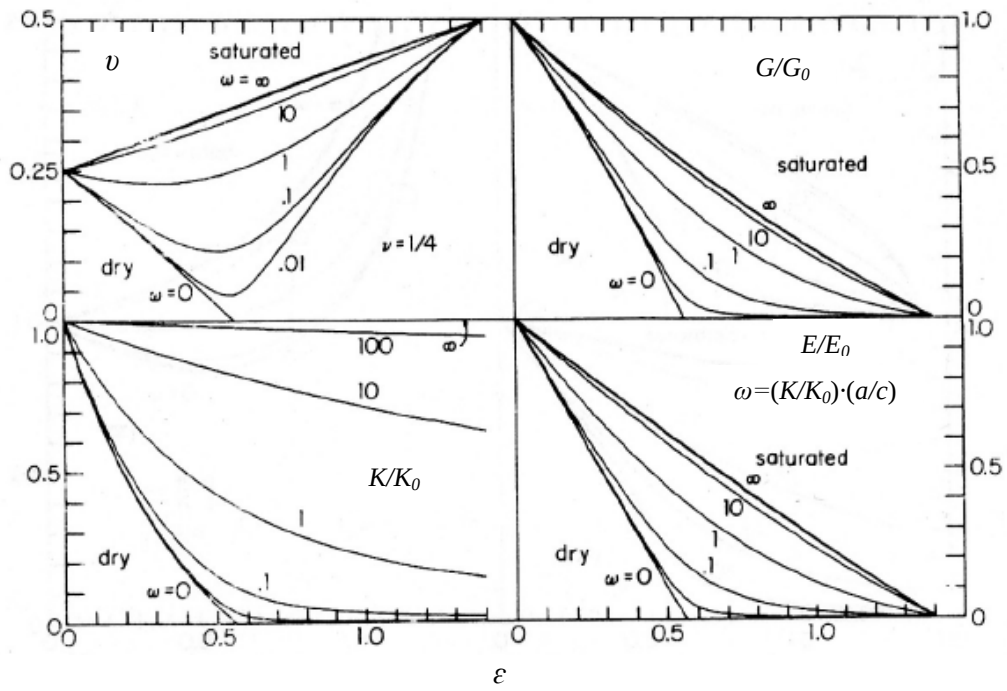

(a)

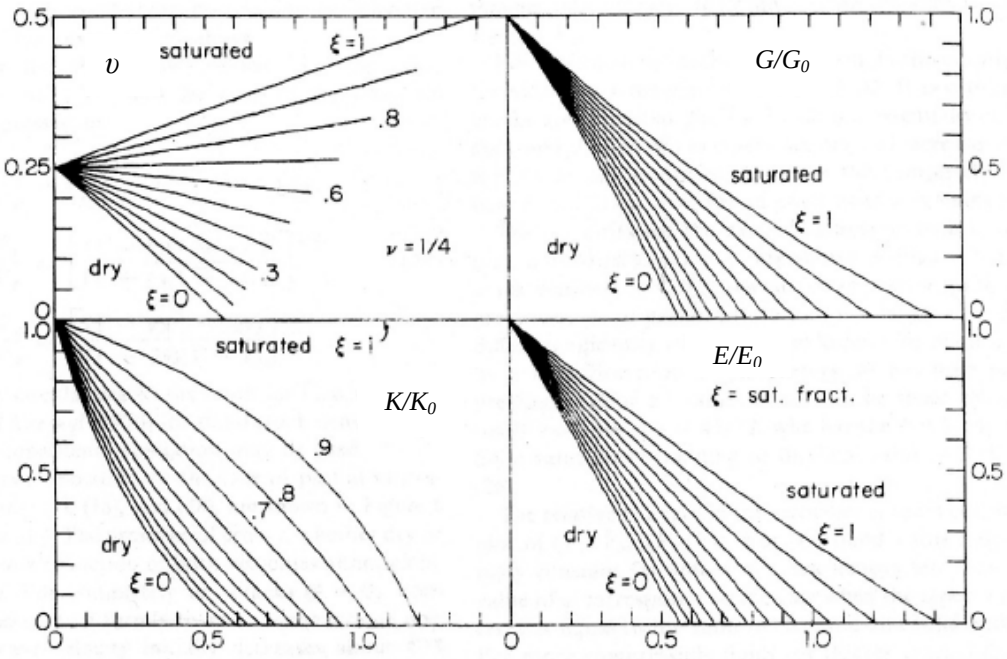

(b)

Figure 5.1 - Effective Elastic Properties of a Solid with Circular Cracks: (a) Effect of Soft-Fluid Saturation (b) Effect of Partial Saturation (O'Connell and Budiansky 1974)

For application to concrete, different geometries and scales of voids and pores are encountered for scales larger than 100 nm (see section 2.3). The larger voids correspond to entrapped air voids of irregular shapes, and entrained air voids often spherical in shape. Capillary pores are typically long and tortuous, compromising a network system surrounding conglomerates of C-S-H particles. Pre-existing cracks at the transition zone (Carrasquillo *et al.* 1981a) are rather thin with irregular shapes surrounding aggregate particles. Any cracks in the mortar phase would also be thin and of irregular shapes. A measurement of ε from a concrete specimen would therefore be an average effect of all these types of voids in the micro- to meso-scale (see section 2.2). Although speculative, the stiffening effect at high frequency vibration is likely to be caused by the thin cracks rather than the larger voids, strains being more significant in the capillary voids and thin cracks than on larger entrained or entrapped air voids where water may contribute mostly with inertial effects (which are accounted for by the value of the density in the calculation of E_d). A measure of ε would therefore be representative of the thin and virtually flat cracks, such as those at the transition zone surrounding large aggregates, modeled as equivalent ellipsoidal cracks of irregular shapes and therefore different area to perimeter ratios.

5.3.3 Analytical Procedure using O'Connell and Budiansky (1974)

The soft-fluid saturation case was analyzed first because it incorporates crack density parameter (ε), crack aspect ratio (a/c) and fluid bulk modulus (K_{fl}). Parameters that could be measured or estimated were G, υ, and K_{fl}, whereas the unknowns were G_0, υ_0, ε and a/c (note that K_0 vanishes when combining Eq. 5.16 and Eq. 5.17). In order to obtain a particular crack density parameter, such as in an undamaged specimen, expanding Eq. 5.14

with Eq. 5.15 gives an expression of G for a given ω_{OB}. For two water content conditions (i.e.: wet and dry), a system of three equations and four unknowns is obtained by developing expressions for G_{wet} and G_{dry} from Eq. 5.14, and setting $\varepsilon_{wet} = \varepsilon_{dry}$ from Eq. 5.15. Exact solution requires values of υ_0, G_0 or a/c to be assumed or be estimated initially. For two crack densities in the same specimen, such as prior to and after high temperature damage, a new set of three equations is introduced, and a system of six equations is obtained with the following six unknowns: ε_1, ε_2, $(a/c)_1$, $(a/c)_2$, υ_0, and G_0. This last solution has the drawback that in order to fully characterize the solid, characteristics at two different crack densities are needed, and therefore damage must be induced in the specimens, losing the 'nondestructive' nature of the test.

For the partial saturation case, a system of three equations and three unknowns is obtained for a given ε and two partial saturation ratios. The system of equations are obtained using Eq. 5.14 for dry and wet conditions and Eq. 5.15 such that $\varepsilon_{wet} = \varepsilon_{dry}$; the system of equations is given by Eq. 5.19 to Eq. 5.22 where the unknowns are G_0, υ_0, and ε. Application to concrete testing is provided in section 5.4, where analytical modifications were incorporated to avoid possible inaccuracies in measurements of the dynamic Poisson's ratios.

$$\frac{G_{dry}}{G_0} = 1 - \frac{32}{45}(1-\upsilon_{dry})\left[1 - \xi_{OB,dry} + \frac{3}{(2-\upsilon_{dry})}\right]\varepsilon \tag{5.19}$$

$$\frac{G_{wet}}{G_0} = 1 - \frac{32}{45}(1-\upsilon_{wet})\left[1 - \xi_{OB,wet} + \frac{3}{(2-\upsilon_{wet})}\right]\varepsilon \tag{5.20}$$

$$\varepsilon_{dry} = \frac{45}{16}\frac{\left(\upsilon_0 - \upsilon_{dry}\right)}{\left(1-\upsilon_{dry}{}^2\right)}\frac{\left(2-\upsilon_{dry}\right)}{\left[\left(1-\xi_{OB,dry}\right)\left(1+3\upsilon_0\right)\left(2-\upsilon_{dry}\right)-2\left(1-2\upsilon_0\right)\right]} \tag{5.21}$$

$$\varepsilon_{wet} = \frac{45}{16}\frac{\left(\upsilon_0 - \upsilon_{wet}\right)}{\left(1-\upsilon_{wet}{}^2\right)}\frac{\left(2-\upsilon_{wet}\right)}{\left[\left(1-\xi_{OB,wet}\right)\left(1+3\upsilon_0\right)\left(2-\upsilon_{wet}\right)-2\left(1-2\upsilon_0\right)\right]} \tag{5.22}$$

Estimating the crack density parameter of concrete disks is therefore possible by nondestructively measuring the dynamic shear modulus and dynamic Poisson's ratio of wet and dry concrete using the same specimen using the partial saturation model. Advantages of using this model are that these properties can be measured on small specimens with ease, changes in crack density with deterioration could be measured independently (unlike the soft-fluid saturation case), and, once the system is defined, a decrease in *G* can be estimated if the $\Delta\varepsilon$ from a damaging event is known.

Application of this model also has some limitations. The first limitation is the need to calculate a dimensionless frequency parameter Ω_0 for each saturation ratio, which would depend on the Poisson's ratio obtained from the stress wave velocity ratio and is subject to the accuracy of the pulse velocity measurement. A second limitation is the estimate of the saturation ratio ξ_{OB}. The model assumes all cracks to be of a same geometry, therefore estimating ξ_{OB} using gravimetric techniques might not necessarily be accurate if changes in the geometry as well as number of cracks change significantly.

Changes in the pore structure or pore size distribution of the matrix will not occur until the structure of the hydrated paste is modified. Since the changes in paste are minor for a short exposure period at temperatures not exceeding 300 °C (Dias *et al.* 1990), the only concern is changes in the general geometry of the transition zone or the significant extension

of pre-existing microcracks. Carrasquillo, Slate and Nilson (1981) found that crack extension was the predominant change in the concrete at loads up to about 50% to 75% of the ultimate strength. These extensions were limited, however. The maximum changes in length were approximately 50% to 100% of the original length, or roughly the original length of the transition zone. Since the ratio of the effective thickness to length of the pre-existing cracks and transition zone lengths are already relatively low, the fundamental geometry of the crack system will likely change very little under the thermal exposures examined in this study, that is, length change will likely predominate the changes in crack characteristics. It was therefore postulated that the equations of O'Connell and Budiansky (1974) could be used, presuming an essentially constant crack thickness, and ξ_{OB} based on differences in mass could be analyzed accurately.

5.4 Experimental Validation

The O'Connell and Budiansky (1974) model for partial saturation provided a practical approach to estimate the crack density parameter of concrete disks. In this section, the analytical technique is validated and calibrated using concrete mixture C, a control mixture of conventional mixture characteristics used in commercial structural applications. Mixture C also served as a control mixture for the very high fly ash mixture (mixture F), therefore it was tested for fluid penetrability at different moisture contents in Phase III as described in section 3.3.1. In this section, only relevant properties for the free-free resonance analysis are presented; fluid penetrability properties and corresponding E_d are presented in Chapter 6.

5.4.1 Measured Properties and Modeling Approach

In order to apply the O'Connell and Budiansky partial saturation model to the free-free resonance analysis of concrete disks, the pulse velocity was incorporated into the test methodology to obtain a measurement of the dynamic Poisson's ratio (υ_d). The dynamic shear modulus (G_d) was calculated from the shear wave speed obtained using Hutchinson's (Hutchinson 1979) solution. The dynamic shear modulus was preferred over E_d to minimize the dependence of the modulus measurement on the value of υ_d. Pulse velocity, G_d, and the corresponding υ_d for each 25 mm thick specimen from mixture C are presented in Table 5.1.

An increase in G_d from G_{DMG}, after the exposure to high temperature, to G_{DRY2}, after a soaking and drying cycle, shows that autogenous healing had occurred after absorption of water. It was therefore preferred to estimate ε under two desorption cycles, that is, G_{SKD} to G_{DRY1} for ε_1, and G_{SAT} to G_{DRY2} for ε_2, where ε_2 for group C1T is the crack density parameter after damage to a 300 °C exposure followed by saturation and drying. Any increase in G_d after high temperature damage with soaking, as in moisture condition CND', has a combined effect of autogenous healing and free water interaction. Soaking in 70% isopropyl alcohol between condition SAT and DRY2 was expected to stop any additional hydration and therefore it was expected that G_d from these two conditions could be used to estimate a value for the crack density parameter at that state (ε_2). Further discussion on autogenous healing is provided in section 6.2.1.

Table 5.1 - Mechanical Properties of 25 mm Thick Concrete Disks From a Conventional Concrete Mixture

Group	Specimen	SKD			DRY1			DMG			SAT			DRY2		
		D		G_d	D		Gd	D		G_d	D		G_d	D		G_d
		kg/m^3		GPa	kg/m^3		GPa	kg/m^3		GPa	kg/m^3		GPa	kg/m^3		GPa
C1T	C11	2360	0.301	15.3	2302	0.275	14.5	*2203*	*0.274*	*11.0*	*2363*	*0.329*	*12.9*	*2262*	*0.292*	*12.5*
	C12	2370	0.325	14.2	2315	0.288	13.9	*2210*	*0.326*	*9.8*	*2374*	*0.343*	*12.4*	*2270*	*0.335*	*11.3*
	C13	2358	0.305	14.6	2289	0.285	13.5	*2194*	*0.327*	*9.1*	*2362*	*0.307*	*12.7*	*2253*	*0.299*	*12.1*
C1U	C14	2367	0.313	14.4	2304	0.291	13.6	—	—	—	2375	0.315	13.8	2296	0.313	12.9
	C15	2360	0.311	14.8	2292	0.295	13.8	—	—	—	2369	0.337	13.7	2285	0.320	12.8
	C16	2377	0.299	15.3	2313	0.286	14.0	—	—	—	2386	0.302	14.5	2306	0.316	13.0

"D" is density, "υ_d" is dynamic Poisson's ratio, and "G_d" is dynamic shear modulus. *Values in italic* represent conditions after damage to high temperature (300 °C). "SKD"= at least 3 days submerged in water, or moist room at 100% RH; "DRY*n*"= Oven dried at 40±2 °C (RH = 25±5 %) for 2 days then sealed and tested within 18 hours; "DMG"= Air dried specimens at 23±2 °C exposed to 300 ± 20 °C for 60±2 min, then sealed and tested at 23±2 °C within 24 hours; "SAT"= water saturated specimens in accordance with ASTM C 1202 (2009). "T" is high temperature treated group, "U" is untreated group

A modification to the approach discussed in section 5.3.2.6 was made to account for variability in the determination of Poisson's ratio from the ratio of stress wave velocities (see Eq. 3.7). During testing, difficulty was experienced in obtaining consistent pulse velocity (v_p) measurements. In addition, the test device was operating near its minimum resolution limit. The wavelength using the largest measured v_p was 9 cm (3.5 in.), calculated by dividing the saturated pulse velocity of 4.85 km/s for specimen C15 by the transducer's frequency of vibration (ASTM Standard C 597, 2002) of 54 kHz, which is very close to the transit length of 10 cm (4 in.) across the disk diameter.

The O'Connell and Budiansky model predicts a higher υ with water content for a given crack density, with more dispersed values of υ as crack density increases (see Figure 5.1). Although a higher measured υ_d is observed for wet measurements paired by crack density, that is, $\upsilon_{SKD} > \upsilon_{DRY1}$ and $\upsilon_{SAT} > \upsilon_{DRY2}$, except for specimen C16, the larger differences expected with higher crack densities such as after high temperature damage were not observed.

Due to the difficulty in reliably measuring υ_{wet} and υ_{dry}, the mean of the measured υ_d for each specimen were used to estimate the value of υ_0 instead, that is, the value of υ_0 was taken as the average of υ_{SKD}, υ_{DRY1}, υ_{SAT} and υ_{DRY2}. Although mathematically convenient, this estimate is also consistent with the physical model, as shown in the first quadrant of Figure 5.1(a) and Figure 5.1(b) for four measurements of dynamic Poisson's ratio such that $\varepsilon_1 < \varepsilon_2 < 0.5$, and υ_{SKD} and υ_{DRY1} would correspond to ε_1, and υ_{SAT} and υ_{DRY2} to ε_2, and the average is an estimate of υ_0. The corresponding υ_{wet} and υ_{dry}, for a particular microstructural

state ε, could then be obtained by numerically finding values for υ_{wet} and υ_{dry} such that $\varepsilon_{wet} = \varepsilon_{dry}$ (Eq. 5.21 and Eq. 5.22). No statistically significant difference was found in the mean υ_d obtained combining υ_{SKD} and υ_{DRY1} data (at state ε_1), compared to the mean υ_d combining υ_{SAT} and υ_{DRY2} data (at state ε_2), by exposure group, providing further evidence on the adequacy of this method to estimate υ_0. This last observation also supports the use of a constant value of equivalent υ_0 by mixture, but individual values of υ_0 for each specimen were preferred, as would be the case of a forensic investigation where specimen availability might be limited.

The model was validated using the best available data, that is, all G_d measurements from a same specimen, therefore the model applied to each specimen used a single value of υ_0 and G_0. A solution for each specimen was found by solving the system for G_0 and ε for a pair of wet and dry shear moduli, in this case G_{SKD} and G_{DRY1} to estimate ε_1, and then finding υ_{DRY2} and ε_2 from G_{DRY2}, and υ_{DMG} and ε_{dmg} from G_{DMG}. Solutions were found using numerical methods to match predicted and measured values of G_{SKD}, G_{DRY1}, G_{DMG}, and G_{DRY2} using Equations 5.19 to 5.22, by numerically selecting values for G_0, υ_{wet1}, υ_{dry1}, υ_{dry2} and υ_{dmg}, such that $\varepsilon_{wet1} = \varepsilon_{dry1} = \varepsilon_1$, $\varepsilon_1 < \varepsilon_2$, and $\upsilon_{wet,i} > \upsilon_{dry,i}$. A description of the analytical method to calculate the crack density parameter is provided in Appendix C.

5.4.2 Model Validation

Two cases of the partial saturation model were analyzed. First, partial saturation was modeled using volumetric water fractions as values for ξ_{OB}. The second case considered

only dry and wet concrete, mathematically modeled as dry ($\xi_{OB} = 0$) and saturated ($\xi_{OB} = 1$) cracked media, where the dry case for shear modulus is equivalent to the saturated isobaric case (O'Connell and Budiansky 1977) at which pore fluid is at constant pressure.

For validation of the partial saturation (PS) model, the values for the crack saturation ratios ξ_{OB} were assumed to be the volumetric water fractions s as discussed in section 5.3.3. The values of s were obtained using Eq. 5.23 and are presented in Table 5.2 for each specimen at each moisture condition of interest; by definition, $s_{SAT} = 1$, and $s_{DMG} = 0$. For group C1U, D_{dry} was estimated using the average D_{DMG} from group C1T which was 2202 kg/m^3 (137 pcf).

$$s = \frac{V_{water}}{V_{voids}} = \frac{D_i - D_{dry}}{D_{sat} - D_{dry}} \simeq \frac{D_i - D_{DMG}}{D_{SAT} - D_{DMG}} \tag{5.23}$$

where

D_i = measured density at condition *i*, kg/m^3

D_{dry} = density without free water, kg/m^3

D_{sat} = density saturated with water, kg/m^3

D_{SAT} = measured density at condition SAT, kg/m^3

D_{DMG} = measured density at condition DMG, kg/m^3

The results of applying the O'Connell and Budiansky PS model, assuming that the value for the crack saturation ratio ξ_{OB} is the same as the volumetric water fraction (s), is given in

Table 5.3. Figure 5.2 plots these results, including G_{SAT} for comparison to the predicted value.

Table 5.2 - Volumetric Water Fractions *s* for Specimens from Control Mixture C

Group	Specimen	s_{SKD}	s_{DRY1}	s_{DRY2}
C1T	C11	0.98	0.62	*0.37*
	C12	0.98	0.64	*0.37*
	C13	0.98	0.57	*0.35*
C1U	C14	0.95	0.59	0.54
	C15	0.95	0.54	0.50
	C16	0.95	0.60	0.57

Values in italic represent conditions after damage to high temperature (300 °C). "SKD"= at least 3 days submerged in water, or moist room at 100% RH; "DRY*n*"= Oven dried at 40±2 °C (RH = 25±5 %) for 2 days then sealed and tested within 18 hours; "DMG"= Air dried specimens at 23±2 °C exposed to 300 ± 20 °C for 60±2 min, then sealed and tested at 23±2 °C within 24 hours; "SAT"= water saturated specimens in accordance with ASTM C 1202 (2009). "T" is high temperature treated group, "U" is untreated group. Values of *s* are 0 for DMG and 1 for SAT by definition.

Table 5.3 - Results of the O'Connell & Budiansky Partial Saturation Model Using Volumetric Saturation Ratios as Crack Saturation Ratios

Group	Specimen	υ_0		Crack Density Parameter			$\Delta\varepsilon$	
				ε_1	ε_{dmg}	ε_2	$\varepsilon_{dmg}-\varepsilon_1$	$\varepsilon_2-\varepsilon_1$
C1T	C11	0.299	18.5	0.199	*0.260*	*0.256*	*0.061*	*0.057*
	C12	0.323	15.6	0.105	*0.243*	*0.223*	*0.138*	*0.118*
	C13	0.299	18.3	0.234	*0.314*	*0.264*	*0.080*	*0.030*
C1U	C14	0.308	17.6	0.207	—	0.235	—	0.028
	C15	0.316	18.2	0.216	—	0.257	—	0.041
	C16	0.301	20.3	0.280	—	0.318	—	0.038

"T" is high temperature treated group, "U" is untreated group, υ_0 is Poisson's ratio of the uncracked solid, "ε_1" is the crack density parameter before damage using shear moduli at conditions SKD and DRY1, "ε_{dmg}" is the crack density parameter after exposure to 300 °C, "ε_2" is the crack density parameter after vacuum saturation using shear moduli at conditions SAT and DRY2. "SKD": at least 3 days submerged in water, or moist room at 100% RH; "DRY*n*"= Oven dried at 40±2 °C (RH = 25±5 %) for 2 days then sealed and tested within 18 hours; "DMG"= Air dried specimens at 23±2 °C exposed to 300 ± 20 °C for 60±2 min, then sealed and tested at 23±2 °C within 24 hours; "SAT"= water saturated specimens in general accordance with ASTM C 1202 (2009)

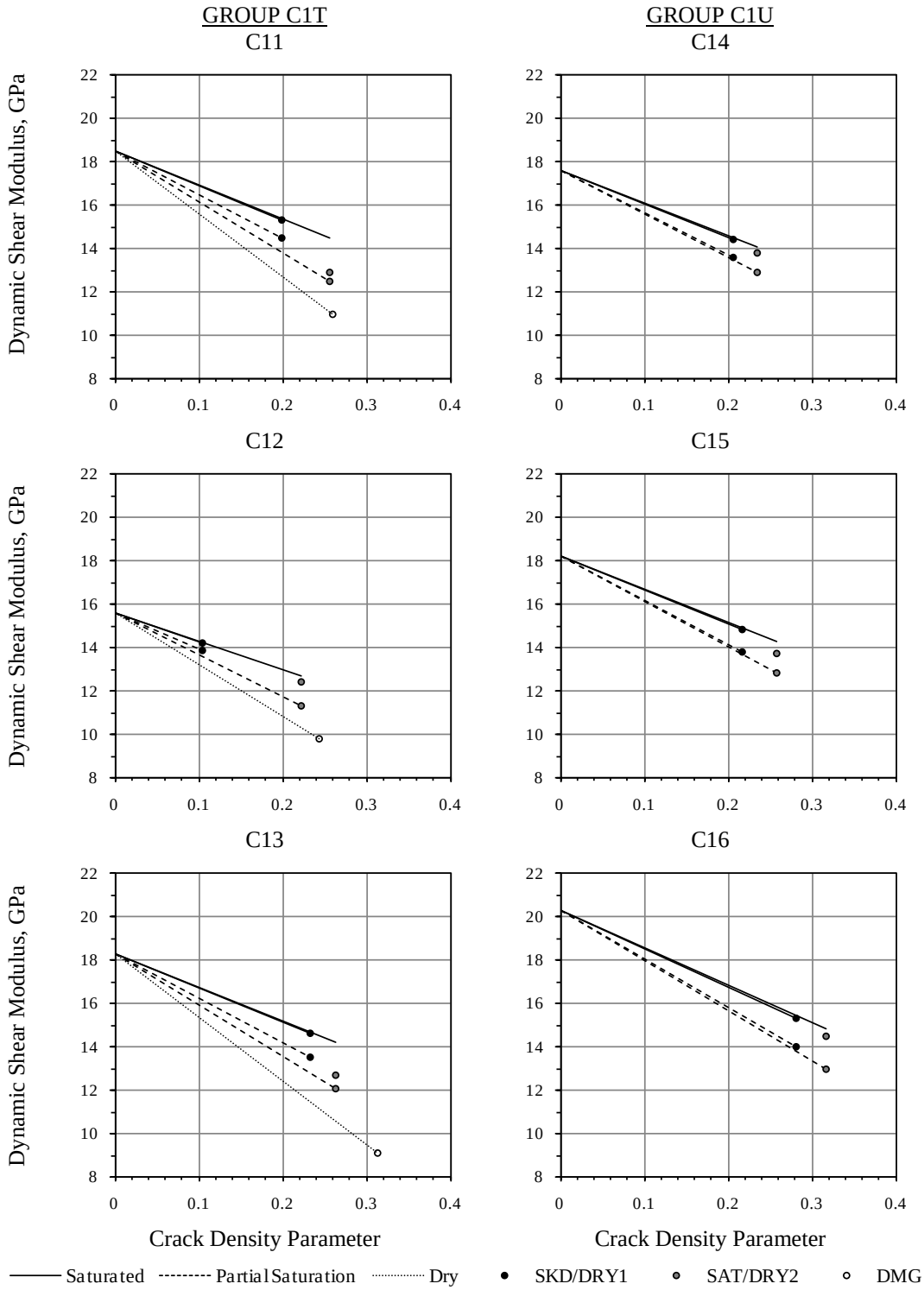

Figure 5.2 - Application of the O'Connell and Budiansky Partial Saturation Model for 25 mm Thick Disk Specimens from Control Mixture C Using Volumetric Water Fractions (1 Mpsi = 6.895 GPa)

Since the values for G_0 and ε_1 were obtained from measurements of G_{SKD} and G_{DRY1}, and ε_2 and ε_{dmg} were calculated from G_{DRY2} and G_{DMG}, respectively, the general validity of the analytical approach can, in part, be evaluated by examining the difference between predicted and measured G_{SAT}, and by examining the expected increase in ε with damage. The results of the analysis match the a priori expectations reasonably well. In all cases an increase in the crack density parameter is found after exposure to 300 °C. This finding is consistent with the reduction in shear modulus and the values themselves appear to be reasonably consistent.

Further analysis of the data from Group C1U shows an increase in crack density after the drying and wetting cycle that may be related to microstructural damage from the vacuum drying procedure. In this regard, measuring the shear modulus soaked, instead of saturated, would be preferred and more representative of an intact condition. For Group C1T, the model appears to capture both an increase in ε with damage, and autogenous healing on specimens C12 and C13. In two of the three specimens (specimen C11 and C12), the prediction of G_{SAT} was inaccurate. The small difference between damaged G_{SAT} and G_{DRY2} of specimens C11 and C13 is more consistent with a drained/relaxed behavior, in which the shear modulus is not affected by the presence of a fluid. These findings suggest that the value of ξ_{OB} might not be valid for the damaged specimens, or that the behavior of concrete is different than predicted by the model at high values of ε. The values of G_{SAT} of specimens from group C1U were virtually the same as predicted by the model.

The precision of the model was analyzed using the variability of the estimated parameters, that is, G_0 and ε_i. A similar value of G_0 was expected between all specimens because they correspond to a same mixture. The mean G_0 was 18.1 GPa, with a standard deviation of 1.5 GPa and a range of 4.7 GPa. Four of the six specimens had a G_0 close to 18 GPa but extreme values of 20.3 and 15.6 GPa were obtained for specimens C16 and C11, respectively. The difference of almost 5 GPa for specimens from the same batch is substantial. Since the estimate of G_0 was obtained from the difference between G_{SKD} and G_{DRY1}, the variability appears to be an artifact of the accuracy of these measurements.

The value of G_0 affects the predicted G_i and corresponding ε_i. This can be observed in the estimates of ε_i for specimens C12 and C16. For specimen C12, ε_1 is half the estimate of the same parameter from the other two specimens, with an ε_2 after damage close to the undamaged ε_1 of the other two specimens. For specimen C16, the high value of G_0 makes the estimate of ε_1 and ε_2 a large value, such that ε_1 for specimen C16 is higher in value than ε_2 of all specimens from Group C1T after damage to high temperature. Variability is also expected from specimens containing larger fractions of aggregates.

It was expected that the crack density parameters obtained using the partial saturation model would give similar values of ε_i by damage condition. The crack density parameter before damage (ε_1) had a mean of 0.207 with a standard deviation of 0.058 and a range of 0.175. Again, specimens C11, C13, C14 and C15, had similar values close to the mean, but specimens C12 and C16, which had extreme G_0 values, also had extreme values of ε_1. The crack density parameter immediately after high temperature damage (ε_{dmg}) had a mean of

0.272 with a standard deviation of 0.037 and a range of 0.071. For ε_2, the mean for group C1T after damage was 0.248 and for the undamaged group C1U was 0.270, inverse to what would be expected; this difference was not significant since the null hypothesis of a zero difference between these two means could not be rejected after conducting a two-sample t-test. Further, a t-test for means using the changes in ε, that is, $\varepsilon_2 - \varepsilon_1$ also resulted in no significant difference between these mean differences at a 95% confidence level. The value of ε_2 using the PS model was therefore not successful at measuring significant microstructural changes after damage by exposure to high temperature.

Although the model seems to capture the measured shear moduli and describe an increase in crack density with damage by specimen, due to the variability of G_0 and ε_i in the sample, values for these parameters that could characterize the mixture could not be found. The fact that no significant difference was found between the mean crack density parameter of the damaged group compared to the undamaged control group suggests that the partial saturation model assuming $\xi_{OB} = s$ is not a useful technique to estimate average crack density parameters, and estimating ξ_{OB} by other means would be difficult.

A second approach to the application of the O'Connell and Budiansky model was to disregard the crack saturation ratios for partial saturation and only model the difference in shear moduli as either dry or wet, cracked material. This assumption seems reasonable since (1) the difference in elastic moduli obtained in Phase I for non-soaked undamaged concrete (conditions DRY, CND, CND') was small (see section 3.4.2), (2) partial saturation is often

modeled using the Reuss average of the fluid bulk moduli, where a small volumetric gas fraction significantly reduces the equivalent bulk modulus of the mixed fluid, and (3) fluid saturation in isobaric conditions (constant fluid pore pressure) has no effect on the equivalent shear modulus, effectively behaving as dry media (O'Connell and Budiansky 1977).

O'Connell and Budiansky (1977) analyzed the cases of saturated isolated cracks, dry cracks and saturated isobaric cracks in a material. The saturated isolated case corresponds to cracks that are not interconnected and therefore local fluid pressure is developed, the case of dry cracks corresponds to cracks without any fluid, and the saturated isobaric case corresponds to a system of interconnected cracks where the fluid pressure is constant such as porous materials at quasi-static conditions or when fluid pressure distributions are negligible. Therefore, the assumption of non-soaked concrete to behave as either dry cracked material or a cracked material saturated with an equivalent air-water fluid seems valid. Modeling soaked concrete as possessing water-saturated isolated cracks implies that local fluid pressure is developed with no water flow, which might be a reasonable approximation when measured at high frequencies and very low strains, consistent with an undrained/unrelaxed condition.

The O'Connell and Budiansky models for dry and saturated (DS) cracked media were applied to the measured shear modulus of soaked and non-soaked concrete by assuming that the shear modulus for the dry case is obtained by setting $\xi_{OB} = 0$ in Eq. 5.19, and the shear modulus of the saturated isolated case is obtained by setting and $\xi_{OB} = 1$ in Eq. 5.20. The shear modulus as a function of ε for the isolated isobaric case describes the same curve as for the dry case, but bulk modulus (K) and Young's modulus (E) behave differently because of the different effects of the isobaric fluid on the cracked Poisson's ratio of the

material (see O'Connell and Budiansky 1977). The results of applying this model to each specimen, assuming G_{SKD} as saturated isolated cracked media and G_{DRY1}, G_{DMG} and G_{DRY2} as dry or saturated isobaric cracked media, is given in Table 5.4. Figure 5.3 shows the values obtained from this model based on the measurements of G_d, where values of G_{SAT} are shown to compare to values predicted by the model.

Table 5.4 - Results of the O'Connell & Budiansky's Dry and Saturated Model Applied on Wet and Dry Concrete

Group	**Specimen**	υ_0		**Crack Density Parameter**			$\Delta\varepsilon$	
				ε_1	ε_{dmg}	ε_2	$\varepsilon_{dmg}-\varepsilon_1$	$\varepsilon_2-\varepsilon_1$
C1T	C11	0.299	16.5	0.085	0.219	0.163	0.134	0.078
	C12	0.323	14.7	0.040	0.221	0.158	0.181	0.118
	C13	0.299	16.2	0.115	0.279	0.170	0.164	0.055
C1U	C14	0.308	15.6	0.091	—	0.120	—	0.029
	C15	0.316	16.3	0.107	—	0.147	—	0.040
	C16	0.301	17.2	0.126	—	0.163	—	0.037

"T" is high temperature treated group, "U" is untreated group, υ_0 is Poisson's ratio of the uncracked solid, "ε_1" is the crack density parameter before damage using shear moduli at conditions SKD and DRY1, "ε_{dmg}" is the crack density parameter after exposure to 300 °C, "ε_2" is the crack density parameter after vacuum saturation using shear moduli at conditions SAT and DRY2. "SKD"= at least 3 days submerged in water, or moist room at 100% RH; "DRY*n*"= Oven dried at 40±2 °C (RH = 25±5 %) for 2 days then sealed and tested within 18 hours; "DMG"= Air dried specimens at 23±2 °C exposed to 300 ± 20 °C for 60±2 min, then sealed and tested at 23±2 °C within 24 hours; "SAT"= water saturated specimens in accordance with ASTM C 1202 (2009)

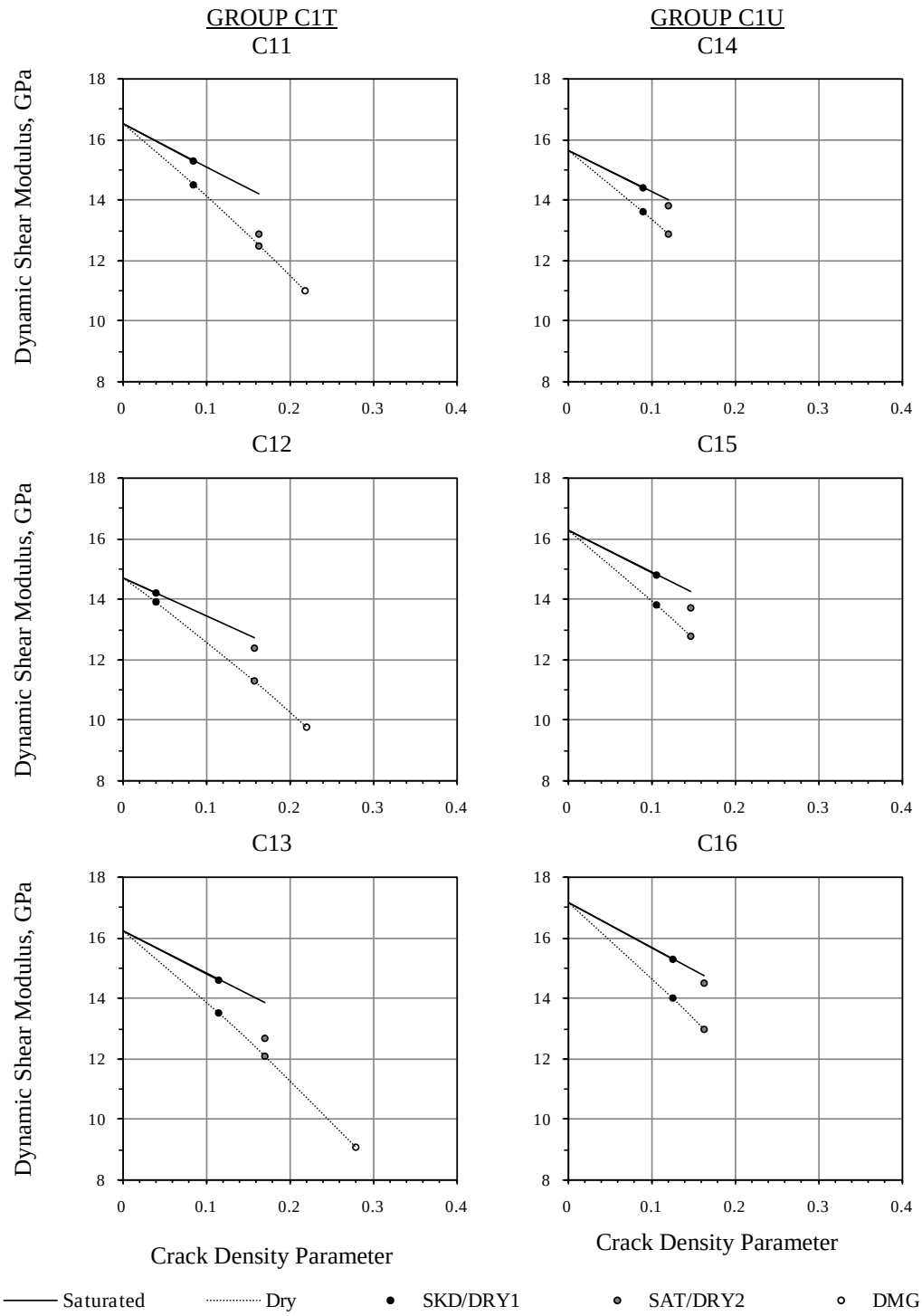

Figure 5.3 - Application of O'Connell and Budiansky Dry and Saturated Model for Wet and Dry 25 mm Thick Disk Specimens from Control Mixture C (1 Mpsi = 6.895 GPa)

The equivalent G_0 had a mean of 16.1 GPa, a standard deviation of 0.9 GPa and a range of 2.5 GPa. The changes in ε describe the expected behavior of an increase in value after damage to high temperature exposure. The effect of autogenous healing is more pronounced as well on damaged specimens, and an increase in ε after a drying and wetting cycle is observed with vacuum drying for saturation of specimens from Group C1U.

The undamaged crack density, ε_1, had a mean of 0.094 with a standard deviation of 0.030, and a range of 0.086; although the coefficient of variation is high (about 32%), it is an artifact of the low value for the mean. The cracked density after high temperature exposure, ε_{dmg}, had a mean of 0.240 with a standard deviation of 0.034, and a range of 0.060. Comparison of these statistics to those from the PS model, including coefficients of variation, is provided in section 5.4.2.3.

For ε_2, after vacuum saturation, the mean ε_2 of Group C1T was 0.164, higher than the mean ε_2 of group C1U which was 0.143. A t-test for means between these two groups revealed that the null hypothesis of a zero mean difference could not be rejected at a 95% confidence level but degrees of freedom are limited (DOF = 4). Further analysis using changes in ε with damage were more promising. The mean increase in crack density ($\varepsilon_2 - \varepsilon_1$) of Group C1T was 0.084, whereas the increase in crack density of control Group C1U was 0.035, changes that were significantly different at a 95% confidence level. The increase in ε immediately after exposure to 300 °C and before healing ($\varepsilon_{dmg} - \varepsilon_1$) was 0.160, with a standard deviation of 0.024 and a range of 0.047.

Means, standard deviations, ranges, and coefficients of variations for G_0, and different crack density parameters for the partial saturation (PS) model and the dry and saturated (DS) model are given in Table 5.5. A lower standard deviation for all properties is observed for the DS model, compared to the PS model. Large coefficients of variation were observed for both, but larger coefficients of variation in the DS model are because of lower values of the means. The DS model captures a larger increase in ε with high temperature damage, and higher values of ε_2 for the damaged group than the undamaged group (as expected), and although not statistically significantly different in both models, a paired analysis of $\varepsilon_2 - \varepsilon_1$ for exposed and non-exposed groups did have a significant difference for the DS model only. The DS model could be applied to determine values for crack density parameter that were consistent with observations in changes in G_d with moisture content, high temperature damage, and healing, and was therefore preferred as the method to determine the crack density parameter. Physically, the DS model for dry concrete is equivalent to a cracked media with interconnected cracks saturated with a fluid (air) at constant pressure. Also, if the fluid is modeled using the Reuss average given in Eq. 5.1, the large volumetric proportion of gas provides negligible changes in the equivalent fluid bulk moduli.

Table 5.5 - Comparison of Statistics of Two Modeling Approaches of the O'Connell and Budiansky Model Applied to Specimens of a Conventional Concrete Mixture

Property	Partial Saturation[1]				Dry and Saturated[2]			
	mean	std. dev.	range	c.v.	mean	std. dev.	range	c.v.
G_0, *GPa*	18.1	1.5	4.7	8.3%	16.1	0.9	2.5	5.6%
ε_1	0.207	0.058	0.175	28.0%	0.094	0.030	0.086	31.9%
ε_{dmg}	0.272	0.037	0.071	13.6%	0.240	0.034	0.060	14.2%
$\varepsilon_{2,C1T}$	0.248	0.022	0.041	8.9%	0.164	0.006	0.012	3.7%
$\varepsilon_{2,C1U}$	0.270	0.043	0.083	15.9%	0.143	0.022	0.043	15.4%
$\varepsilon_{dmg} - \varepsilon_1$	+0.093	0.040	0.077	43.0%	+0.160	0.024	0.047	15.0%
$(\varepsilon_2 - \varepsilon_1)_{C1T}$	+0.068	0.045	0.088	66.2%	+0.084	0.032	0.063	38.1%
$(\varepsilon_2 - \varepsilon_1)_{C1U}$	+0.036	0.007	0.013	19.4%	+0.035	0.006	0.011	17.1%

"T" is high temperature treated group, "U" is untreated group, G_0 is shear modulus of the uncracked solid, "ε_1" is the crack density parameter before damage using shear moduli at conditions SKD and DRY1, "ε_{dmg}" is the crack density parameter after exposure to 300 °C, "ε_2" is the crack density parameter after vacuum saturation using shear moduli at conditions SAT and DRY2. "SKD"= at least 3 days submerged in water, or moist room at 100% RH; "DRY*n*"= Oven dried at 40±2 °C (RH = 25±5 %) for 2 days then sealed and tested within 18 hours; "DMG"= Air dried specimens at 23±2 °C exposed to 300 ± 20 °C for 60±2 min, then sealed and tested at 23±2 °C within 24 hours; "SAT"= water saturated specimens in accordance with ASTM C 1202 (2009). "std.dev" is the sample standard deviation, "c.v." is the coefficient of variation. [1]: considers water volume fractions as crack saturation ratios; [2]: considers shear modulus of dry concrete as media with cracks either empty or saturated with a fluid at constant pressure, and wet concrete as cracked media with saturated isolated cracks.

5.4.3 Model Implications and Limitations

In section 5.4.2, it was determined that the O'Connell and Budiansky (1974; 1977) dry and saturated (DS) cracked media model could be applied to the dynamic shear modulus of dry and wet concrete to determine values for crack density parameter that were consistent with observations in changes in G_d with moisture content, high temperature damage, and healing. This model assumes that G_d of wet concrete at high frequency vibration behaves in undrained/unrelaxed conditions with no pore fluid pressure diffusion, producing a stiffening

effect (as observed in Phase I) and can be modeled as isolated cracks saturated with water. Further, it assumes that G_d of dry concrete behaves as either media with empty cracks, or media saturated with a fluid at constant pressure. Considering that air inside a concrete specimen in a dry condition would allow for gas compressibility, compared to an almost negligible compressibility of water, it is expected that pore air in the specimen would create an isobaric condition. Values of crack density parameters obtained by the DS model therefore allow quantifying the amount voids and microcracks as an equivalent density measure of ellipsoidal cracks in a manner consistent with other observations.

An increase in the value of the crack density parameter is expected from an increase in either the number of cracks (N), an increase in crack area (A), a decrease in crack perimeter (P) (which is unlikely except in healing), or a combined effect (see Eq. 5.11). From the results by Carrasquillo, Slate and Nilson (1981), an extension of existing microcracks is expected with damage, rather than the creation of new cracks, therefore, assuming N remains approximately constant, an increase in ε is a measure of the increase in $\sum A_c^2 / P_c$. Since A_c and P_c are expected to increase in value with damage, at least on average, the increase in ε indicates that the overall increase in squared crack area is higher than the overall increase in crack perimeter. Similarly, a reduction in ε, such as observed with autogenous healing, would be because of a decrease in $\sum A_c^2 / P_c$ rather than a decrease in N, assuming that the unhydrated cement was exposed after extension of existing microcracks.

O'Connell and Budiansky (1974) provide expressions that relate ε with crack trace mean lengths and densities, from counting line segments formed by intersections of cracks with a plane section. The scenarios considered are uniform sized cracks of convex shape and

elliptical cracks of various sizes but uniform ellipticity. Assuming uniform size and any convex shape, as expected to be the case for transition zone cracks surrounding uniform sized aggregates, ε is related to the mean crack trace length ($\bar{L}$) and crack trace density (M), measured as number of crack line segments per unit area, according to the relation given in Eq. 5.24 (Kenall and Moran 1963).

$$\varepsilon = \frac{8}{\pi^3} M \left(\bar{L}\right)^2 \tag{5.24}$$

Measurements of ε before and after damage on the same specimen therefore allows estimating changes in the equivalent crack trace lengths, commonly found with two-dimensional microscopic investigations and image analysis (see, for example, Carrasquillo *et al.* 1981; Mitchell and Leming 1998; Ringot and Bascoul 2001). By defining $\varepsilon_a = \left(8/\pi^3\right) M_a \left(\bar{L}_a\right)^2$ and $\varepsilon_b = \left(8/\pi^3\right) M_b \left(\bar{L}_b\right)^2$ as the crack density parameters before and after microstructural changes respectively, then the ratio between these two measurements is the relation given by Eq. 5.25. If the microstructural change is dominated by the extension of cracks, rather than the creation of new cracks as observed by Carrasquillo *et al.* (1981), then values for M_a and M_b are approximately the same, and consequently $\varepsilon_a/\varepsilon_b \approx \left(\bar{L}_a/\bar{L}_b\right)^2$. The $\varepsilon_a/\varepsilon_b$ ratio can therefore be used to estimate the proportional changes in mean crack trace lengths, to relate to results from two-dimensional microstructural investigations. Further research in crack changes due to damage and healing in concrete are strongly encouraged to compare to the nondestructive measurements of ε.

$$\frac{\varepsilon_a}{\varepsilon_b} = \frac{M_a}{M_b}\left(\frac{\bar{L}_a}{\bar{L}_b}\right)^2 \tag{5.25}$$

Table 5.6 presents the estimates of mean crack trace length proportional increase, measured as the square root of the $\varepsilon_a/\varepsilon_b$ ratio, obtained for the specimens of the conventional concrete mixture using the selected dry and saturated model. Values of crack density parameter are repeated for reference. The estimates of proportional increases in crack trace lengths ($\bar{L}$) are very consistent, except for specimen C12, which had a very low estimate of ε_1. Excluding specimen C12, an increase in $\bar{L}$ of about 60% was estimated from the high temperature damage, and the unrecoverable $\bar{L}$ after healing was between 20% and 40% of the original mean crack trace length. For the healing process, measurement of $\sqrt{\varepsilon_2/\varepsilon_{dmg}}$ provided an estimate of the reduction in $\bar{L}$ of the extended (high temperature damaged) cracks with healing, resulting in recoveries of around 80% for all three specimens. For the control group, the vacuum drying followed by saturation produced an increase in estimated $\bar{L}$ of about 15%, with minor variability between the three specimens. Quantitative estimates of mean increases in crack trace length, to the best of the author's knowledge, have not been previously reported for concrete. Further research with microscopic investigations confirming the adequacy of estimating these proportional changes in $\bar{L}$ is recommended.

Quantifying the changes in crack density parameter with damage would also be useful in evaluating the amount of degradation in the material. Once the system can be defined by measuring G_{wet}, G_{dry} and estimating υ_0, a crack density parameter can be determined. If the expected increase in ε by type of exposure can be established, then the degradation in G_d can be predicted for a given exposure. Applying this analytical procedure could therefore be

a powerful forensic tool since it provides an estimate of previous or future condition of the material depending on the amount of damage (or healing treatment) provided.

Table 5.6 - Estimates of Increases in Mean Crack Trace Lengths from Crack Density Parameter Measurements for Specimens of a Conventional Concrete Mixture

Group	Specimen	Crack Density Parameters			Crack Trace Length Ratio Estimates		
		ε_1	ε_{dmg}	ε_2	$\sqrt{\varepsilon_{dmg}/\varepsilon_1}$ [a]	$\sqrt{\varepsilon_2/\varepsilon_1}$ [b]	$\sqrt{\varepsilon_2/\varepsilon_{dmg}}$ [c]
C1T	C11	0.085	0.219	0.163	1.61	1.38	0.86
	C12	0.040	0.221	0.158	2.35	1.99	0.85
	C13	0.115	0.279	0.170	1.56	1.22	0.78
C1U	C14	0.091	—	0.120	—	1.15	—
	C15	0.107	—	0.147	—	1.17	—
	C16	0.126	—	0.163	—	1.14	—

"T" is high temperature treated group, "U" is untreated group, υ_0 is Poisson's ratio of the uncracked solid, "ε_1" is the crack density parameter before damage using shear moduli at conditions SKD and DRY1, "ε_{dmg}" is the crack density parameter after exposure to 300 °C, "ε_2" is the crack density parameter after vacuum saturation using shear moduli at conditions SAT and DRY2. "SKD"= at least 3 days submerged in water, or moist room at 100% RH; "DRY*n*"= Oven dried at 40±2 °C (RH = 25±5 %) for 2 days then sealed and tested within 18 hours; "DMG"= Air dried specimens at 23±2 °C exposed to 300 ± 20 °C for 60±2 min, then sealed and tested at 23±2 °C within 24 hours; "SAT"= water saturated specimens in accordance with ASTM C 1202 (2009). "—": data not taken (no exposure). [a]: estimate of L_{dmg}/L_1; b: estimate of L_2/L_1; c: estimate of L_2/L_{dmg}

A limitation of the model is that it requires that $G_{wet} > G_{dry}$ mathematically and this ΔG might be affected by the degree of damage (i.e.: porous material without water interaction where $G_{wet} \simeq G_{dry}$), by measurement variations, or both. This factor may be contributing to the difference between measured and predicted value for G_{SAT} of specimens C11, C13 and C15, where G_{SAT} was lower than predicted by the model, and close in value to G_{DRY2} (see Figure 5.3). If G_{SAT} and G_{DRY2} are used to evaluate G_0 for these disks, lower values of G_0

are obtained, and therefore different values for ε. Modeling can be corrected because G_{SKD} would have to be plotted over the saturated curve.

5.5 Model Application to Results from Phase I

The mechanical properties of specimens from Phase I (see section 4.3) were analyzed by applying the analytical technique developed in section 5.4, using the O'Connell and Budiansky model considering only data for dry or wet specimens (dry/saturated model). Table 5.7 shows the measured G_d and the model output for G_0 and ε using two values of υ_0. Values of G_d were obtained assuming a dynamic Poisson's ratio (υ_d) of 1/6, since this value was assumed to determine Ω_0 (see Eq. 5.3 and discussion in section 3.4.2). Since the measurements of υ_d for specimens from mixture C were closer to 0.3 than to 1/6, these two values of υ_0 were used to analyze the sensitivity of the model to variability in υ_0 in the estimates of G_0 and ε. Dynamic Poisson's ratios (υ_d) closer to 0.25 are commonly reported (Philleo 1994; Weiss 2006), therefore the values obtained using υ_0 of 1/6 and 0.3 provide a low and high range for comparison. The large υ_d measured in specimens from mixture C might be an artifact of the difference in frequency at which the stress wave velocities were measured, since the transducers for pulse velocity operate at 54 kHz and the standing shear waves during disk resonance have frequencies closer to 10 kHz, or due to geometrical limitations for the pulse wave (see discussion in section 5.4.1).

Table 5.7 - Results of the O'Connell and Budiansky Model for Dry and Saturated Specimens of Two Thicknesses, Two Mixtures, and Two Values of Uncracked Solid Poisson's Ratio

Group	Specimen	Dynamic Shear Modulus			υ_0 = 1/6					υ_0 = 0.3				
								Δ	$\sqrt{\frac{\varepsilon_{dmg}}{\varepsilon_1}}$				**Δ**	$\sqrt{\frac{\varepsilon_{dmg}}{\varepsilon_1}}$
		GPa	**GPa**	**GPa**	**GPa**					**GPa**				
L1T	L11	9.7	8.5	*6.9*	11.4	0.156	*0.238*	*0.082*	*1.24*	11.3	0.167	*0.252*	*0.085*	*1.23*
	L12	9.1	7.9	*6.2*	10.8	0.164	*0.256*	*0.092*	*1.25*	10.7	0.175	*0.269*	*0.094*	*1.24*
	L13	9.5	8.1	*6.1*	11.4	0.178	*0.279*	*0.101*	*1.25*	11.3	0.189	*0.292*	*0.103*	*1.24*
L1U	L14	9.5	8.3	—	11.2	0.159	—	—	—	11.1	0.170	—	—	—
	L15	9.8	8.5	—	11.6	0.165	—	—	—	11.5	0.176	—	—	—
	L16	9.4	7.7	—	11.7	0.207	—	—	—	11.5	0.218	—	—	—
N1T	N11	12.1	10.7	*8.2*	14.1	0.148	*0.252*	*0.104*	*1.30*	14.0	0.159	*0.266*	*0.107*	*1.29*
	N12	12.1	10.8	*8.9*	13.9	0.140	*0.220*	*0.080*	*1.25*	13.9	0.151	*0.234*	*0.083*	*1.24*
	N13	12.6	10.8	*8.6*	15.1	0.174	*0.259*	*0.085*	*1.22*	15.0	0.185	*0.272*	*0.087*	*1.21*
N1U	N14	12.0	10.6	—	14.0	0.149	—	—	—	13.9	0.160	—	—	—
	N15	12.4	10.6	—	14.9	0.176	—	—	—	14.8	0.187	—	—	—
	N16	11.1	9.9	—	12.8	0.140	—	—	—	12.8	0.152	—	—	—
L2T	L21	10.5	9.2	*5.1*	12.3	0.156	*0.346*	*0.190*	*1.49*	12.3	0.167	*0.358*	*0.191*	*1.46*
	L22	10.5	9.2	*5.8*	12.3	0.156	*0.315*	*0.159*	*1.42*	12.3	0.167	*0.328*	*0.161*	*1.40*
	L23	10.3	9.2	*5.4*	11.9	0.139	*0.324*	*0.185*	*1.53*	11.8	0.150	*0.336*	*0.186*	*1.50*
L2U	L24	10.8	9.4	—	12.7	0.162	—	—	—	12.7	0.173	—	—	—
	L25	11.4	9.5	—	14.0	0.195	—	—	—	13.8	0.206	—	—	—
	L26	10.3	8.7	—	12.5	0.185	—	—	—	12.4	0.196	—	—	—
N2T	N21	12.3	10.6	*7.3*	14.6	0.170	*0.299*	*0.129*	*1.33*	14.6	0.181	*0.312*	*0.131*	*1.31*
	N22	12.6	10.9	*7.9*	15.0	0.167	*0.283*	*0.116*	*1.30*	14.9	0.178	*0.296*	*0.118*	*1.29*
	N23	12.7	11.0	*7.9*	15.1	0.166	*0.285*	*0.119*	*1.31*	15.0	0.177	*0.298*	*0.121*	*1.30*
N2U	N24	13.6	11.6	—	16.3	0.178	—	—	—	16.2	0.189	—	—	—
	N25	13.2	11.0	—	16.2	0.195	—	—	—	16.0	0.206	—	—	—
	N26	13.4	10.8	—	16.8	0.218	—	—	—	16.6	0.228	—	—	—

"L": low strength mixture; "N": moderate strength mixture. *Values in italic* are conditions after damage; "SKD": at least 3 days submerged in water, or moist room at 100% RH; "DRY": 1 day at 40±2 °C, then at least 1 day sealed at 23±2 °C; "DMG"= air dried specimens at 23±2 °C exposed to 300 ± 20 °C (25 mm disks for 30±2 min and 50 mm disks for 60±2 min) , then sealed and tested at 23±2 °C within 24 hours ; "T" is high temperature treated group, "U" is untreated group, "υ_0" is Poisson's ratio of the uncracked solid, "G_0" is shear modulus of the uncracked solid, "ε_1" is the crack density parameter before damage; "ε_{dmg}" is crack density parameter after damage, $\Delta\varepsilon = \varepsilon_{dmg} - \varepsilon_1$; "—" is data not taken (no exposure).

An increase in the value of υ_0 from 1/6 to 0.3 increased the individual values of ε between +0.010 and +0.014. Considering that υ_0 can only be estimated, either by assuming a reasonable value or obtaining a mean of measured wet and dry Poisson's ratios as discussed above, crack density parameters for each specimen were accurate within ±0.01 from variability of υ_0 alone. A higher accuracy is achieved for changes in crack density parameter ($\Delta\varepsilon$), however, since the increase in υ_0 from 1/6 to 0.3 created individual increases in $\Delta\varepsilon$ after high temperature damage between +0.001 and +0.003. Measurements of $\Delta\varepsilon$ by specimen were therefore accurate within ±0.005 from variability of υ_0 alone. It was therefore concluded that due to the limitation of estimating a precise value of υ_0 in this investigation, the individual values of ε and $\Delta\varepsilon$ could be reported to the nearest 0.01 with an accuracy of ±0.01. For the value of G_0, an increase in υ_0 from 1/6 to 0.3 produced a decrease in G_0 of up to -0.2 GPa, therefore an accuracy of ±0.1 GPa was reasonable from the uncertainty in the estimated value of υ_0.

Estimates of increases in mean crack trace length ($\bar{L}$) with high temperature damage were very consistent, with increases between 20% to 25% for group L1T, between 20% and 30% for group C1T, between 40% and 55% for group L2T, and about 30% for group N2T. Accuracy to nearest 2½ significant figures was found for these estimates from the uncertainty in the estimated value of υ_0; 2½ significant figures are consistent with reporting requirements of dynamic elastic moduli of concrete (ASTM-C215 2008). These values appear to be in reasonable agreement with those obtained from specimens of mixture C.

Figure 5.4 shows ε and G_d by mixture and specimen thickness obtained after applying the model using υ_0 = 1/6. For mixture L, although the estimates of G_0 are higher for the 50 mm (2 in.) thick disks than the 25 mm (1 in.) thick disks (see section 4.3), the mean ε before damage (ε_1) were statistically the same for both disk thicknesses. The mean ε was estimated as 0.051 ± 0.015 for the 25 mm (1 in.) groups and 0.056 ±0.017 for the 50 mm (2 in.) groups, using 95% confidence levels. This statement was not true for mixture N, where the mean ε_1 obtained using 25 mm (1 in.) thick disks was significantly different from the ε_1 obtained from the 50 mm (2 in.) thick disks (a mean of 0.036 ±0.013 for the 25 mm groups and 0.052 ±0.016 for the 50 mm groups). The mean increases in ε for the exposed groups were 0.09 ±0.02 for Group L1T, 0.09±0.03 for Group N1T, 0.18 ±0.04 for Group L2T and 0.12±0.02 for Group N2T. The analysis using the O'Connell and Budiansky model considering only dry or saturated conditions found a larger increase in ε with damage for the 50 mm thick disks than for the 25 mm thick disks per mixture, consistent with a longer exposure to a 300 °C temperature. The 30 minute exposure had similar damaging effect on the 25 mm (1 in.) groups, and the 60 min exposure had a higher damaging effect on Group L2T than on Group N2T.

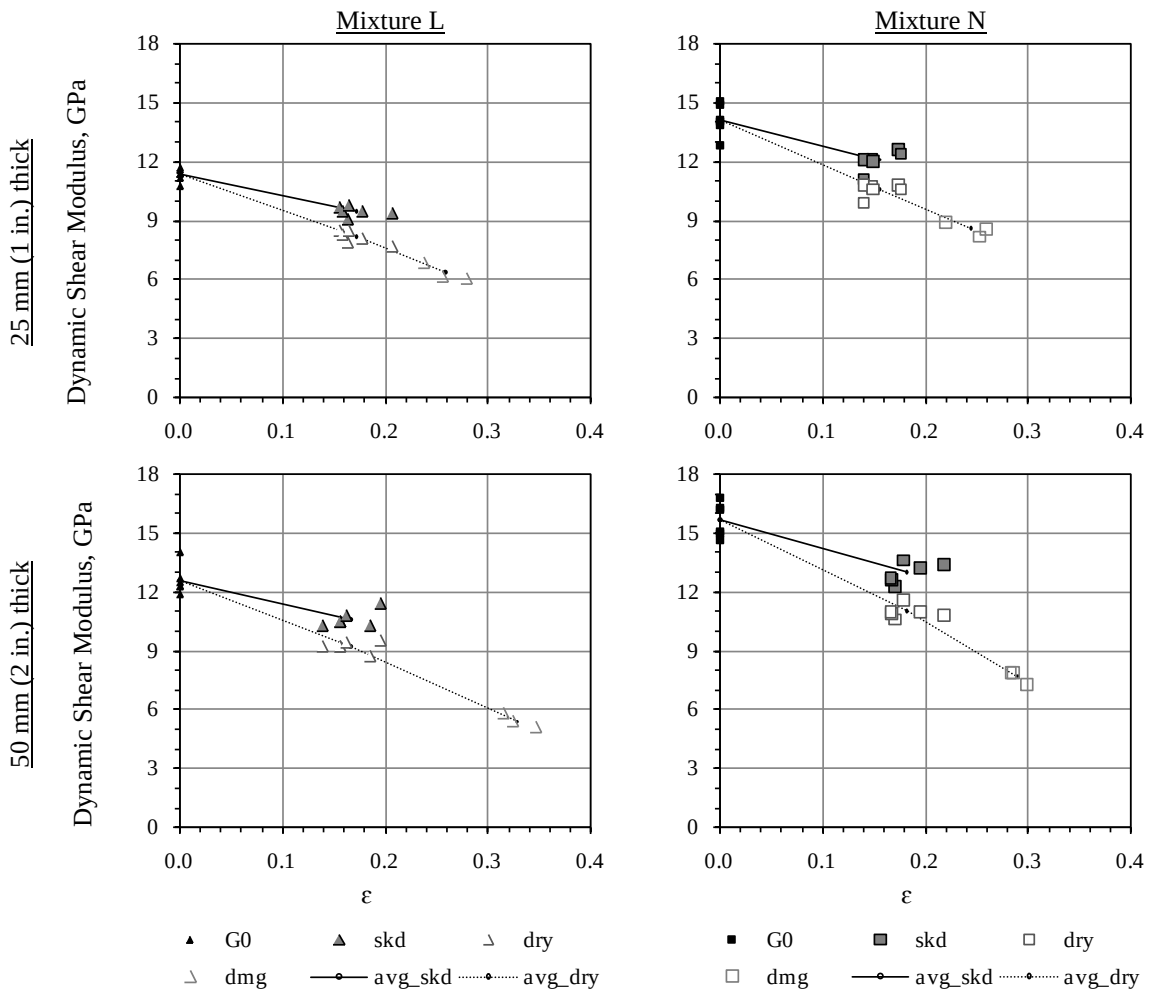

Figure 5.4 - Output for the Saturated/dry O'Connell and Budiansky Model for a Low Strength and a Nominal Strength Mixture and Two Specimen Thicknesses

5.6 Summary

This chapter presented the search for an applicable model that could use the difference in measured wet and dry dynamic shear moduli to characterize the microstructure of concrete. The effective moduli of dry and saturated cracked media, using the relations developed by O'Connell and Budiansky (1974; 1977) provided a way to obtain a value for the crack density parameter (ε). Tests using dry or saturated media provided more reliable estimates of ε than using partial saturation. A limitation of the experimental method is that obtaining an estimate of Poisson's ratio for the equivalent uncracked solid (υ_0) is not possible, but the sensitivity of ε was of ±0.01 for values of υ_0 between 1/6 to 0.3 (typical for concrete). Changes in crack density parameter ($\Delta\varepsilon$) were practically insensitive to the value of υ_0, however. Ratios of ε before and after damage allow quantifying estimates of average increase of crack trace lengths, which have not been previously reported for concrete. The analytical tool was successfully applied on three different conventional concrete mixtures, and was able to characterize the microstructure by obtaining values of the crack density parameter of concrete disks before and after high temperature damage and quantify recovery in ε by autogenous healing after damage.

CHAPTER 6.

CHANGES IN DURABILITY PROPERTIES WITH HIGH TEMPERATURE DAMAGE OF CEMENTITIOUS MATERIALS WITH ENHANCED SUSTAINABILITY (PHASE III)

6.1 Introduction

In this chapter, the results of an experimental program on changes in mechanical properties, fluid penetrability, and microstructural characteristics due to high temperature damage of three sustainable cementitious materials and a conventional concrete mixture as the control are presented and analyzed. Microstructural changes were quantitatively analyzed using changes in the dynamic shear modulus, ultrasonic pulse velocity, crack density parameter, air permeability index, and rates of absorption of water. These characteristics were used to compare the response of cementitious materials with enhanced sustainability to conventional concrete for possible use as a screening tool.

Changes in mechanical properties with damage were characterized by measuring the dynamic shear modulus (G_d). Differences in G_d with water content, before and after high temperature damage, were used to calculate crack density parameters using the analytical technique explained in section 5.4. The changes in fluid penetrability properties were analyzed, and the relationships between all measured properties, and changes in these properties, were investigated. Conclusions and recommendations are given on the nature of the enhanced sustainability materials and the utility of the non-destructive microstructural characterization technique with these materials.

Phase II and Phase III occurred simultaneously, therefore adjustments were made during the experimental plan as progress in both Phases were achieved. The experimental plan originally consisted of testing specimens from mixtures C, F and M in a moisture conditioning sequence similar to Phase I, that is, SKD, CND, DRY1, DMG, CND', and, at the end, test the specimens in a saturated state (condition SAT) to avoid possible microstructural damage from vacuum drying, a damaging factor that was later confirmed (see section 5.4.2.2). Changes in properties were measured on 25 mm (1 in.) thick disk specimens, and 50 mm (2 in.) thick specimens were used as companion specimens to characterize undamaged conditions only. Specimens from Mixture G were obtained at a later time, and progress in Phase II allowed an accelerated testing plan involving selected moisture conditions. Specimens of mixture F were re-tested along with specimens from mixture G since there were concerns on the validity of G_d measurements obtained at early ages used for the determination of the crack density parameter. Measurements for the re-testing of specimens from mixture F are labeled with a "*" in the tables and figures of this chapter. After measuring properties at saturated conditions (SAT) for the set of groups from mixtures C, F, and M, the test specimens were soaked in alcohol to minimize healing and, since the bulk moduli of alcohol and water are slightly different, to evaluate the possible benefits and applicability of the soft-fluid saturation model, described in section 5.3.2.6; these values are provided in Appendix D.

A final factor that significantly affected the results in this investigation was that autogenous healing was not detected until late in the investigation, complicating analysis and model development, since the increase in G_d of damaged specimens from dry to wet

conditions were originally thought to be due to water content alone. Evidence of autogenous healing was provided by specimens from Mixture M, which had no change in G_d with water presence when undamaged, but after damage and soaking, the value of G_d increased to a value similar to that undamaged. Further testing after air drying the specimens and testing in desorption (condition DRY2), confirmed the autogenous healing effect on the four mixtures.

6.2 Phase III Results

6.2.1 Changes in Mechanical Properties

Values of density (ρ) and ultrasonic pulse velocity (v_p) are given in Table 6.1 and Table 6.2, respectively; these measurements were used in determining G_d. Ultrasonic pulse velocity was measured to estimate the dynamic Poisson's ratio (υ_d), and also is indicative of changes in elastic properties, although there are concerns with its precision due to the size and geometry of the specimens (see discussion in section 5.4.1). Figure 6.1 shows the relationship between density and v_p for each mixture.

Table 6.1 - Density of Specimens from a Control and Three Sustainability Enhanced Cementitious Materials at Different Moisture Conditions and Before and After High Temperature Damage

Group	Spe-cimen	Volume cm^3	Density, kg/m^3										
			SKD	**CND**	**DRY1**	**DMG**	**CND'**	**SKD'**	**SAT**	**DRY2**	**DMG***	**SAT***	**DRY2***
C1T	C11	211.3	2360	2343	2302	*2203*	*2229*	*2347*	*2363*	*2262*	—	—	—
	C12	214.0	2370	2356	2315	*2210*	*2239*	*2358*	*2374*	*2270*	—	—	—
	C13	203.6	2358	2340	2289	*2194*	*2226*	*2346*	*2362*	*2253*	—	—	—
C1U	C14	203.5	2367	2346	2304	—	2299	2356	2375	2296	—	—	—
	C15	198.8	2360	2334	2292	—	2288	2351	2369	2285	—	—	—
	C16	206.2	2377	2357	2313	—	2309	2370	2386	2306	—	—	—
F1T	F11	205.4	2299	2285	2236	*2128*	*2152*	*2283*	*2298*	*2180*	*2137*	*2301*	*2183*
	F12	207.7	2324	2308	2266	*2155*	*2179*	*2310*	*2324*	*2210*	*2170*	*2325*	*2210*
	F13	210.1	2301	2285	2241	*2132*	*2156*	*2288*	*2303*	*2190*	*2151*	*2305*	*2192*
F1U	F14	221.7	2317	2299	2256	—	2247	2307	2321	2226	—	2322	2227
	F15	199.3	2288	2274	2227	—	2217	2278	2293	2200	—	2296	2200
	F16	212.4	2316	2296	2255	—	2247	2304	2317	2229	—	2320	2229
M1T	M11	205.2	2106	2086	2048	*1938*	*1944*	*2108*	*2161*	*2031*	—	—	—
	M12	206.0	2084	2062	2024	*1912*	*1916*	*2085*	*2137*	*2008*	—	—	—
	M13	221.3	2119	2094	2061	*1978*	*1975*	*2120*	*2170*	*2040*	—	—	—
M1U	M14	203.4	2120	2098	2061	—	2060	2122	2171	2048	—	—	—
	M15	203.1	2105	2087	2046	—	2044	2107	2154	2032	—	—	—
	M16	230.2	2115	2094	2060	—	2058	2119	2167	2046	—	—	—
G1T	G11	224.1	2321	—	2270	*2198*	—	—	*2358*	*2258*	—	—	—
	G12	213.7	2315	—	2266	*2208*	—	—	*2351*	*2253*	—	—	—
	G13	201.0	2355	—	2306	*2239*	—	—	*2391*	*2294*	—	—	—
G1U	G14	203.1	2362	—	2312	—	—	—	2399	2315	—	—	—
	G15	220.8	2319	—	2271	—	—	—	2362	2273	—	—	—
	G16	214.6	2335	—	2285	—	—	—	2374	2289	—	—	—

"C" is conventional concrete, "F" is very high fly ash concrete, "M" is Grancrete™ mortar, "G" is Grancrete™ concrete, "*" indicates specimens that were re-tested at a later age. "T" is high temperature exposure (300°C) group, "U" is unexposed/undamaged group. "SKD" and "SKD'": in water for 1 day with one face exposed to ambient air, then at least 1 day submerged in water or moist room at 100 % RH and tested immediately after removal from water; "CND" and "CND'": 3 days at 50±2 °C and 80% RH, then at least 1 day sealed at 23±2 °C; "DRY1" and "DRY2": oven dried at 40±2 °C (RH = 25±5 %) for 2 days then sealed and tested within 18 hours; "DMG": air dried specimens at 23 ± 2 °C exposed to 300 ± 20 °C for 60 ± 1 min, then sealed and tested at 23 ± 2 °C within 24 hours; "SAT": oven dried at 40 ± 2 °C for 2 days, then vacuum saturated in general accordance with ASTM Standard C1202(2009); "—" is data not taken. Conversion factor: 1 pcf = 16.02 kg/m^3

Table 6.2 - Ultrasonic Pulse Velocity of Specimens from a Control and Three Sustainability Enhanced Cementitious Materials at Different Moisture Conditions and Before and After High Temperature Damage

Group	Spe-cimen	Ultrasonic Pulse Velocity, km/s										
		SKD	**CND**	**DRY1**	**DMG**	**CND'**	**SKD'**	**SAT**	**DRY2**	**DMG***	**SAT***	**DRY2***
C1T	C11	4.77	4.57	4.51	*4.01*	*4.15*	*4.38*	*4.64*	*4.34*	—	—	—
	C12	4.81	4.62	4.49	*4.15*	*4.17*	*4.27*	*4.67*	*4.49*	—	—	—
	C13	4.70	4.65	4.42	*4.01*	*3.98*	*4.29*	*4.39*	*4.33*	—	—	—
C1U	C14	4.73	4.76	4.47	—	4.51	4.55	4.64	4.54	—	—	—
	C15	4.79	4.67	4.54	—	4.58	4.54	4.85	4.60	—	—	—
	C16	4.74	4.61	4.49	—	4.42	4.56	4.62	4.58	—	—	—
F1T	F11	4.29	4.38	3.75	*3.36*	*3.06*	*3.70*	*4.00*	*3.62*	*3.36*	*4.05*	*3.65*
	F12	4.38	4.37	4.15	*3.13*	*3.17*	*3.74*	*4.02*	*3.58*	*3.37*	*4.11*	*3.65*
	F13	4.27	4.26	3.72	*3.04*	*3.17*	*3.67*	*3.81*	*3.61*	*3.34*	*4.07*	*3.70*
F1U	F14	4.58	4.41	4.16	—	3.98	4.14	4.19	3.94	—	4.33	4.16
	F15	4.37	4.32	4.13	—	4.02	4.10	4.09	4.01	—	4.31	4.14
	F16	4.38	4.32	4.16	—	3.98	3.92	3.99	4.08	—	4.31	4.14
M1T	M11	3.70	3.77	3.78	*2.98*	*3.28*	*3.70*	*3.94*	*3.89*	—	—	—
	M12	3.70	3.76	3.80	*3.15*	*3.26*	*3.70*	*3.95*	*3.88*	—	—	—
	M13	3.76	3.79	3.82	*3.18*	*3.40*	*3.73*	*3.95*	*3.84*	—	—	—
M1U	M14	3.76	3.78	3.81	—	3.82	3.83	3.95	3.88	—	—	—
	M15	3.77	3.79	3.82	—	3.83	3.80	3.93	3.83	—	—	—
	M16	3.79	3.80	3.83	—	3.84	3.84	3.99	3.86	—	—	—
G1T	G11	4.01	—	3.81	*3.00*	—	—	*4.24*	*3.82*	—	—	—
	G12	4.04	—	3.69	*2.95*	—	—	*4.35*	*3.73*	—	—	—
	G13	4.04	—	3.81	*3.12*	—	—	*4.33*	*3.88*	—	—	—
G1U	G14	4.01	—	3.68	—	—	—	4.36	3.79	—	—	—
	G15	4.05	—	3.76	—	—	—	4.39	3.83	—	—	—
	G16	4.10	—	3.79	—	—	—	4.38	3.79	—	—	—

"C" is conventional concrete, "F" is very high fly ash concrete, "M" is Grancrete™ mortar, "G" is Grancrete™ concrete, "*" indicates specimens that were re-tested at a later age. "T" is high temperature exposure (300°C) group, "U" is unexposed/undamaged group. "SKD" and "SKD'": in water for 1 day with one face exposed to ambient air, then at least 1 day submerged in water or moist room at 100 % RH and tested immediately after removal from water; "CND" and "CND'": 3 days at 50±2 °C and 80% RH, then at least 1 day sealed at 23±2 °C; "DRY1" and "DRY2": oven dried at 40±2 °C (RH = 25±5 %) for 2 days then sealed and tested within 18 hours; "DMG": air dried specimens at 23 ± 2 °C exposed to 300 ± 20 °C for 60 ± 1 min, then sealed and tested at 23 ± 2 °C within 24 hours; "SAT": oven dried at 40 ± 2 °C for 2 days, then vacuum saturated in general accordance with ASTM Standard C1202-09; "—" is data not taken. Conversion factor: 1 km/s= 3281 ft/s

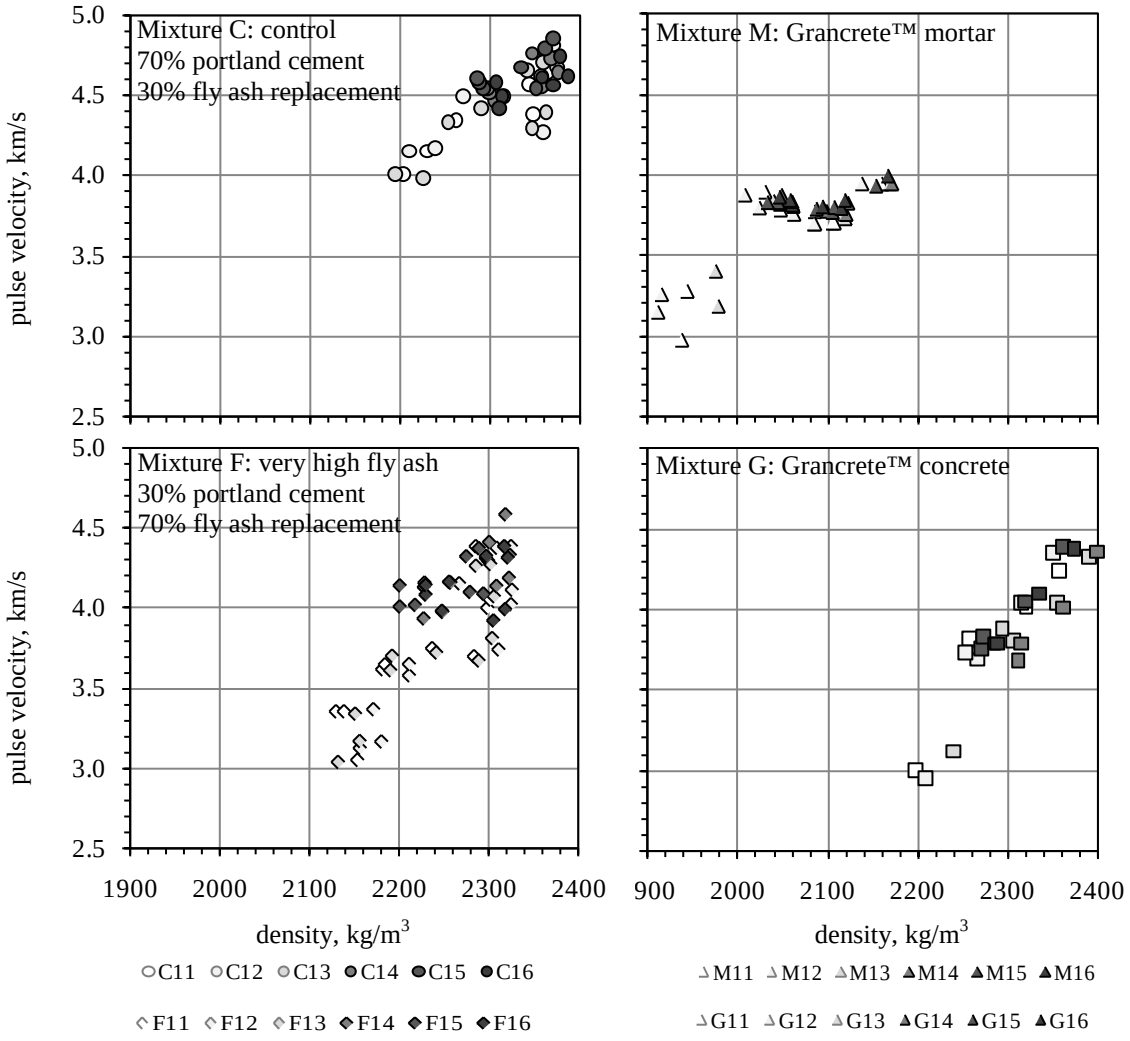

Figure 6.1 - Relationship Between Ultrasonic Pulse Velocity and Changes in Density Due to High Temperature Exposure and Water Content

An increase in v_p with density is observed for the three concrete mixtures (C, F and G), whereas the magnesium phosphate cement mortar exhibited no change in v_p with density after healing. Figure 6.1 suggests a patchy type of saturation for concrete, and a homogeneous type of saturation for mortar, suggesting that the interfacial transition zone in

concrete plays a major role in the behavior of seismic wave propagation in unsaturated concrete, consistent with the discussion in section 5.3.2.6. Increases in v_p in concrete of up to 10% higher when wet than when dry were observed, a value higher than the expected maximum of 5% (ASTM-C597 2003; Weiss 2006). A higher v_p for the magnesium phosphate cement based mortar (mixture M) when saturated than when soaked or dry is consistent with observations in sandstone and other rocks (Mavko *et al.* 2003; Berryman *et al.* 2000) suggesting homogeneous saturation up to very high water contents and then patchy saturation behavior when approaching complete saturation.

The calculated dynamic shear modulus (G_d) for each specimen is presented in Table 6.3. Figure 6.2(a) shows the average G_d and range of measurements for each moisture condition for the portland cement mixtures (mixtures C and F), and Figure 6.2(b) shows the average G_d and range of measurements for the magnesium phosphate cementitious materials (mixtures M and G). Re-testing of specimens from mixture F (labeled with a "*") are shown contiguously in Figure 6.2(a) according to the test chronology. Resonant frequency, specimen geometry, and calculated dynamic Poisson's ratio, measurements also used in determining G_d (see Eq. 5.3), are provided in Appendix D.

Table 6.3 - Dynamic Shear Modulus of Specimens from a Control and Three Sustainability Enhanced Cementitious Materials at Different Moisture Conditions and Before and After High Temperature Damage

Group	Spe-cimen	Dynamic Shear Modulus, GPa										
		SKD	**CND**	**DRY1**	**DMG**	**CND'**	**SKD'**	**SAT**	**DRY2**	**DMG***	**SAT***	**DRY2***
C1T	C11	15.3	14.2	14.5	*11.0*	*10.7*	*11.7*	*12.9*	*12.5*	—	—	—
	C12	14.2	13.5	13.9	*9.8*	*10.1*	*11.1*	*12.4*	*11.3*	—	—	—
	C13	14.6	14.2	13.5	*9.1*	*9.7*	*10.7*	*12.7*	*12.1*	—	—	—
C1U	C14	14.4	13.5	13.6	—	13.5	14.4	13.8	12.9	—	—	—
	C15	14.8	13.3	13.8	—	13.5	14.8	13.7	12.8	—	—	—
	C16	15.3	15.1	14.0	—	14.6	14.7	14.5	13.0	—	—	—
F1T	F11	11.8	10.6	10.8	*5.0*	*5.5*	*7.3*	*9.1*	*7.1*	*5.0*	*8.3*	*5.3*
	F12	11.2	12.0	8.9	*4.6*	*4.7*	*7.0*	*9.0*	*7.0*	*5.4*	*8.3*	*5.5*
	F13	11.5	11.4	9.7	*6.5*	*6.2*	*7.2*	*9.9*	*7.3*	*6.1*	*8.7*	*5.8*
F1U	F14	11.4	11.3	9.0	—	9.2	10.5	10.6	8.0	—	10.4	7.1
	F15	11.4	11.4	8.5	—	9.1	9.9	10.2	7.6	—	9.5	7.0
	F16	12.0	12.4	10.1	—	10.9	11.5	12.2	8.8	—	11.3	8.2
M1T	M11	8.3	8.8	8.9	*3.9*	*4.9*	*7.5*	*8.4*	*8.8*	—	—	—
	M12	8.3	8.7	8.5	*3.7*	*4.7*	*7.8*	*8.3*	*8.8*	—	—	—
	M13	8.8	9.3	9.1	*5.0*	*6.0*	*8.1*	*8.6*	*9.5*	—	—	—
M1U	M14	8.6	9.3	9.1	—	9.2	8.9	9.1	9.0	—	—	—
	M15	8.5	9.1	9.0	—	9.0	9.0	9.1	9.2	—	—	—
	M16	8.6	9.2	9.2	—	9.4	9.1	9.0	9.3	—	—	—
G1T	G11	9.1	—	9.8	*4.4*	—	—	*9.1*	*8.7*	—	—	—
	G12	8.9	—	10.4	*5.4*	—	—	*9.0*	*8.9*	—	—	—
	G13	9.2	—	10.2	*5.0*	—	—	*9.4*	*8.8*	—	—	—
G1U	G14	9.1	—	10.4	—	—	—	9.6	9.5	—	—	—
	G15	8.6	—	9.8	—	—	—	9.2	9.3	—	—	—
	G16	9.2	—	9.8	—	—	—	9.5	9.5	—	—	—

"C" is conventional concrete, "F" is very high fly ash concrete, "M" is Grancrete™ mortar, "G" is Grancrete™ concrete, "*" indicates specimens that were re-tested at a later age. "T" is high temperature exposure (300°C) group, "U" is unexposed/undamaged group. "SKD" and "SKD'": in water for 1 day with one face exposed to ambient air, then at least 1 day submerged in water or moist room at 100 % RH and tested immediately after removal from water; "CND" and "CND'": 3 days at 50±2 °C and 80% RH, then at least 1 day sealed at 23±2 °C; "DRY1" and "DRY2": oven dried at 40±2 °C (RH = 25±5 %) for 2 days then sealed and tested within 18 hours; "DMG": air dried specimens at 23 ± 2 °C exposed to 300 ± 20 °C for 60 ± 1 min, then sealed and tested at 23 ± 2 °C within 24 hours; "SAT": oven dried at 40 ± 2 °C for 2 days, then vacuum saturated in general accordance with ASTM Standard C1202-09; "—" is data not taken. Conversion factor: 1 Mpsi = 6.895 GPa

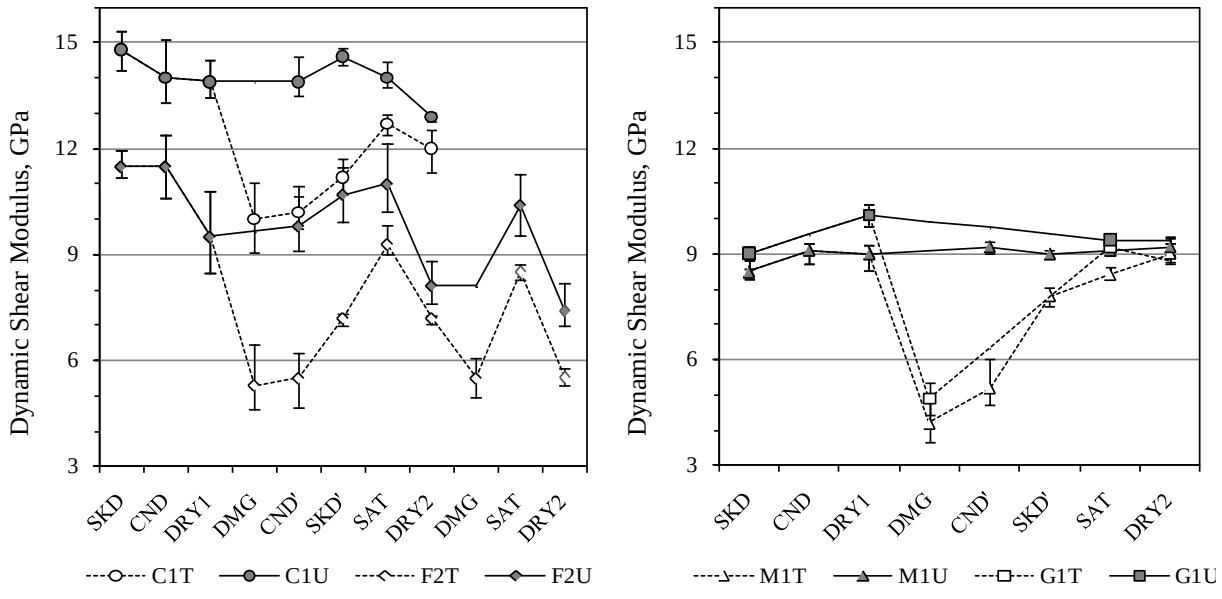

Portland Cement Mixtures:
C: concrete; F: 70% fly ash replacement
(a)

Magnesium Phosphate Cement Mixtures:
M: mortar; G:concrete
(b)

Figure 6.2 - Dynamic Shear Modulus of a Control and Three Sustainability Enhanced Cementitious Materials at Different Moisture Conditions and High Temperature (300 °C) Damage: (a) Portland Cement Concrete Mixtures, (b) Magnesium Phosphate Cement Based Mortar and Concrete (1 Mpsi = 6.895 GPa)

Dry shear moduli were used to compare the shear modulus between mixtures to minimize any density and water interaction effects. The dry shear modulus G_{DRY1} was considered as representative of undamaged conditions. Using 95% confidence intervals, the mean G_{DRY1} of mixtures C, F, M and G were 14.0±1.3, 9.8±2.4, 8.8±0.8, and 10.1±0.8 GPa, respectively. Results are as expected, with higher G_d for mixture C than for mixture F due to the inverted cement/fly-ash proportions, and higher G_d for mixture G than mixture M due to the inclusion of coarse aggregate. Similar G_d values for mixtures G and F were surprising, however, considering that the concrete based on magnesium phosphate cement (mixture G) had higher compressive strengths than the very high fly ash mixture (mixture F) (see Table 3.1).

Analysis of the stress-strain curve for these two types of mixtures, with emphasis on behavior at very low strains may be useful.

The value of G_{DMG}, measured at room temperature after the high temperature exposure and therefore prior to major water ingress, was considered to be representative of damaged conditions. The mean G_{DMG}, of mixtures C, F, M and G were 10.0±2.4, 5.4±2.5, 4.2±1.7and 4.9±1.3 GPa, respectively, using 95% confidence intervals. The residual shear modulus of mixture C was therefore about two times the residual shear moduli of the other three mixtures (see Figure 6.2). The normalized ratios of the residual shear moduli after damage, calculated as G_{DMG}/G_{DRY1}, were 0.70, 0.55, 0.48 and 0.49, for mixtures C, F, M and G, respectively. These residual ratios are within expected ranges for a 300 °C exposure (see, for example, Phan and Carino 1998), with mixture C being close to the upper limit and the enhanced sustainability mixtures near the lower limit. Decreases in G_d are analyzed later in this section.

Measurements of G_{DRY2} were obtained after vacuum saturation and subsequent redrying, and then measured dry. They therefore represent elastic characteristics after any autogenous healing for the damaged specimens, and any damage due to the vacuum saturation procedure for the undamaged specimens. For the exposed groups, the mean G_{DRY2} of mixtures C, F, M and G were 12.0±1.5, 7.1±0.1, 9.0±1.0, and 8.8±0.2 GPa, respectively. These correspond to normalized ratios G_{DRY2}/G_{DRY1} of 0.86, 0.72, 1.02 and 0.87 for mixtures C, F, M and G, respectively, providing evidence of autogenous healing occurring on the four mixtures, with complete healing for mixture M, and significant healing for mixture G. A lower residual ratio after healing for mixture F is consistent with lower cement content in the mixture.

For the undamaged groups, mean G_{DRY2} for mixtures C, F, M and G were 12.9±0.2, 8.1±1.5, 9.2±0.4, and 9.4±0.3 GPa, respectively. These mean shear moduli correspond to normalized ratios (G_{DRY2}/G_{DRY1}) of 0.92, 0.83, 1.05, and 0.93, for mixtures C, F, M and G, respectively, indicative of damage possibly due to the vacuum drying required for the saturation procedure. No residual damage on specimens from mixture M is consistent with the autogenous capabilities exhibited by this mortar, where microstructural damage from vacuum drying healed after saturation.

For the re-exposure of specimens from mixture F, mean G_{DMG*} was 5.5±1.4 GPa, the mean G_{DRY2*} of the exposed group was 5.5±0.6 GPa, and of the unexposed group was 7.4±1.7 GPa. These means provide evidence of similar damage to the first exposure, and of healing occurring only once for similar exposures. The G_{DMG*}/G_{DRY1} and G_{DRY2*}/G_{DRY1} ratios for the exposed group had the same value of 0.56. The G_{DRY2*}/G_{DRY1} ratio of the unexposed group was 0.76, lower than the G_{DRY2}/G_{DRY1} ratio, providing evidence of further damage after the second vacuum saturation procedure, but not to the extent of the damage caused by the high temperature exposure.

Effects of damage by high temperature exposure and the stiffening effect of water in resonant testing of G_d were analyzed using paired differences from changes on the same specimen. This technique allows reducing specimen-to-specimen variability and can identifying changes that might not be detected from analysis of means of absolute values (Box *et al.* 1978; and see, for example, Recalde and Leming 2009). The difference $\Delta G_T = G_{DMG} - G_{DRY1}$ measures the decrease in G_d from the 60±1 minute exposure to 300 °C, and the difference $\Delta G_V = G_{DRY2} - G_{DRY1}$ measures the decrease in G_d after high temperature

damage and healing for the damaged groups, and the decrease in G_d from the vacuum saturation procedure on the undamaged groups. For the water interaction effects on the measured G_d of the specimens, the differences between wet and dry conditions are measured by the differences $\Delta G_1 = G_{SKD} - G_{DRY1}$, prior to any microstructural modification, and by $\Delta G_2 = G_{SAT} - G_{DRY2}$ after microstructural modification by high temperature damage and autogenous healing for exposed specimens, and by the vacuum saturation for the unexposed specimens. Individual values of these selected differences are given in Table 6.4, along with mean estimates of these differences using 95% confidence intervals.

The 60±1 minute exposure to 300 °C produced similar mean decreases in G_d with all mixtures, with decreases of 4.0±1.1, 4.4±3.2, 4.6±1.2 and 5.2±0.5 GPa for mixtures C, F, M and G, respectively, as measured by $\Delta G_T = G_{DMG} - G_{DRY1}$. After the vacuum saturation procedure, the difference of the damaged specimens, as measured by $\Delta G_V = G_{DRY2} - G_{DRY1}$, was -2.0±1.5, -2.7±2.3, +0.2±0.7, and -1.3±0.5 GPa for mixtures C, F, M and G, providing evidence of significant unrecoverable decreases in G_d for mixtures C, F and G, since the difference was not significant for mixture M. For the undamaged specimens, the decreases in G_d after vacuum saturation were significant for mixtures C and F only, with similar decreases of 0.9±0.4 for mixture C, and 1.1±0.5 for mixture F.

Table 6.4 - Changes in Dynamic Shear Modulus of Specimens of a Control and Three Sustainability Enhanced Cementitious Materials Between Selected Moisture Conditions and High Temperature Damage

Group	Specimen	Changes in Dynamic Shear Modulus, GPa				Mean Estimates of Changes in Dynamic Shear Modulus, GPa [1]			
		Δ	Δ	Δ	Δ	Δ	Δ	Δ	Δ
C1T	C11	-3.5	-2.0	+0.4	+0.8	-4.0 ±1.1	-2.0 ±1.5	+0.7 ±0.9	+0.9 ±0.4
	C12	-4.1	-2.6	+1.1	+0.3				
	C13	-4.4	-1.4	+0.6	+1.1				
C1U	C14	—	-0.7	+0.9	+0.8	—	-0.9 ±0.4	+1.1 ±0.9	
	C15	—	-1.0	+0.9	+1.0				
	C16	—	-1.0	+1.5	+1.3				
F1T	F11	-5.8	-3.7	+2.0	+1.0	-4.4 ±3.2	-2.7 ±2.3	+2.2 ±0.9	+2.1 ±0.7
	F12	-4.3	-1.9	+2.0	+2.3				
	F13	-3.2	-2.4	+2.6	+1.8				
F1U	F14	—	-1.0	+2.6	+2.4	—	-1.1 ±0.5	+2.9 ±1.1	
	F15	—	-0.9	+2.6	+2.9				
	F16	—	-1.3	+3.4	+1.9				
M1T	M11	-5.0	-0.1	-0.4	-0.6	-4.6 ±1.2	+0.2 ±0.7	-0.6 ±0.7	-0.5 ±0.2
	M12	-4.8	+0.3	-0.5	-0.2				
	M13	-4.1	+0.4	-0.9	-0.3				
M1U	M14	—	-0.1	+0.1	-0.5	—	+0.1 ±0.4	-0.1 ±0.5	
	M15	—	+0.2	-0.1	-0.5				
	M16	—	+0.1	-0.3	-0.6				
G1T	G11	-5.4	-1.1	+0.4	-0.7	-5.2 ±0.5	-1.3 ±0.5	+0.4 ±0.6	-1.1 ±0.4
	G12	-5.0	-1.5	+0.1	-1.5				
	G13	-5.2	-1.4	+0.6	-1.0				
G1U	G14	—	-0.9	+0.1	-1.3	—	-0.6 ±0.8	+0.0 ±0.2	
	G15	—	-0.5	-0.1	-1.2				
	G16	—	-0.3	+0.0	-0.6				

"C" is conventional concrete, "F" is very high fly ash concrete, "M" is Grancrete™ mortar, "G" is Grancrete™ concrete, "T" is high temperature exposure (300°C) group, "U" is unexposed/undamaged group. "SKD": in water for 1 day with one face exposed to ambient air, then at least 1 day submerged in water or moist room at 100 % RH and tested immediately after removal from water; "DRY1" and "DRY2": oven dried at 40±2 °C (RH = 25±5 %) for 2 days then sealed and tested within 18 hours; "DMG": air dried specimens at 23 ± 2 °C exposed to 300 ± 20 °C for 60 ± 1 min, then sealed and tested at 23 ± 2 °C within 24 hours; "SAT": oven dried at 40 ± 2 °C for 2 days, then vacuum saturated in general accordance with ASTM Standard C1202-09; "—" is data not taken. [1]: using 95% confidence intervals. Conversion factor: 1 Mpsi = 6.895 GPa

The presence of water in the specimens had considerably different effects on the portland cement mixtures than on the mixtures based on magnesium phosphate cement. The differences $\Delta G_1 = G_{SKD} - G_{DRY1}$ and $\Delta G_2 = G_{SAT} - G_{DRY2}$ for specimens from mixtures C and F were all positive, meaning that $G_{SKD} > G_{DRY1}$ and $G_{SAT} > G_{DRY2}$, consistent with observations in Phase I for mixtures L and N and confirming the stiffening effect of water in portland cement based concrete in the resonant behavior of these types of specimens. The differences between G_{wet} and G_{dry} are also consistent with the O'Connell and Budiansky (1974; 1979) models, and allow calculating values of the crack density parameter. Crack density parameters and implications on the larger difference between G_{SKD} and G_{DRY1} for mixture F than in mixture C in estimating crack density parameters are analyzed in section 6.2.2.

For mixtures M and G, the undamaged G_d remained practically the same regardless of water content (see Figure 6.2). Analysis of the difference $\Delta G_1 = G_{SKD} - G_{DRY1}$ showed a significant increase for mixtures M and G, that is, G_{DRY} was higher than G_{SKD}, which is contrary to what was expected from observations of mixtures C, F, and from Phase I. No significant difference was found between G_{SAT} and G_{DRY1} on each specimen, however. The lack of dependence of measured G_d on water content for mixtures M and G imply that the squared resonant frequency decreases such that it counteracts the increase in density with water content (see Eq. 5.3), and that water acts simply as a mass held in the capillary pores contributing only inertially to the dynamic system without the stiffening effect observed in specimens of portland cement concrete mixtures. Further research on pore size effects in mortar on the resonant behavior of fluid-filled concretes would be useful. The fact that G_{wet} was not higher than G_{dry} means that crack density parameters cannot be calculated for

mixtures M and G as originally developed in Phase II. This issue is addressed in section 6.2.2.

The stiffening effect of water observed on the portland cement based mixtures, and no effect on the magnesium phosphate cement mixtures, is shown in Figure 6.3, where differences in G_d are shown with changes in density for all available data. The autogenous healing observed on all specimens, and the stiffening effect of water on the portland cement based mixtures also imply that the increase in G_d from G_{DMG} to G_{SKD} in damaged specimens of mixtures C and F is therefore a combined effect of healing and stiffening due to capillary water.

Table 6.5 shows the calculated dynamic Young's modulus of elasticity for comparison to results from Phase I and from previous investigations (Dilek *et al.* 2004; Recalde 2005; Recalde and Leming 2009). These values were obtained using the measured dynamic Poisson's ratio (υ_d) estimated from the ratio of v_p to shear wave velocity (v_s). The values of υ_d and v_s were obtained simultaneously when solving for the dimensionless frequency parameter Ω_0 (see section 3.4.2). Discussions on observations in measured G_d apply equally for E_d.

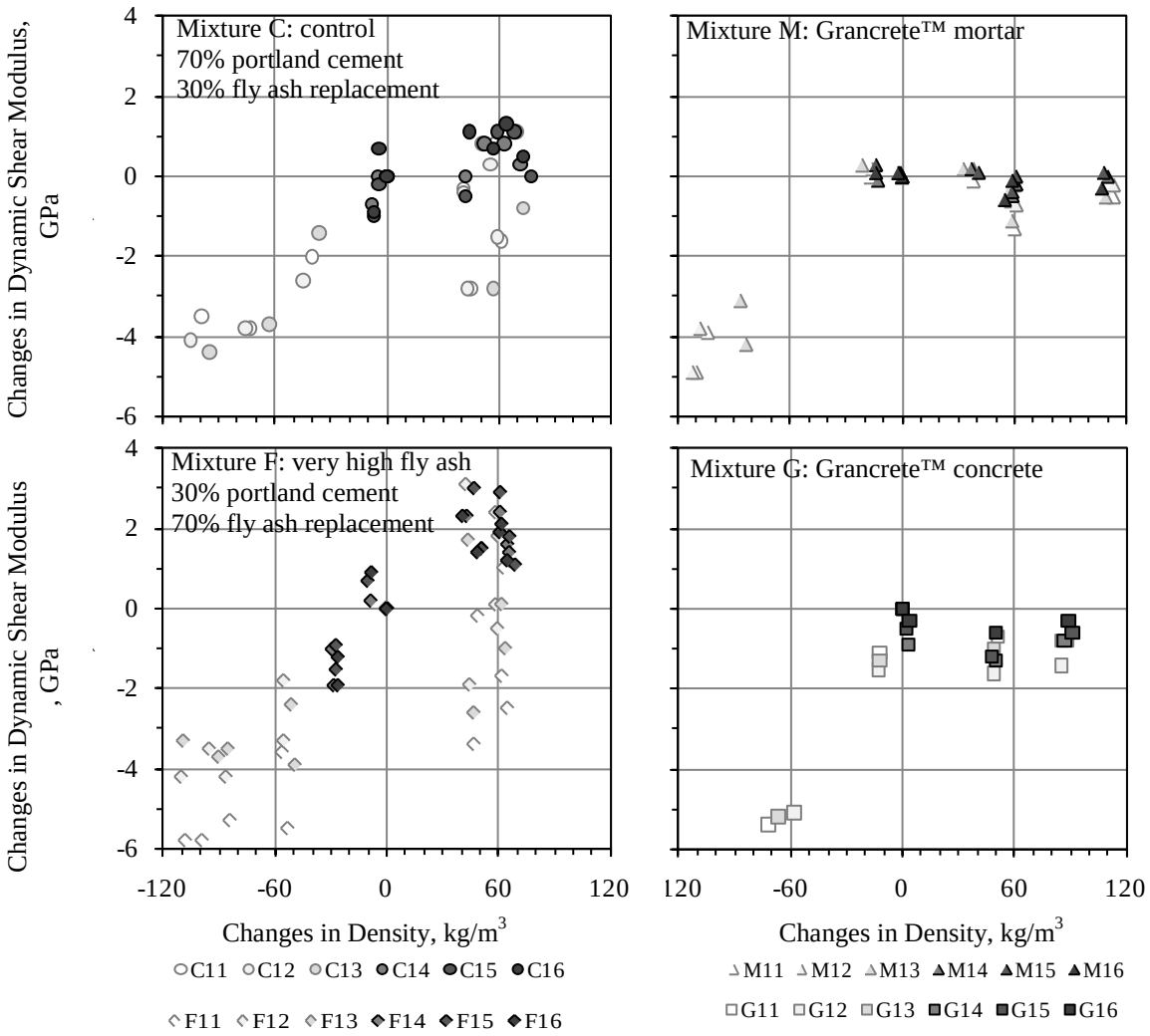

Figure 6.3 - Changes in Dynamic Shear Modulus (ΔG_d) with Changes in Density Based on a Dry Undamaged Condition (DRY1) of Specimens from a Control and Three Sustainability Enhanced Cementitious Materials

Table 6.5 - Dynamic Young's Modulus of Specimens from a Control and Three Sustainability Enhanced Cementitious Materials at Different Moisture Conditions and Before and After High Temperature Damage

Group	Spe-cimen	Dynamic Young's Modulus of Elasticity, GPa										
		SKD	**CND**	**DRY1**	**DMG**	**CND'**	**SKD'**	**SAT**	**DRY2**	**DMG***	**SAT***	**DRY***
C1T	C11	39.7	36.8	37.0	*28.1*	*27.9*	*31.1*	*34.4*	*32.4*	—	—	—
	C12	37.7	35.6	35.8	*26.1*	*26.8*	*29.4*	*33.3*	*30.2*	—	—	—
	C13	38.1	37.1	34.6	*24.1*	*25.5*	*28.6*	*33.2*	*31.5*	—	—	—
C1U	C14	37.8	36.0	35.0	—	35.1	37.1	36.4	33.8	—	—	—
	C15	38.9	35.2	35.6	—	35.2	38.0	36.7	33.8	—	—	—
	C16	39.8	38.7	35.9	—	36.9	37.9	37.6	34.3	—	—	—
F1T	F11	30.8	28.4	26.7	*13.6*	*14.4*	*19.8*	*24.2*	*19.0*	*13.7*	*22.6*	*14.7*
	F12	29.9	31.5	24.0	*12.5*	*12.8*	*19.1*	*24.1*	*18.8*	*14.6*	*22.7*	*15.3*
	F13	30.3	29.9	24.7	*16.2*	*16.2*	*19.3*	*25.5*	*19.4*	*16.2*	*23.6*	*16.0*
F1U	F14	30.7	30.0	24.3	—	24.4	27.8	28.1	21.5	—	27.8	19.7
	F15	30.2	30.1	23.0	—	24.3	26.3	26.9	20.7	—	25.8	19.4
	F16	31.5	32.1	26.7	—	28.0	28.9	30.5	23.7	—	29.8	22.4
M1T	M11	21.5	22.7	22.7	*10.7*	*13.2*	*19.9*	*22.4*	*22.9*	—	—	—
	M12	21.5	22.5	22.1	*10.1*	*12.8*	*20.5*	*22.1*	*22.7*	—	—	—
	M13	22.8	23.7	23.4	*13.3*	*15.9*	*21.2*	*22.9*	*24.0*	—	—	—
M1U	M14	22.3	23.6	23.3	—	23.5	23.1	24.0	23.3	—	—	—
	M15	22.2	23.3	23.0	—	23.2	23.2	23.8	23.6	—	—	—
	M16	22.4	23.6	23.7	—	23.9	23.6	23.8	23.8	—	—	—
G1T	G11	24.4	—	25.3	*12.0*	—	—	*24.8*	*23.0*	—	—	—
	G12	23.9	—	26.0	*14.0*	—	—	*24.7*	*23.3*	—	—	—
	G13	24.7	—	26.1	*13.5*	—	—	*25.8*	*23.5*	—	—	—
G1U	G14	24.5	—	26.0	—	—	—	26.2	24.6	—	—	—
	G15	23.2	—	25.1	—	—	—	25.3	24.3	—	—	—
	G16	24.8	—	25.2	—	—	—	26.0	24.6	—	—	—

"C" is conventional concrete, "F" is very high fly ash concrete, "M" is Grancrete™ mortar, "G" is Grancrete™ concrete, "*" indicates specimens that were re-tested at a later age. "T" is high temperature exposure (300°C) group, "U" is unexposed/undamaged group. "SKD" and "SKD'": in water for 1 day with one face exposed to ambient air, then at least 1 day submerged in water or moist room at 100 % RH and tested immediately after removal from water; "CND" and "CND'": 3 days at 50±2 °C and 80% RH, then at least 1 day sealed at 23±2 °C; "DRY1" and "DRY2": oven dried at 40±2 °C (RH = 25±5 %) for 2 days then sealed and tested within 18 hours; "DMG": air dried specimens at 23 ± 2 °C exposed to 300 ± 20 °C for 60 ± 1 min, then sealed and tested at 23 ± 2 °C within 24 hours; "SAT": oven dried at 40 ± 2 °C for 2 days, then vacuum saturated in general accordance with ASTM Standard C1202-09; "ALC": 1 day standing in 70% isopropyl alcohol (one face immersed, one face exposed to the atmosphere), then at least 1 day submerged. "—" is data not taken Conversion factor: 1 Mpsi = 6.895 GPa

6.2.2 Changes in Crack Density Parameter

The analytical technique described in Chapter 5, developed to determine the crack density parameter (ε) using the O'Connell and Budiansky (1974) model for dry and saturated (DS) cracked media (see section 5.4.2.2) using G_d measurements from dry and wet concrete disk specimens, was applied to specimens of concrete mixture F, a very high fly ash concrete mixture, using the methodology described in section 5.4.2. For mixtures M and G, G_{wet} was not higher than G_{dry} (see section 6.2.1), therefore representative values of ε could not be obtained, but changes in ε for mixtures M and G could be estimated, however, by using the relations for dry cracked media only. The values for Poisson's ratio of the uncracked solid (υ_0) were estimated for each specimen as the mean of the dynamic Poisson's ratio at selected wet and dry moisture conditions υ_{SKD}, υ_{DRY1}, υ_{SAT}, and υ_{DRY2}. For mixture F, the difference between dynamic shear moduli G_{SKD} and G_{DRY1} was used to determine the equivalent dynamic shear modulus of the uncracked solid (G_0) and the value of the crack density parameter before damage (ε_1). The crack density parameters after a 60±1 minute exposure to 300 °C (ε_{DMG}) and after vacuum saturation (ε_2) were determined from G_{DMG} and G_{DRY2}, respectively. For mixtures G and M, since G_0 and ε_1 could not be determined, the largest measured value of G_d from each specimen was taken as G_0 to then measure changes in crack density parameter ($\Delta\varepsilon$) using the dry curve of the O'Connell and Budiansky (1974) model.

Table 6.6 shows the results of the calculated crack density parameters ε_1, ε_{dmg}, and ε_2. Results for specimens from Mixture C are those already presented in sections 5.4.2.2 and

5.4.3, and are repeated in Tables and Figures of this section for ease of comparison. The values of ε presented in Table 6.6 are absolute values for mixtures C and F, and represent relative values for mixtures M and G, therefore comparison of ε can only be made between mixtures C and F. The value of ε_2 characterizes the microstructure after autogenous healing for damaged specimens, and the effect of the vacuum saturation procedure for the undamaged specimens of the control group. For mixture F, ε_{dmg*} is the crack density parameter after a second exposure to high temperature, and ε_{2*} is the crack density parameter after re-saturating and drying. The values of υ_0 used are also presented in Table 6.6, along with values of G_0 which were output for mixtures C and F, and selected input for mixtures M and G. Although an accuracy of ±0.01 was determined from uncertainty in the value of υ_0 (see section 5.5), values of ε are reported to the nearest 0.001 so statistical analyses could be conducted using three significant figures. This is consistent with a higher accuracy in measuring changes in crack density parameter from uncertainty in υ_0 (see section 5.5), and the 2½ significant figures reporting accuracy (nearest 0.05 GPa) for elastic moduli of concrete (ASTM-C215 2008). Estimates of mean crack density parameter at each state are also provided in Table 6.6, using 95% confidence intervals.

Table 6.6 - Results of the O'Connell and Budiansky Model Considering Dry and Saturated Specimens for Specimens of a Control and Three Sustainability Enhanced Concrete Mixtures

Group	Specimen	υ_0		Crack Density Parameters					Mean Estimates of Crack Density Parameters[b]				
C1T	C11	0.299	16.5	0.085	*0.219*	*0.163*			0.094 ±0.032	*0.240 ±0.085*	*0.164 ±0.015*	—	—
	C12	0.323	14.7	0.040	*0.221*	*0.158*							
	C13	0.299	16.2	0.115	*0.279*	*0.170*							
C1U	C14	0.308	15.6	0.091		0.120				—	0.143 ±0.054	—	—
	C15	0.316	16.3	0.107		0.147							
	C16	0.301	17.2	0.126		0.163							
F1T	F11	0.327	13.2	0.128	*0.380*	*0.296*	*0.380*	*0.369*	0.215 ±0.054	*0.373 ±0.096*	*0.304 ±0.028*	*0.368 ±0.046*	*0.367 ±0.020*
	F12	0.352	13.9	0.241	*0.407*	*0.317*	*0.378*	*0.374*					
	F13	0.322	13.8	0.199	*0.331*	*0.300*	*0.347*	*0.358*					
F1U	F14	0.350	14.3	0.245		0.285		0.319		—	0.283 ±0.068	—	0.309 ±0.069
	F15	0.351	14.7	0.275		0.309		0.331					
	F16	0.321	14.4	0.201		0.254		0.278					
M1T	M11	0.303	8.9	0.000[a]	*0.346*[a]	*0.008*[a]	—	—	N/A	N/A	N/A	—	—
	M12	0.305	8.8	0.025[a]	*0.356*[a]	*0.000*[a]	—	—					
	M13	0.293	9.5	0.030[a]	*0.298*[a]	*0.000*[a]	—	—					
M1U	M14	0.298	9.3	0.015[a]	—	0.023[a]	—	—		—	N/A	—	—
	M15	0.294	9.2	0.016[a]	—	0.000[a]	—	—					
	M16	0.296	9.4	0.015[a]	—	0.008[a]	—	—					
G1T	G11	0.327	9.8	0.000[a]	*0.343*[a]	*0.080*[a]	—	—	N/A	N/A	N/A	—	—
	G12	0.316	10.4	0.000[a]	*0.304*[a]	*0.101*[a]	—	—					
	G13	0.330	10.2	0.000[a]	*0.321*[a]	*0.098*[a]	—	—					
G1U	G14	0.315	10.4	0.000[a]	—	0.062[a]	—	—		—	N/A	—	—
	G15	0.329	9.8	0.000[a]	—	0.037[a]	—	—					
	G16	0.325	9.8	0.000[a]	—	0.023[a]	—	—					

"T" is high temperature treated group, "U" is untreated group, "υ_0" is Poisson's ratio of the uncracked solid, "$_1$" is the crack density parameter before damage, "$_{dmg}$" is the crack density parameter after exposure to 300 °C, "$_2$" and "$_{2*}$" are crack density parameters after vacuum saturation; "$_{dmg*}$" is crack density parameter after a second exposure to 300 °C; "—": data not taken; "N/A": value not available[a]; [a]: relative values since G_0 could not be determined; [b]: mean estimates with 95% confidence intervals.

Table 6.7 presents the changes in crack density parameter ($\Delta\varepsilon$) using paired differences for each specimen based on ε_1, the crack density parameter without any deterioration. Mean estimates of these differences are also provided in Table 6.7, using 95% confidence intervals. Estimates of the mean crack trace length ratios with damage of mixtures C and F are also presented in Table 6.7, estimated from the square root of the ratio of crack density parameters before and after damage (see discussion in section 5.4.3). Although mean estimates in Table 6.6 and Table 6.7 are given using three significant figures, these will be referred to in the discussions using only 2½ significant figures for ease of comparison.

The results of applying the O'Connell and Budiansky DS model to specimens of mixture F is presented in Figure 6.4, which shows the values of ε obtained from measurements of G_d. Figure 6.5 presents the results for specimens of mixture C, previously presented in Figure 5.3, but repeated here using the same scale used in Figure 6.4 for ease of comparison. For mixture F, the model successfully captures changes in ε associated with high temperature damage, autogenous healing, damage from vacuum drying, and re-damage after the second exposure with no healing after re-saturation and drying. Measured values of G_{SAT} are plotted at ε_2 for comparison to the saturated curve.

Table 6.7 - Estimates of Mean Crack Trace Length, Changes in Crack Density Parameter and Mean Estimates of From Specimens of a Control and Three Sustainability Enhanced Concrete Mixtures

		Mean Crack Trace Length ($\bar{L}$) Ratio Estimates[a]					Changes in Crack Density Parameter ( )		Mean Estimates of	
Group	**Specimen**	$\sqrt{\frac{\varepsilon_{dmg}}{\varepsilon_1}}$	$\sqrt{\frac{\varepsilon_2}{\varepsilon_1}}$	$\sqrt{\frac{\varepsilon_{dmg*}}{\varepsilon_1}}$	$\sqrt{\frac{\varepsilon_{2*}}{\varepsilon_1}}$	$\sqrt{\frac{\varepsilon_2}{\varepsilon_{dmg}}}$	( )	(ε_2)	( )	(ε_2)
C1T	C11	*1.61*	*1.38*	—	—	*0.86*	*+0.134*	*+0.078*	*+0.160* *±0.059*	*+0.084* *±0.079*
	C12	*2.35*	*1.99*	—	—	*0.85*	*+0.181*	*+0.118*		
	C13	*1.56*	*1.22*	—	—	*0.78*	*+0.164*	*+0.055*		
C1U	C14	—	1.15	—	—	—	—	+0.029	—	+0.035 ±0.014
	C15	—	1.17	—	—	—	—	+0.040		
	C16	—	1.14	—	—	—	—	+0.037		
F1T	F11	*1.72*	*1.52*	*1.72*	*1.70*	*0.88*	*+0.252*	*+0.168*	*+0.183* *±0.154*	*+0.115* *±0.118*
	F12	*1.30*	*1.15*	*1.25*	*1.25*	*0.88*	*+0.166*	*+0.076*		
	F13	*1.29*	*1.23*	*1.32*	*1.34*	*0.95*	*+0.132*	*+0.101*		
F1U	F14	—	1.08	—	1.14	—	—	+0.040	—	+0.042 ±0.024
	F15	—	1.06	—	1.10	—	—	+0.034		
	F16	—	1.12	—	1.18	—	—	+0.053		
M1T	M11	N/A	N/A	—	—	N/A	*+0.346*	*+0.008*	*+0.315* *±0.103*	*-0.016* *±0.051*
	M12	N/A	N/A	—	—	N/A	*+0.331*	*-0.025*		
	M13	N/A	N/A	—	—	N/A	*+0.268*	*-0.030*		
M1U	M14	—	N/A	—	—	—	—	+0.008	—	-0.005 ±0.030
	M15	—	N/A	—	—	—	—	-0.016		
	M16	—	N/A	—	—	—	—	-0.007		
G1T	G11	N/A	N/A	—	—	N/A	*+0.343*	*+0.080*	*+0.323* *±0.049*	*+0.093* *±0.028*
	G12	N/A	N/A	—	—	N/A	*+0.304*	*+0.101*		
	G13	N/A	N/A	—	—	N/A	*+0.321*	*+0.098*		
G1U	G14	—	N/A	—	—	—	—	+0.062	—	+0.041 ±0.049
	G15	—	N/A	—	—	—	—	+0.037		
	G16	—	N/A	—	—	—	—	+0.023		

"T" is high temperature treated group, "U" is untreated group, "υ_0" is Poisson's ratio of the uncracked solid, " $_1$" is the crack density parameter before damage, " $_{dmg}$" is the crack density parameter after exposure to 300 °C, " $_2$" and " $_{2*}$" are crack density parameters after vacuum saturation; " $_{dmg*}$" is crack density parameter after a second exposure to 300 °C; "—": data not taken; "N/A": value not available (ε could not be determined); [a]:$\bar{L}_{before}/\bar{L}_{after}$, considering similar crack count densities in both states ; [b]: mean estimates with 95% confidence intervals.

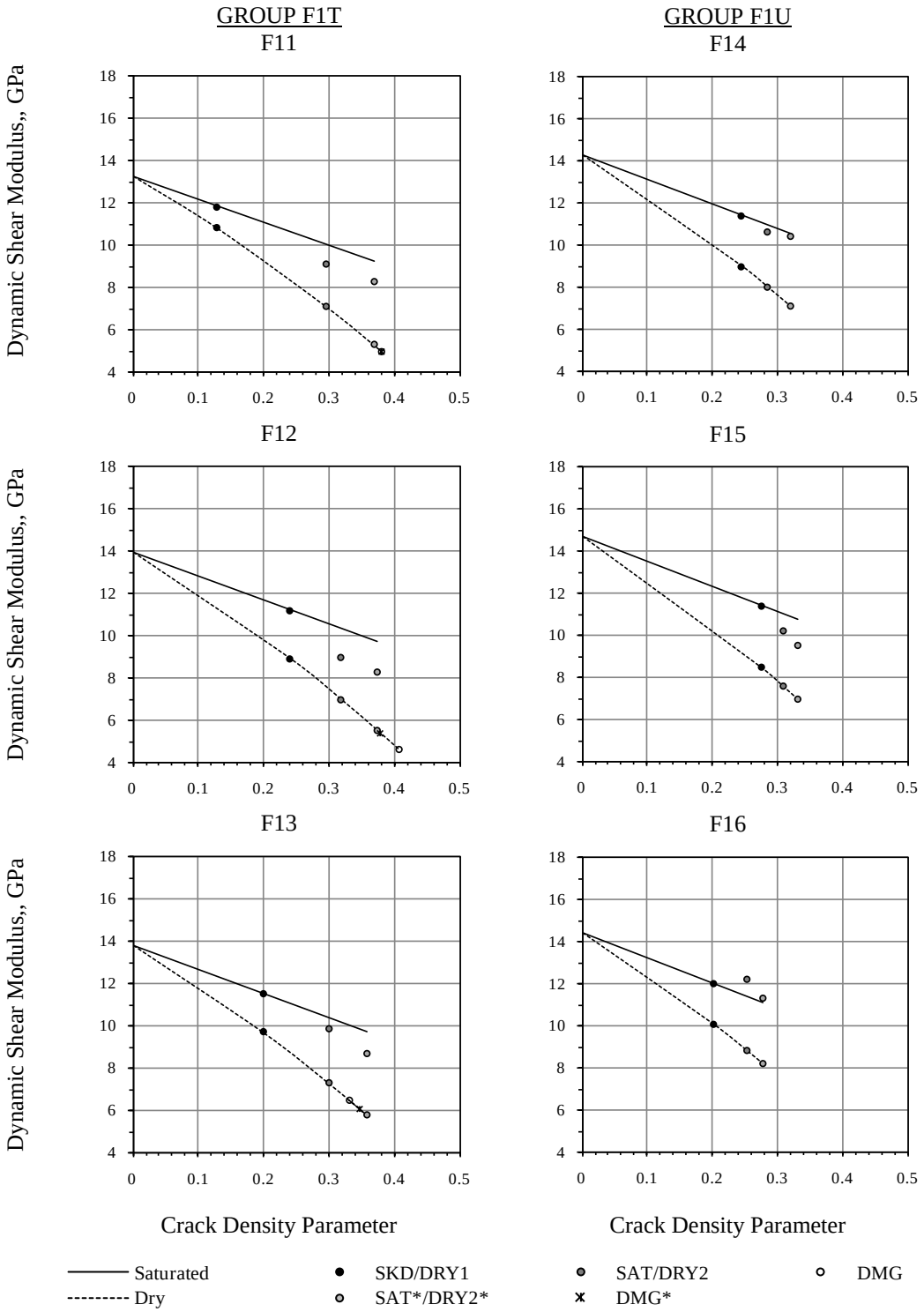

Figure 6.4 - Application of the O'Connell and Budiansky Dry and Saturated Model for Wet and Dry Disk Specimens of a Very High Fly Ash Concrete Mixture (1 Mpsi = 6.895 GPa)

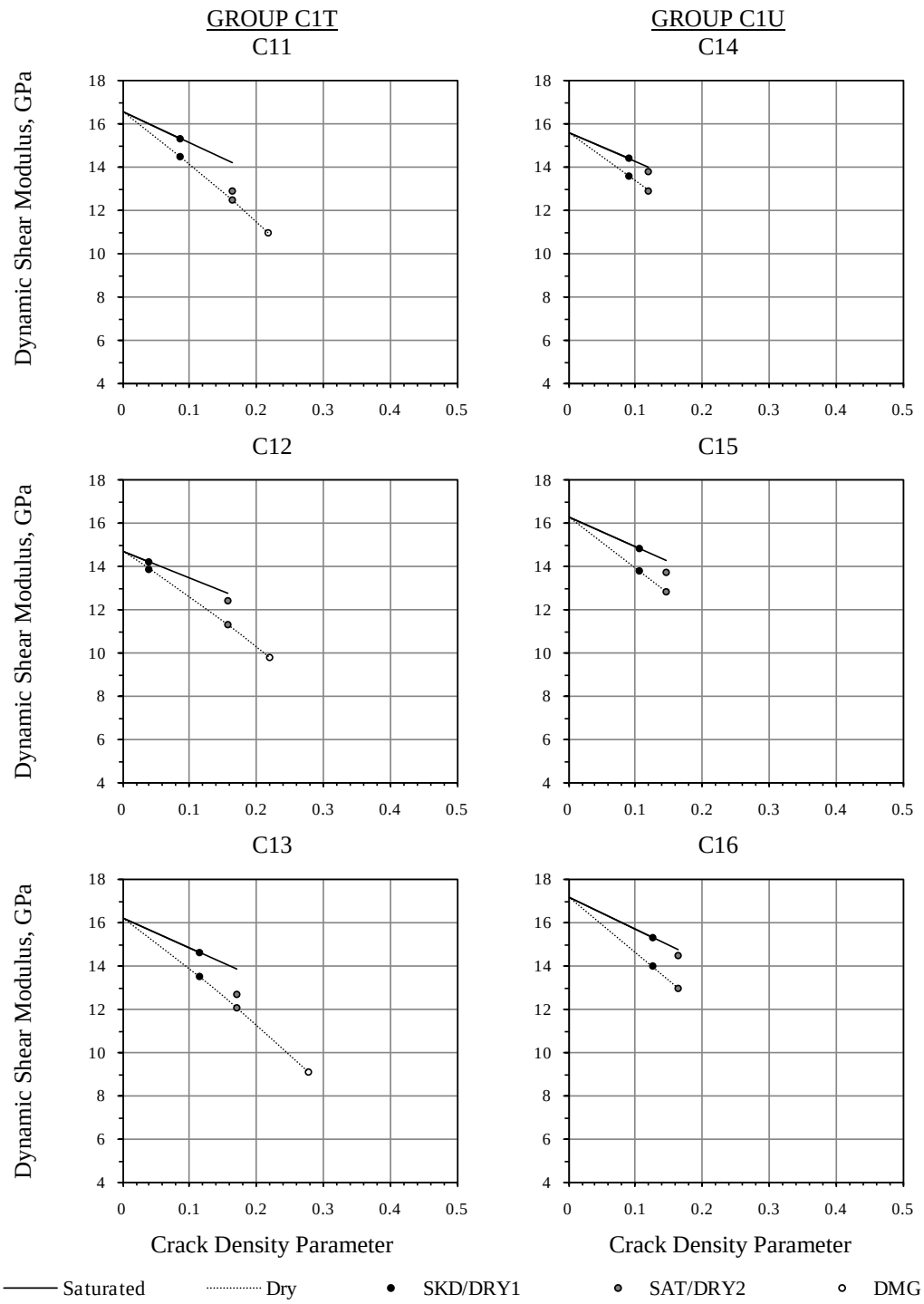

Figure 6.5 - Application of the O'Connell and Budiansky Dry and Saturated Model for Wet and Dry Disk Specimens of a Conventional Control Concrete Mixture (1 Mpsi = 6.895 GPa)

Small differences between predicted and measured G_{SAT} with ε_2 suggest that the model is adequate in characterizing portland cement concrete mixtures. The results also tend to support the conclusion that G_d measurements at early ages are sufficient to characterize the undamaged crack density parameter (ε_1) and G_0 of mixture F. No healing after the second exposure was indicated; this issue is statistically analyzed later in this section.

The undamaged crack density parameter (ε_1) of mixture F was 0.215±0.055, about twice the value of ε_1 of mixture C, which was 0.095±0.030, despite having otherwise similar mixture proportions. The larger values of ε_1 for mixture F were obtained because of the large difference between G_{SKD} and G_{DRY1}, compared, for example, to those measured with mixture C (see Figure 6.5 and Table 6.3). These results are consistent with mixture F having a lower compressive strength than mixture C, since compressive failure for concrete occurs because of crack interconnection (see, for example, Hsu *et al.* 1963). The technique to determine the crack density parameter therefore appears promising in characterizing portland cement based concrete mixtures. Discussion on mixtures based on magnesium phosphate cement is provided later in this section.

For conditions immediately after high temperature damage, a t-test for ε_{dmg} between mixtures C and F showed a significant difference, with mean ε_{dmg} of 0.375±0.095 of mixture F being significantly different than the mean ε_{dmg} of 0.240±0.085 of mixture C. The mean ε_{dmg} of mixture C was similar in value to the mean ε_1 of mixture F, indicating that specimens from mixture C, immediately after the 300 °C temperature damage, were at a

similar microstructural condition as specimens of mixture F without damage. Values of G_{DMG} of mixture C were also similar to the values of G_{DRY1} of mixture F, despite the slightly lower values of G_0 for specimens from mixture F.

For ε_2, a Fisher's Protected Least Significant Difference (Fisher's LSD) procedure was conducted to identify differences in mean ε_2 between groups C1T, C1U, F1T and F1U, which were 0.165±0.015, 0.145±0.055, 0.305±0.030, and 0.285±0.070, respectively. A Fisher's LSD procedure allows making pairwise comparisons among a set of more than two population means, after an *F* test for means shows that at least one of the groups is significantly different, by providing a 'least significant difference' that uses the pooled estimator of the population variance from all samples, the number of observations from each sample being compared, and a critical *t* value from a t-distribution of *N–T* degrees of freedom, where *N* is the total number of observations and *T* is the number of 'treatment' groups (Ott and Longnecker, 2001).

At a 95% confidence level, the mean ε_2, after vacuum saturation, of group C1T was not significantly different than the mean ε_2 of group C1U (as previously determined in section 5.4.2.2). Similarly, the mean ε_2 of group F1T was not significantly different than the mean ε_2 of group F1U, but the mean ε_2 of groups C1T and C1U were significantly lower than mean ε_2 of groups F1T and F1U. This result indicates that no significant difference was found for ε_2 between damaged and undamaged groups of the same mixture (with 2 degrees of freedom), but provides further evidence of a higher crack concentration for the very high fly ash mixture. Analysis of the mean difference $\Delta\varepsilon_2 = \varepsilon_2 - \varepsilon_1$ for mixture C in section

5.4.2.2 determined that the mean difference of +0.085±0.080 of the exposed group was significantly higher than the mean difference of +0.035±0.015 of the unexposed group. A similar analysis of paired differences for specimens from mixture F did not show, at a 95% confidence level, that the mean difference of +0.115±0.120 of the exposed group was significantly higher than the mean difference of +0.040±0.02 of the unexposed group. This is likely due to the low value of ε_1 obtained for specimen F11 (see Table 6.6). The use of larger sample sizes is recommended for future research to increase the degrees of freedom of the statistical tests.

Despite neither mean ε_2 nor $\Delta\varepsilon_2$ of mixture F being significantly different between exposure groups, the mean ε_{2^*} of group F1T was significantly higher than that of group F1U, with a mean ε_{2^*} of 0.365±0.020 for the re-exposed group and 0.310±0.070 for the non-exposed group. The mean ε_{2^*} of 0.365±0.020 was similar in value to the mean ε_{dmg} after the first exposure and to the mean $\hat{\varepsilon}_{dmg^*}$ after the second exposure, of 0.375±0.095 and 0.370±0.045 respectively, providing insight into changes in the microstructure with more than one exposure. No significant difference was found after conducting an analysis of variance F-test for these means, and no significant difference was found after conducting a paired difference analysis of mean ε_{dmg^*} and ε_{2^*}. These observations indicates that the very high fly ash concrete after the second high temperature exposure went to a damage state similar to the state immediately after the first exposure, and that autogenous healing occurred only once with mixture F for the same type of exposure. Although speculative, this is consistent with healed cracks having reformed or re-extended, but after which no remaining

unhydrated cement in the crack faces was available. Additional research would be useful to determine if this phenomenon is in fact occurring, as suspected.

Analysis of the estimates of increases in mean crack trace lengths ($\bar{L}$) (see section 5.4.3) for specimens from mixture F, ignoring those based on ε_1 of specimen F11, indicate that the mean crack trace length prior to exposure ($\bar{L}_1$) increased to about $1.30\,\bar{L}_1$ after the first exposure, and healing after vacuum saturation reduced $\bar{L}$ to about $1.15\,\bar{L}_1$ to $1.25\,\bar{L}_1$. For the undamaged specimens, the vacuum saturation procedure increased $\bar{L}$ by $1.06\,\bar{L}_1$ to $1.12\,\bar{L}_1$. For mixture C, as analyzed in section 5.4.3, $\bar{L}$ was about $1.6\,\bar{L}_1$ after high temperature damage (ignoring value for specimen C12), between $1.2\,\bar{L}_1$ and $1.4\,\bar{L}_1$ after healing of the damaged specimens, and around $1.15\,\bar{L}_1$ for the undamaged specimens after the vacuum saturation procedure. For the second exposure of specimens from mixture F, $\bar{L}$ were practically the same as after the first exposure, with no further evidence of healing, and the undamaged specimens had slight increases in $\bar{L}$ after vacuum saturation to around $1.1\,\bar{L}_1$ to $1.2\,\bar{L}_1$ (see Table 6.7). Similar levels of healing as in mixture C were observed for mixture F, as measured by $\sqrt{\varepsilon_2/\varepsilon_{dmg}}$, with recoveries between 0.85 and 0.95 of the $\bar{L}$ after high temperature damage.

Analysis of changes in crack density parameter ($\Delta\varepsilon$) using paired differences, allowed quantifying the different effects in microstructural changes for mixture M and G. Values for

these differences were provided in Table 6.7, and are shown Figure 6.6 as related to changes in G_d.

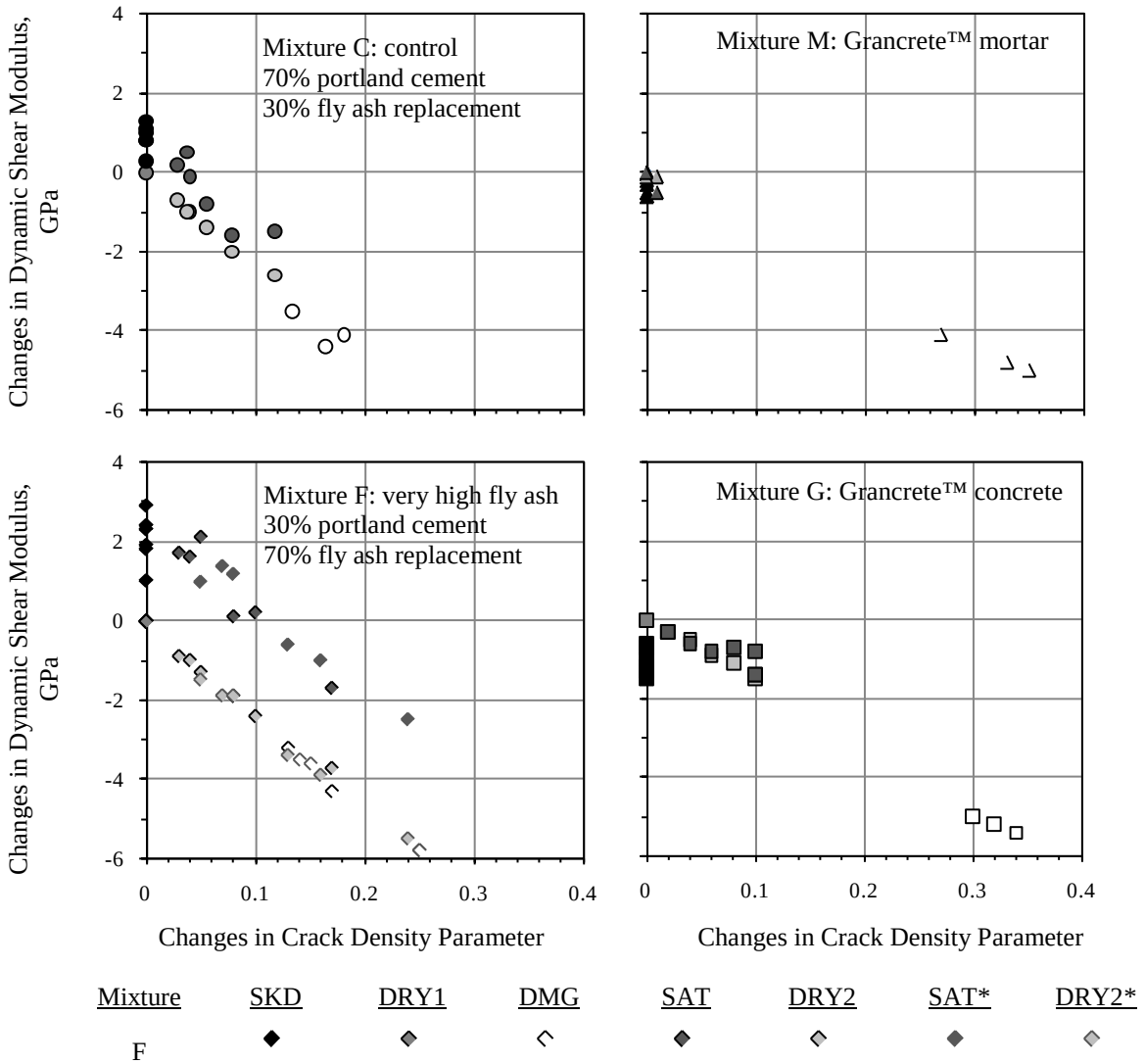

Figure 6.6 - Changes in Dynamic Shear Modulus and Changes in Crack Density Parameter of Specimens from a Control Concrete Mixture and Three Sustainability Enhanced Mixtures

Damage by high temperature exposure was measured by $\Delta\varepsilon_T = \varepsilon_{dmg} - \varepsilon_1$, the increase in crack density parameter from its original undamaged state. A Fisher's LSD procedure was

conducted for the mean estimate of $\Delta\varepsilon_T$ to identify differences in $\Delta\varepsilon$ between the four mixtures with high temperature damage before healing. The results show no statistically significant difference in mean $\Delta\varepsilon_T$ between mixture C and F, and no significant difference in mean $\Delta\varepsilon_T$ between mixture M and G; significant differences between the portland cement based mixtures and the magnesium phosphate based cement mixtures were observed, however. The high temperature exposure resulted in increases in ε of 0.160±0.060 for mixture C, 0.185±0.155 for mixture F, both significantly lower than an increase of 0.315±0.105 for mixture M and 0.325±0.050 for mixture G (see Table 6.7). The high temperature exposure therefore created more damage to the magnesium phosphate based cement mixtures than the portland cement based mixtures.

The similarity in changes in estimated crack density parameter after high temperature damage between the high fly ash mixture and the conventional concrete mixture implies that the changes in the microstructure are similar for this exposure. The microstructural behavior of the magnesium phosphate based cement appears to be different. These findings imply that current design methodologies and standard test procedures developed for conventional portland cement concrete exposed to moderately high temperatures, those not exceeding 300 °C, should be applicable to otherwise similar, portland cement based concretes with very high fly ash contents. Conversely, the findings indicate that current design and test methods may not be appropriate for this particular magnesium phosphate cement. The larger crack density parameter found with this cement implies a different fundamental, microstructural behavior. Additional research is strongly recommended, including microscopic analysis of

changes in the matrix and transition zone of concrete produced with magnesium phosphate cement prior to any use as a structural material.

The same mean $\Delta\varepsilon_T$ found for mixtures M and G is consistent with deterioration of the mortar phase, dominating over the effects in the transition zone present only in mixture G. Since the paste composition is so different, the dominant effect in mixtures C and F is consistent with the transition zone considering that both had the same aggregates and coarse aggregate proportions, therefore similar density of transition zone areas. This finding is also generally consistent with the findings reported by Carrasquillo *et al.* (1981).

The difference $\Delta\varepsilon_2 = \varepsilon_2 - \varepsilon_1$ measures the residual characteristics after vacuum saturation, and therefore unrecoverable damage after high temperature exposure and healing for the exposed groups, and damage by vacuum drying for the unexposed groups. Mixture M healed completely, returning to its original, undamaged mechanical properties. Mixture G also exhibited healing, but did not recover to its original undamaged properties, since the mean increase in $\Delta\varepsilon_2$ was +0.095±0.030. This value is an unrecoverable damage, very likely occurring in the transition zone, since the mortar was expected to heal completely as observed with mixture M.

Further research on the autogenous healing capabilities for multiple exposures is suggested, especially for the magnesium phosphate cement materials made with Grancrete™, since the mortar recovered completely after the first exposure, but is unknown if after a second exposure the ε and G_d would stay severely damaged, considering that mixtures G and M were affected the most by the high temperature damage prior to healing

Vacuum saturation had similar effects on all undamaged control groups. The procedure for vacuum saturation and re-drying produced an increase in ε of 0.035±0.015 for mixture C, 0.040±0.025 for mixture F, no damage with mixture M (healing would be expected), and no significant damage with mixture G despite having a similar sample mean increase of 0.04 as mixtures C and F.

The finding that magnesium phosphate cementitious materials had a higher degree of microcracking with high temperature damage than portland cement mixtures, and that the high temperature exposure created the same degree of microcracking by type of cement, regardless of its mixture characteristics, was further examined by evaluating $\Delta\varepsilon_T$ of specimens from Phase I. A finding that the mean $\Delta\varepsilon_T$ for different concrete mixtures were statistically the same would have important implications in service life estimates of concrete structures since the damaged G_d and ε could be predicted from a prior state, measured directly or estimated from tests on similar materials after a high temperature event. These analyses were done with only two significant figures, due to the uncertainty in the estimate of υ_0 (see section 5.5).

A Fisher's LSD procedure was conducted on mean $\Delta\varepsilon_T$ of groups C1T, F1T, M1T, G1T, L1T from Phase III, and L1T, N1T, L2T and N2T from Phase I. Significant differences in mean $\Delta\varepsilon_T$ were found among certain sets of groups. The first set, of the least affected groups, is composed of groups N1T, L1T and N2T. These samples were found to have mean $\Delta\varepsilon_T$ that were statistically the same (+0.09, +0.09, and +0.12, respectively) but significantly different from the mean $\Delta\varepsilon_T$ of all other groups. The set of groups that had the highest

increase in ε after high temperature exposure were groups M1T and G1T, with mean $\Delta\varepsilon_T$ of +0.34 and +0.32, respectively, which were significantly higher than the mean $\Delta\varepsilon_T$ of all other groups. The intermediate set is composed of groups C1T, L2T and F1T, whose mean $\Delta\varepsilon_T$ (+0.16, +0.18, and +0.18, respectively) were statistically the same. No significant difference was found between mean $\Delta\varepsilon_T$ of groups C1T and N2T, however. Considering that groups L1T and N1T were exposed to 300 °C only for 30±2 minutes, and all other groups were exposed for 60±2 minutes, the latter exposure produced similar changes in crack density for the four types of portland cement based concrete mixtures tested in this investigation, with minor significant differences for group N2T only. The 60±2 minute exposure to 300 °C therefore produced mean increases in ε between 0.12 and 0.18 on different portland cement based concrete mixtures, regardless of specimen thickness. Having the ability to determine exposure time, temperature, or both, from differences in ε between damaged and undamaged concrete after a fire event can be a useful resource in forensic investigations. For example, an increase in ε between 0.12 and 0.18 was indicative of a 60 minute exposure to 300 °C from results of this investigation. Relating increases in ε with different levels of high temperature exposure (i.e.: time, temperature) for portland cement based concrete mixtures appears promising; additional study is strongly recommended.

6.2.3 Fluid Penetrability Properties

Measured properties for air permeability index (API), and rates of absorption of water (*S*) for individual specimens in dry conditions are presented in Table 6.8. The API of mixtures C and F for conditions SKD, CND and DRY1 were determined using adhesive tape as A sealant for the edges of the disk, whereas all other API measurements were measured using

impermeable clay to ensure proper sealing and to avoid measurement errors, especially at locations where absorbed lubricant remained after conducting the ultrasonic pulse velocity test. Average values for each group and corresponding average measurements of at least two companion 50 mm (2 in.) thick disks are given in Table 6.9. Figure 6.7 shows the average API and measurement ranges as a function of moisture condition.

Measurements of API_{CND}, API_{DRY1}, and API_{DMG} for mixtures C and F, which were measured using adhesive tape, were excluded from the analysis because of concerns of air leak between the adhesive tape and the specimen side surface. This assumption seems valid since no significant difference is observed between API_{DRY1} and API_{DMG} after high temperature damage for both mixtures. These API measurements were also an order of magnitude higher than $API_{CND'}$, which, from G_d results, was expected to be similar in value to API_{DMG} for exposed groups C1T and F1T, and similar or higher in value to API_{DRY1} for unexposed groups C1U and F1U. Values of API for mixture M, none of which were measured using adhesive tape, did exhibit the expected behavior considering G_d and ε results, that is, API_{DMG} higher than API_{DRY1} after high temperature exposure, same API_{DMG} and $API_{CND'}$ before autogenous healing, complete healing after saturating and drying, and for undamaged group C1U, dry measurements of API (API_{DRY1}, $API_{CND'}$ and API_{DRY2}) remained the same throughout the drying and wetting cycles.

Table 6.8 - Air Permeability Index and Rates of Absorption of Water of Concrete Disks from Two Mixtures for Different Moisture Conditioning Methods and Before and After High Temperature Damage

Group	Specimen	CND	DRY1	DMG	CND'	DRY2	DMG*	DRY2*	Initial	Secondary
		m^2/s	m^2/s	m^2/s	m^2/s	m^2/s	m^2/s	m^2/s	$\times 10^{-4}$ $mm/sec^{0.5}$	$\times 10^{-4}$ $mm/sec^{0.5}$
C1T	C11	8.6E-07[a]	8.2E-06[a]	*1.0E-05[a]*	*3.8E-07*	*1.5E-07*	—	—	*198.3*	*7.9*
	C12	9.7E-07[a]	1.3E-05[a]	*1.7E-05[a]*	*4.3E-07*	*2.3E-07*	—	—	*179.5*	*8.2*
	C13	2.4E-06[a]	1.3E-05[a]	*9.6E-06[a]*	*5.3E-07*	*1.8E-07*	—	—	*195.3*	*5.6*
C1U	C14	2.2E-08[a]	1.3E-05[a]	—	9.5E-08	1.6E-07	—	—	60.1	N/A
	C15	1.6E-06[a]	1.0E-05[a]	—	5.4E-08	1.9E-07	—	—	66.1	N/A
	C16	6.4E-06[a]	8.8E-06[a]	—	6.1E-08	2.1E-07	—	—	59.9	N/A
F1T	F11	7.8E-06[a]	8.7E-06[a]	*1.5E-05[a]*	*6.4E-07*	*5.0E-07*	*7.1E-07*	*1.2E-06*	*172.0*	*8.6*
	F12	1.8E-07[a]	1.3E-05[a]	*6.8E-06[a]*	*5.6E-07*	*6.2E-07*	*6.5E-07*	*1.2E-06*	*166.2*	*10.3*
	F13	1.6E-06[a]	1.5E-05[a]	*5.3E-06[a]*	*5.6E-07*	*3.5E-07*	*6.3E-07*	*7.4E-07*	*153.8*	N/A
F1U	F14	2.7E-06[a]	1.0E-05[a]	—	1.8E-07	2.0E-07	—	7.3E-07	85.1	N/A
	F15	1.2E-06[a]	1.2E-05[a]	—	1.8E-07	3.8E-07	—	3.6E-07	74.3	N/A
	F16	1.6E-06[a]	1.3E-05[a]	—	2.1E-07	2.1E-07	—	6.7E-07	76.7	N/A
M1T	M11	3.9E-07[a]	1.5E-06	*5.6E-06*	*5.4E-06*	*1.4E-06*	—	—	*204.7*	*8.1*
	M12	6.2E-07[a]	1.7E-06	*4.8E-06*	*5.3E-06*	*1.0E-06*	—	—	*209.3*	*7.5*
	M13	6.6E-07[a]	1.4E-06	*4.4E-06*	*4.5E-06*	*9.3E-07*	—	—	*168.0*	*7.3*
M1U	M14	4.1E-07[a]	1.2E-06	—	1.2E-06	1.1E-06	—	—	131.8	7.0
	M15	3.5E-07[a]	1.1E-06	—	1.1E-06	1.0E-06	—	—	133.5	5.9
	M16	3.7E-07[a]	1.1E-06	—	1.1E-06	9.0E-07	—	—	129.3	8.8
G1T	G11	—	4.8E-07	*1.9E-06*	—	*3.1E-07*	—	—	—	—
	G12	—	5.3E-07	*1.8E-06*	—	*3.7E-07*	—	—	—	—
	G13	—	2.8E-07	*1.8E-06*	—	*4.4E-07*	—	—	—	—
G1U	G14	—	3.5E-07	—	—	5.7E-07	—	—	—	—
	G15	—	3.5E-07	—	—	4.2E-07	—	—	—	—
	G16	—	4.4E-07	—	—	3.1E-07	—	—	—	—

Values in italic represent conditions after damage to high temperature (300 °C) "T" is high temperature treated group, "U" is untreated group. "DRY*n*": oven dried at 40±2 °C (RH = 25±5 %) for 2 days then sealed and tested within 18 hours; "DMG": Air dried specimens at 23±2 °C exposed to 300 ± 20 °C for 60±2 min, then sealed and tested at 23±2 °C within 24 hours;" "* ": F1T/U specimens were re-tested for DMG, SAT and DRY2;; "—": data not-taken (no exposure); "N/A": Secondary Rate of Absorption of Water not valid since $r < 0.98$. [a]: measurement taken using adhesive impermeable tape to seal the test specimen

Table 6.9 - Average Air Permeability Index and Rates of Absorption of Water of Concrete Disks for Different Moisture Conditioning Methods and Before and After High Temperature Damage

Group	Air Permeability Index, m^2/s							Rate of Absorption of Water, $\times 10^{-4}$ $mm/s^{0.5}$	
	CND	**DRY1**	**DMG**	**CND'**	**DRY2**	**DMG***	**DRY2***	**Initial**	**Secondary**
C1T	2.1E-06[a]	1.1E-05[a]	*1.2E-05[a]*	*4.5E-07*	*1.8E-07*	—	—	*191.0*	*7.2*
C1U			—	7.0E-08	1.9E-07	—	—	62.0	[b]
C2U	4.1E-06[a]	2.8E-05[a]	—	1.1E-07	—	—	—	38.5	3.6
F1T	2.5E-06[a]	1.2E-05[a]	*9.1E-06[a]*	*5.9E-07*	*4.9E-07*	*6.6E-07*	*1.1E-06*	*164.0*	*9.5*
F1U			—	1.9E-07	2.6E-07	—	5.9E-07	78.7	[b]
F2U	6.9E-09[a]	2.0E-05[a]	—	2.1E-07	—	—	—	78.6	3.6
M1T	4.7E-07	1.3E-06	*4.9E-06*	*5.1E-06*	*1.1E-06*	—	—	*194.0*	*7.6*
M1U			1.1E-06	1.0E-06	1.1E-06	—	—	131.5	7.2
M2U	4.8E-07	1.3E-06	—	1.2E-06	—	—	—	124.8	3.3
G1T	—	4.0E-07	*1.8E-06*	—	*3.7E-07*	—	—	—	—
G1U			—	—	4.3E-07	—	—	—	—
G2U	—	—	—	—	—	—	—	9.5[c]	6.4

Values in italic represent conditions after damage to high temperature (300 °C) "T" is high temperature treated group, "U" is untreated group. "DRY*n*": oven dried at 40±2 °C (RH = 25±5 %) for 2 days then sealed and tested within 18 hours; "DMG": Air dried specimens at 23±2 °C exposed to 300 ± 20 °C for 60±2 min, then sealed and tested at 23±2 °C within 24 hours;" "[*] ": F1T/U specimens were re-tested for DMG, SAT and DRY2; "—": data not-taken; [a]: measurement taken using adhesive impermeable tape to seal the test specimen.; [b]: Secondary Rate of Absorption of Water not valid since r < 0.98; [c]: 31.5 $\times 10^{-4}$ obtained after drying for 1 day at 40 °C (RH≈ 25%) and sealing for 18 hours.

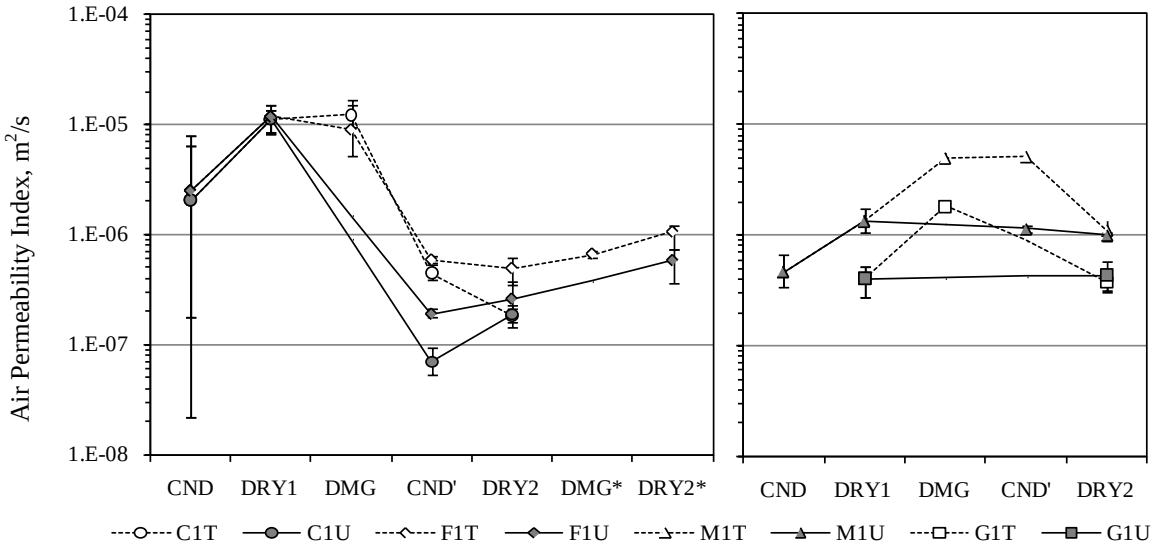

Figure 6.7 - Air Permeability Index at Different Moisture Content Conditions for a Control and Three Sustainability Enhanced Cementitious Materials

For the analysis of the effect of high temperature exposure on measured API, individual measurements of $API_{CND'}$ of mixtures C and F were considered as representative of damaged conditions for groups C1T and F1T, in lieu of API_{DMG} data, and of undamaged dry conditions for groups C1U and F1U in lieu of API_{DRY1}. Mixture M had a complete data set and Mixture G had measurements of API_{DRY1}, API_{DMG} and API_{DRY2} only, because the accelerated testing program excluded moisture conditions CND and CND'. Using a Fisher's LSD procedure with logarithmic transformed data, significant differences among mean log(API) were established for all groups, except for no significant difference between means of groups C1T and G1U. The mean log(API) for each group, in decreasing order, are -5.30, -5.74, -5.94, -6.23, -6.35, -6.42, -6.72 and -7.17 log(m^2/s) for groups M1T, G1T, M1U, F1T, C1T, G1U, F1U and C1U, respectively. In this regard, the log(API) was effective in

identifying differences in fluid penetrability between mixtures and with high temperature damage.

A similar analysis for $\log(API_{DRY2})$, after vacuum saturation and drying and therefore including the effects of autogenous healing of damaged specimens, resulted in three sets of groups with no statistically significant difference among their means. The first set consists of groups C1T, C1U and F1U, whose means of -6.74, -6.73 and -6.60 $\log(m^2/s)$ were statistically the same. The second set consists of groups G1T, G1U and F1T with sample means of -6.43, -6.38 and -6.32 $\log(m^2/s)$, respectively. The third set, with the highest log(API), consists of groups M1U and M1T, with means of -6.00 and -5.96 $\log(m^2/s)$, respectively. No significant difference was found between mean log(API) of groups F1U and G1T, however. These results is consistent with the hypothesis that autogenous healing occurred in specimens from mixtures C, G, and M, whereas mixture F showed no statistically meaningful API recovery. Re-exposure of specimens from mixture F produced a statistical significant, though minor, increase in API measurements for API_{DMG*} and API_{DRY2*}, with no evidence of healing.

Sorptivity measurements of undamaged specimens resulted in lower initial rates of absorption of water (S_i) for mixture C than mixture F, and a lower S_i for mixture G than mixture M, using the standard, 50 mm (2 in.) thick specimens. The initial rate of absorption of water of 25 mm (1 in.) thick disks were similar in value measurements with the 50 mm (standard) disks for mixtures F and M; the 25 mm (1 in.) thick disks of mixture C had higher S_i than the standard measurement, however. For mixture G, the standard S_i was 9.5×10^{-4} $mm/sec^{0.5}$, which was very low compared to standard S_i of other groups. In order to mimic

the drying cycle undergone by specimens from other mixtures prior to the sorptivity test (condition CND'), specimens from mixture G were dried for one day at 40 °C and sealed for at least 18 hours and re-tested for S_i. The repeated test resulted in an initial rate of absorption of water of 31.5×10^{-4} mm/sec$^{0.5}$. The undamaged S_i measurements were high compared to those obtained during Phase I. The dependence of the rate of absorption on initial water content is consistent with the findings by Nokken and Hooton (2002), but further studies for moisture conditioning of concrete in desorption is needed. Drying specimens prior to moisture conditioning is recommended in order to avoid different water contents from moisture conditioning in desorption compared to sorption, using the methodology in ASTM Standard C 1585 (2004). Sorptivity measurements for each specimen are provided in Appendix D.

Initial rates of absorption of water increased with high temperature damage, as expected. Group M1T had the highest S_i, at 191.0×10^{-4} mm/sec$^{0.5}$, followed by group C1T at 191.0×10^{-4} mm/sec$^{0.5}$ and group F1T at 164.0×10^{-4} mm/sec$^{0.5}$. Sorptivity was not measured on 25 mm (1 in.) thick specimens from mixture G since moisture conditions CND and CND' were eliminated from the accelerated testing program, whose purpose was to determine values for crack density parameter only. The relationship between API and S_i is addressed in section 6.3.2.

6.3 Relationships between Measured Properties

6.3.1 Correlation Matrix

Relationships between measured properties were assessed by the sample correlation coefficients (r) combining data from all mixtures. Measurements excluded from the analysis

were absolute values of ε for mixtures G and M (see section 6.2.2), API of mixtures C and F measured with adhesive tape (see section 6.2.3), and values of ε_1 at condition SKD since these were analyzed at condition DRY1 only ($\varepsilon_{SKD} = \varepsilon_{DRY1} = \varepsilon_1$). The selected data sets are summarized in Table 6.10, and the resulting correlation matrix is given in Table 6.11. A scatterplot matrix of selected properties is given in Figure 6.8. Several of the correlations are known to be exact as the relationship between G_d and E_d, so very high sample correlation coefficients reflect simple conformance of the data and should be considered only a measure of variability. An analysis of the relationship between v_p and G_d is provided in Appendix D.

Table 6.10 - Summary of data Sets Used to Determine Sample Correlation Coefficients Between Measured Properties

Condition	Property				
	G_d		**API**		
SKD	C,F,M,G	—	—	—	—
CND	C,F,M	—	M	—	—
DRY1	C,F,M,G	C,F	M,G	—	—
DMG	C,F,M,G	C,F	M,G	—	—
CND’	C,F,M	—	C,F,M	C,F,M	C,F,M
SKD’	C,F,M	—	—	—	—
SAT	C,F,M,G	—	—	—	—
DRY2	C,F,M,G	C,F	C,F,M,G	—	—
DMG*	F	F	F	—	—
DRY2*	F	F	F	—	—

“C” is conventional concrete, “F” is very high fly ash concrete, “M” is Grancrete™ mortar, “G” is Grancrete™ concrete, and “—” is data not taken “SKD” and “SKD’”: in water for 1 day with one face exposed to ambient air, then at least 1 day submerged in water or moist room at 100 % RH and tested immediately after removal from water; “CND” and “CND’”: 3 days at 50±2 °C and 80% RH, then at least 1 day sealed at 23±2 °C; “DRY1”, “DRY2” and “DRY2*”: oven dried at 40±2 °C (RH = 25±5 %) for 2 days then sealed and tested within 18 hours; “DMG” and “DMG*”: air dried specimens at 23 ± 2 °C exposed to 300 ± 20 °C for 60 ± 1 min, then sealed and tested at 23 ± 2 °C within 24 hours; “SAT”: oven dried at 40 ± 2 °C for 2 days, then vacuum saturated in general accordance with ASTM Standard C1202 (2009). “G_d” is dynamic shear modulus, “ε” is crack density parameter, “API” is air permeability index, “S_i” is initial rate of absorption of water, and “S_s” is secondary rate of absorption of water.

Table 6.11 - Correlation Matrix of Measured Properties Combining Data for All Mixtures

	G_d	**E_d**		**API**	**log(API)**		
G_d	1.00						
E_d	1.00	1.00					
	-0.98	-0.97	1.00				
API	-0.60	-0.61	0.78	1.00			
log(API)	-0.75	-0.77	0.87	0.84	1.00		
	-0.71	-0.71	—	0.57	0.78	1.00	
	-0.42	-0.42	—	-0.08	-0.14	0.01	1.00

“v_p” is ultrasonic pulse velocity, “G_d” is dynamic shear modulus, “ε” is crack density parameter, “API” is air permeability index, “S_i” is initial rate of absorption of water, and “S_s” is secondary rate of absorption of water. “—” is no available paired data.

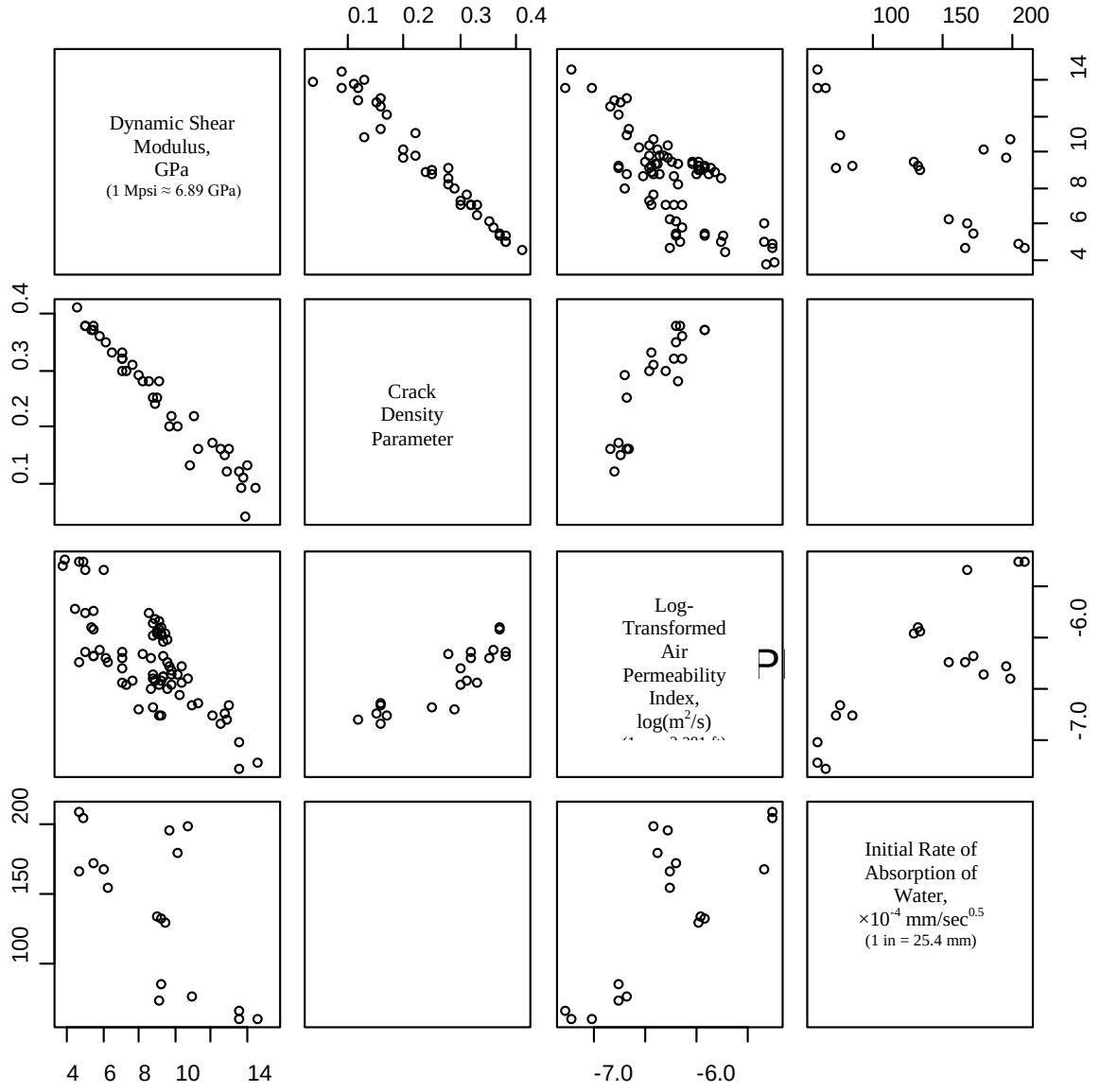

Figure 6.8 - Scatterplot Matrix of Selected Measured Properties Combining Data of a Conventional Concrete Mixture and Three Sustainability Enhanced Mixtures

6.3.2 Relationship between Fluid Penetrability Properties

The sample correlation coefficient between log(API) and S_i was +0.78. The relationship between API and S_i for mixtures C, F and M is presented in Figure 6.9, demonstrating the increase in both API and S_i of damaged specimens, and similar to that reported by Recalde and Leming (2009). Data clusters by mixtures follow different trends from undamaged to damaged groups therefore analysis by a linear regression model was not appropriate. Figure 6.9 confirms the results from Phase I of this investigation, showing that the 25 mm (1 in.) thick disks can be used to determine the initial rate of absorption of water.

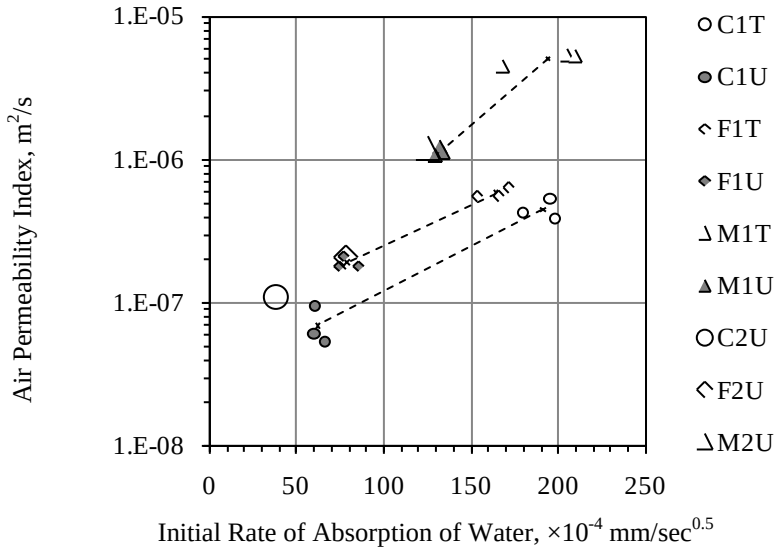

Figure 6.9 - Relationship Between Initial Rate of Absorption of Water and Air Permeability Index for a Conventional and Two Sustainability Enhanced Cementitious Materials and Two Disk Thicknesses

6.3.3 Relationship between Dynamic Shear Modulus and Air Permeability Index

The sample correlation coefficient between G_d and log(API) was -0.75; a plot of these properties is presented in Figure 6.10. Data for mixtures C and G plot along the regression line, whereas data from mixture M are above the expected log(API) and data for mixture F are below the expected log(API) line. This last observation indicates that a linear model is not appropriate for the combined data since the residuals plot does not show randomness for all mixtures. The changes in properties seem similar, however, changes in these properties are addressed in section 6.4. The corresponding plot of dynamic elastic Young's modulus (E_d) and log(API) is given in Figure 6.11, where E_d was calculated using each individual measured dynamic Poisson's ratio, instead of assuming a value of 1/6 as in previous studies (Recalde and Leming 2009; Dilek *et al.* 2004). The *r* between E_d and log(API) was -0.77, showing only a slightly higher correlation than between G_d and log(API). A linear regression model of E_d and log(API) is also not appropriate because of the same limitations observed with G_d.

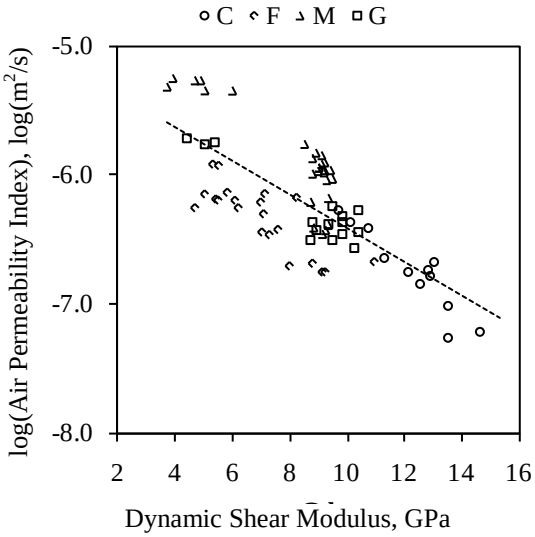

Figure 6.10 - Relationship Between Dynamic Shear Modulus (G_d) and Log-Transformed Air Permeability Index (API) for a Conventional Concrete Mixture and Three Sustainability Enhanced Mixtures

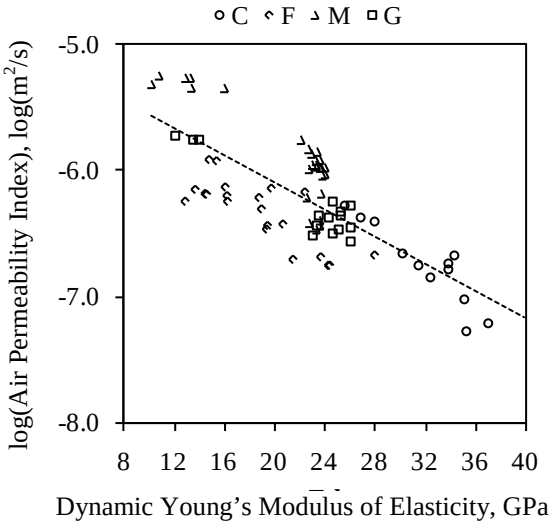

Figure 6.11 - Relationship Between Dynamic Elastic Modulus (E_d) and Log-Transformed Air Permeability Index (API) for a Conventional Concrete Mixture and Three Sustainability Enhanced Mixtures

6.3.4 Relationships between Crack Density Parameter and Fluid Penetrability Properties

The relationship between ε and log(API) was found to be relatively strong with an *r* value of +0.87, as shown in Figure 6.12(a). This data set was limited since it used only data of mixtures C and F in moisture condition DRY2, and data for mixture F in conditions DMG* and DRY2* (see discussion in section 6.3.1). Crack density parameter data from mixtures M and G were excluded due to limitations in obtaining absolute values for ε.

Since clusters of data per mixture do not overlap for ε, analysis by a simple linear regression was not appropriate. In order to improve any possible relationship using these two mixtures, the data sets of log(API) were completed using values of $API_{CND'}$ instead of API_{DMG*} for exposed groups C1T and F1T and instead of API_{DRY1} for non-exposed groups C1U and F1U, since these measurements were taken at dry conditions prior to vacuum saturation, and therefore generally representative of the microstructure at ε_1. The *r* between ε and log(API) augmented with $API_{CND'}$ data was +0.86 where the $API_{CND'}$ data contributed with intermediate data points between the original clusters, as seen in Figure 6.12(b). The results of incorporating data for mixture M, are addressed in section 6.4.

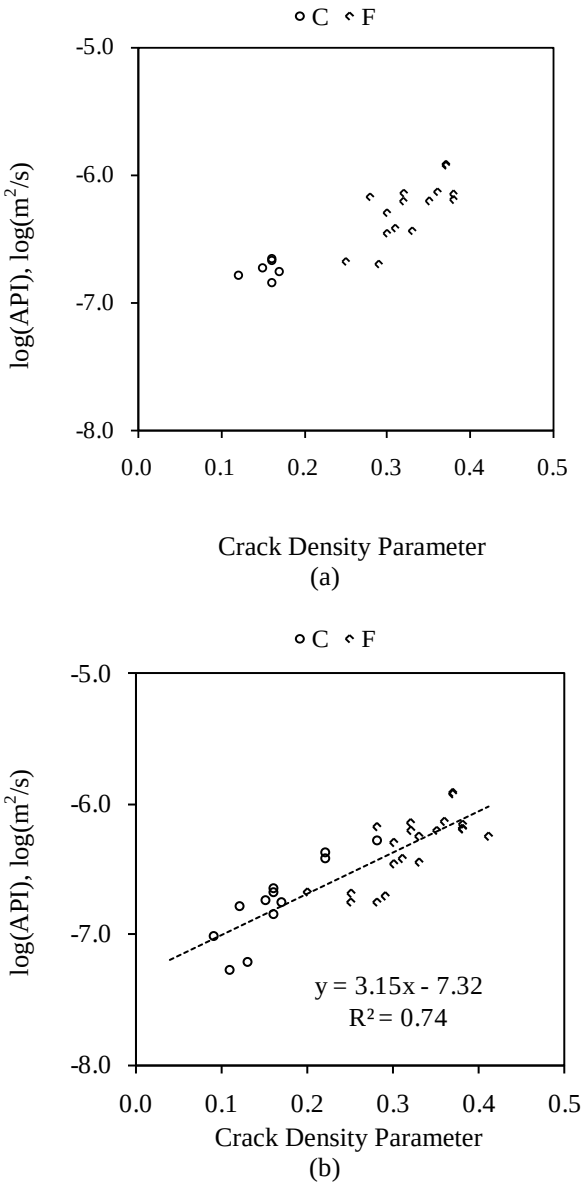

Figure 6.12 - Relationship Between Crack Density Parameter and Log-Transformed Air Permeability Index: (a) Original Paired Data; (b) Augmented log($API_{CND'}$) Data

The relationships between log(API) and ε is physically appealing but the results must be viewed recalling that ε was calculated using G_d results and log(API) was shown in previous studies to be approximately linearly related to E_d, and therefore with G_d. The finding that ε

and log(API) are approximately linearly related is important for several reasons, however. The relationship does indicate that the crack density parameter, as calculated using the methodology described in section 5.4, is changing in the correct direction and with relative values that appear to be reasonable.

For the relationship between sorptivity and ε, no paired data was available between ε and S_i since ε was obtained at DRY1 and DMG conditions, and S_i after condition CND' only. In order to analyze any possible relationship between these properties, representative data sets for each crack density parameter condition for mixtures C and F were used. The S_i of exposed groups C1T and F1T were representative of ε_{DMG}, and the S_i of non-exposed groups C1U and F1U were representative of ε_1. Figure 6.14 plots the initial rates of absorption of water and crack density parameter for these four groups, where only a general relationship is seen between undamaged and damaged specimens with the same raw materials. As before, this finding is useful primarily in supporting the validity of estimating the crack density parameter using the methods and techniques described previously. Additional research is suggested to further investigate the relationship between changes in ε and changes in S_i with commonly used concrete mixtures.

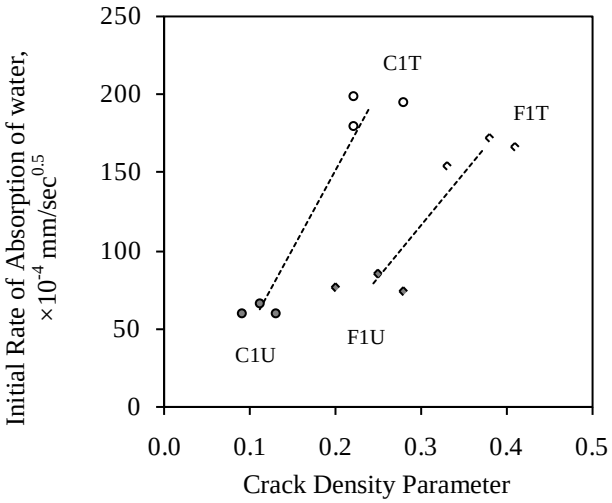

Figure 6.13 - Relationship Between Crack Density Parameter and Initial Rate of Absorption of Water

6.4 Relationships between Changes in Dynamic Shear Modulus, Crack Density Parameter, and Air Permeability Index

Relationships in changes in G_d, E_d, API and ε were examined using paired differences by specimen, therefore reducing specimen-to-specimen variability. Measuring differences was possible because of the nondestructive nature of the tests. The datum from which differences were calculated was the dry, undamaged condition DRY1. Since API_{DRY1} of mixtures C and F were excluded (see sections 6.2.3 and 6.3.1), these values were estimated from measurements of $API_{CND'}$. For the undamaged specimens from non-exposed groups C1U and F1U, the value of $API_{CND'}$ was repeated as API_{DRY1}, and for the specimens in exposed groups C1T and F1T, API_{DRY1} was estimated as the average $API_{CND'}$ of groups C1U and F1U, respectively. Likewise, values of $API_{CND'}$ of damaged specimens from groups C1T and F1T were taken as representative of API_{DMG}. Additional research is recommended to

provide directly obtained values. Figure 6.14 shows a scatterplot matrix of the changes for properties of interest that are discussed in the following sections.

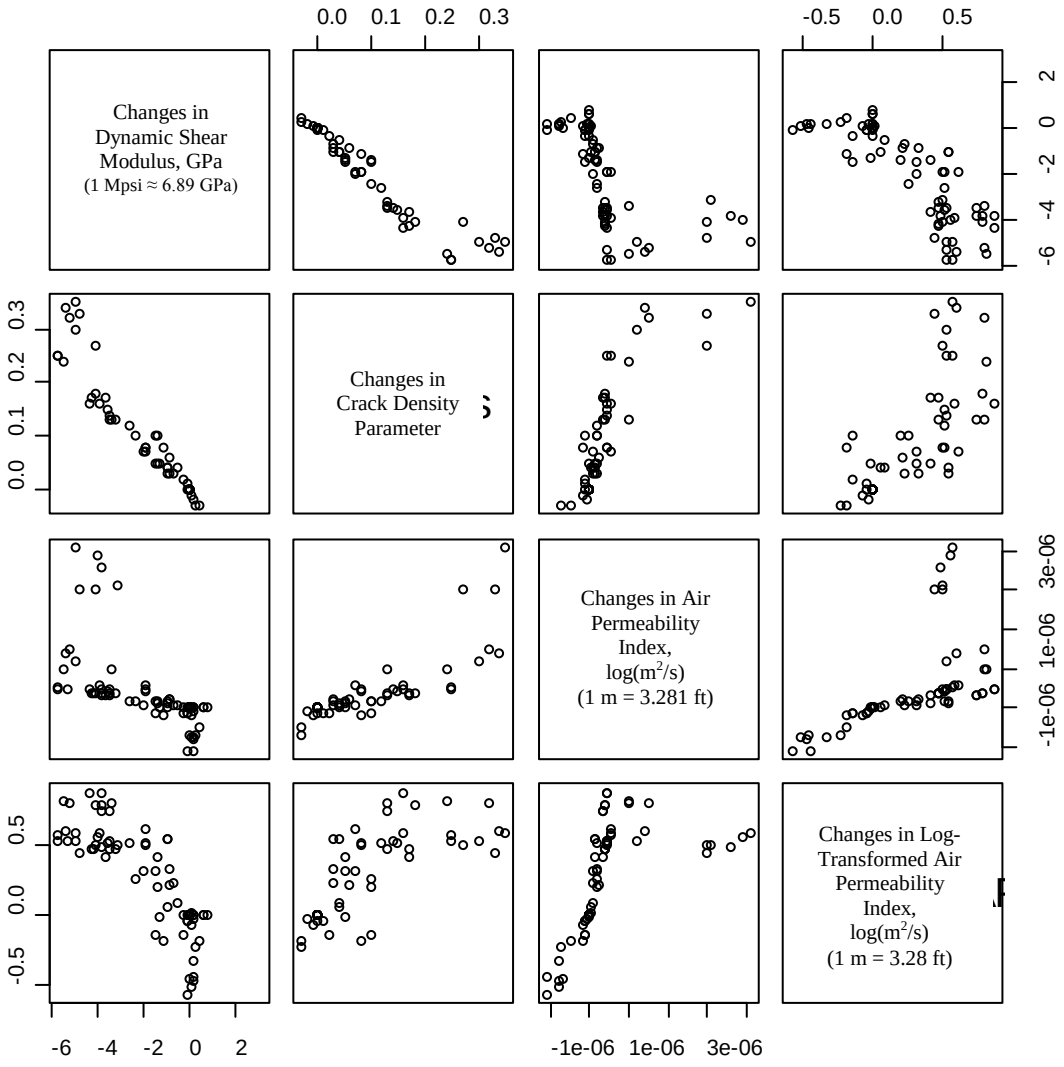

Figure 6.14 - Scatterplot Matrix of Changes in Measured Properties Combining Data of a Conventional Concrete Mixture and Three Sustainability Enhanced Mixtures

The sample correlation coefficient between ΔG_d and Δlog(API) was –0.84, higher than -0.75 found between log(API) and G_d (see Table 6.11). Figure 6.15(a) shows the relationship between ΔG_d and Δlog(API). A linear regression model was not found to be appropriate since the residuals plot did not show random error; further, data for mixture C was above the regression line and most of the data for mixture M was below the regression line. Regardless, Figure 6.10 and Figure 6.15(a) show strong correlations between these two properties, and although a single coefficient relating the increase in log(API) with a unitary decrease in G_d for all data is not appropriate, the behavior is very similar between mixtures. Figure 6.15(b) shows the corresponding plot for ΔE_d and Δlog(API), for comparison.

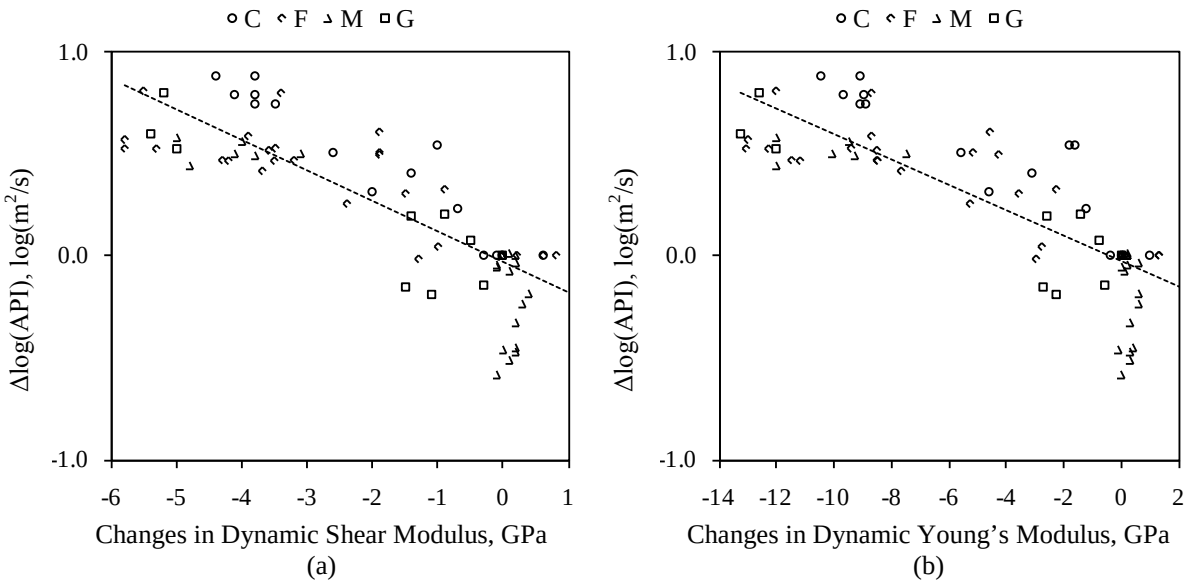

Figure 6.15 - Relationships Between Changes in Mechanical Properties and Log-Transformed Air Permeability Index: (a) Changes in Dynamic Shear Modulus, (b) Changes in Dynamic Young's Modulus

Figure 6.16 shows the changes in API with changes in ε. The r between the $\Delta\varepsilon$ and Δlog(API) was +0.76, and the r between $\Delta\varepsilon$ and ΔAPI was +0.81. In contrast with Figure 6.12, the data for mixtures M and G were incorporated since values of $\Delta\varepsilon$ for these mixtures were available (see section 6.2.2).

Differences in behavior by mixture are observed in Figure 6.16(a), where log(API) of the portland cement based mixtures had a higher increase in log(API) than the magnesium phosphate based mixtures for a similar increase in ε (data for mixtures C and F are above the regression line, whereas data for mixtures C and M are below). This observation provides additional evidence that the magnesium phosphate cement based materials have much different characteristics than portland cement mixtures. Since the values of ε were obtained from measurements of G_d, Figure 6.16(a) mimics the behavior observed between ΔG_d and Δlog(API) in Figure 6.15(a), and the same limitations on applying a linear model were encountered.

A stronger correlation was found between $\Delta\varepsilon$ and ΔAPI (r = +0.81), a plot of which is presented in Figure 6.16(b). A difference between behavior of mortar samples and concrete samples is evident and not surprising. The concrete specimens appear to form a coherent sample set, regardless of cementitious material characteristics. The relationship between changes in API for concrete materials (mixtures C, F and G) appears linear, for differences below $+2\times10^{-6}$ m^2/s. Further research on changes in ε and changes in API is recommended, incorporating portland cement based mortars of different water-cement ratios.

Air Permeability Index is a measure of the interconnected pore system, in particular for transport through the larger voids, whereas the value of ε measures an overall effect of cracks

despite of interconnectivity. Additionally, the O'Connell and Budiansky (O'Connell and Budiansky 1977) model for dry shear modulus is the same for dry isolated and dry isobaric (interconnected) cracks, and since all values of $\Delta\varepsilon$ correspond to changes in dry conditions, values of ε are therefore unaffected by the degree of interconnectivity between cracks. Further research incorporating microscopic investigation is strongly recommended, in order to relate measurable crack properties to values of ε obtained nondestructively, for different types of damage exposures and to relate those properties directly to fluid transport properties.

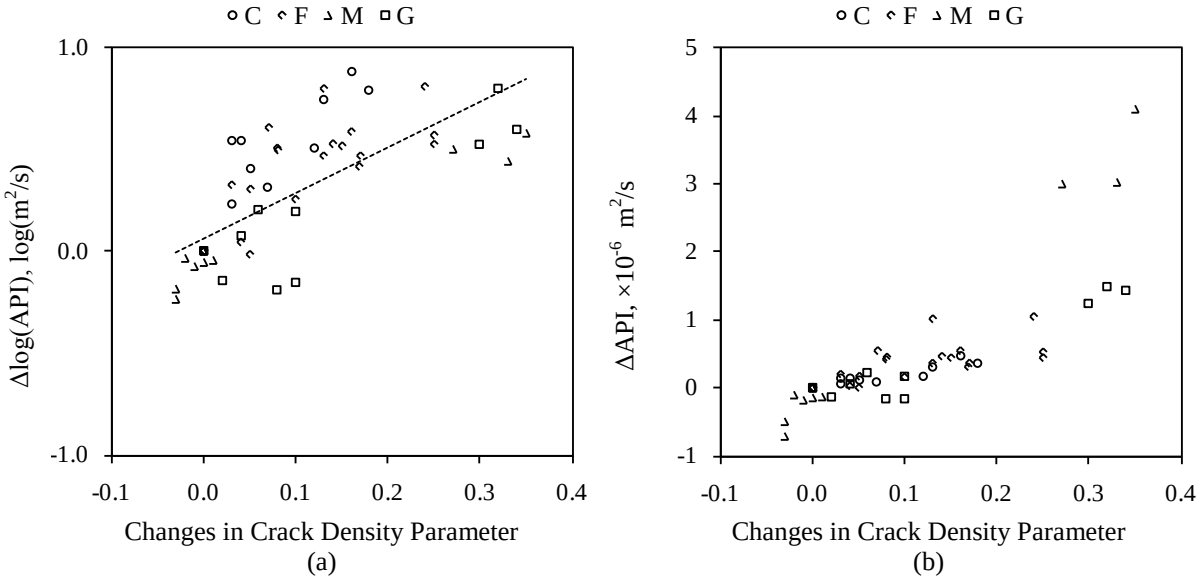

Figure 6.16 - Relationship Between Changes in Crack Density Parameter and Changes in Air Permeability Index: (a) Changes in log(API), (b) Changes in API

Mixture C, before damage, had the lowest log(API) and S_i of all mixtures. Despite the relatively low increase in ε, mixture C had the largest increases in log(API) and also had a larger difference in S_i between damaged and undamaged specimens. This observation is consistent with the behavior of high strength concrete with exposure to high temperature, where a less interconnected porous system is more susceptible to damage from exposure to high temperature (see, for example, Phan and Carino 1998; Recalde and Leming 2009). It is speculated that this larger degree of damage is caused by high gas pressures unable to dissipate because of a low gas permeability (Bazant 1997), which becomes more critical with wet, high strength concrete which is more susceptible to explosive spalling (see, for example, Hannant 1964; and Anderberg 1997).

6.5 Phase III Summary

Phase III of this investigation analyzed changes in dynamic shear modulus (G_d), air permeability index (API) and initial rate of absorption of water (S_i) of a control and three sustainable cementitious materials mixtures with damage resulting from a high temperature exposure. Microstructural changes were quantified using the crack density parameter (ε), as calculated using the analytical technique developed in Phase II. Relationships between measured properties were analyzed, and differences in fundamental behavior between mixtures were identified and compared.

The following is a list of conclusions obtained from the last phase of this investigation:

- The three enhanced sustainability concrete mixtures analyzed had a lower undamaged mean G_d than the control concrete mixture C, consistent with the strength of mixture F, but not of mixtures M and G.

- Decreases between 4 and 5 GPa were observed after an exposure of 60±1 minutes to 300 °C for all mixtures, reducing the G_d of the enhanced sustainability concrete mixtures to about half their original undamaged conditions, compared to about ¾ of the original undamaged condition of mixture C. These relative residual characteristics were within the expected ranges, although they were close to the range limits.
- Autogenous healing occurred in all mixtures after soaking in water. Mixtures based on magnesium phosphate cement (Grancrete™) exhibited significant autogenous healing, with mortar (Mixture M) recovering to its original undamaged state. The very high fly ash concrete mixture (Mixutre F) exhibited autogenous healing, but to a lesser extent.
- Water held in the capillaries produced the stiffening effect observed in Phase I for mixtures C and F during resonant testing, resulting in higher G_d for wet concrete than for dry concrete. The magnesium phosphate based cements behaved differently, with minor water interaction in the resonant behavior.
- Values for crack density parameter using the analytical technique developed in Phase II of this investigation, could be determined for specimens of portland cement based mixtures. For mixtures M and G, only changes in ε could be determined.
- Higher crack density parameters obtained for mixture F than for mixture C are consistent with fluid penetrability results. The analytical method to determine ε has potential as an analytical tool for research and forensic investigations on conventional portland cement based concrete mixtures.

- Mixtures M and G had high fluid penetrability properties, and similar increases in log(API) with high temperature damage. Although speculative, a more porous matrix with these mixtures may be related to the extremely rapid (less than 10 minutes) development of the microstructure, known to produce a coarser microstructure in portland cement based materials. This observation is consistent with a high log(API) of both mixtures and high S_i of mixture M. The significant healing after crack extension by high temperature damage followed by water saturation is consistent with the rapid development of the microstructure, leaving substantial unreacted product available for later hydration.
- Strong correlations were found between G_d and log(API), and between ΔG_d and Δlog(API), with slight differences observed between mixtures. Values for changes in crack density parameter were consequently also correlated to changes in API.
- No meaningful difference was found in initial rate of absorption of water of 25 mm (1 in.) and 50 mm (2 in.) thick specimens, therefore 25 mm (1 in.) thick disks can be used to determine the initial rate of absorption of water.

The following is a list of recommendations:

- The use of clay is preferred over duct tape to seal the edges of the disk for the measurement of API.
- Drying the specimens prior to moisture conditioning for sorptivity testing is recommended. Studies in this area are needed for improvement of the reproducibility of the test measurements.

- Estimates of increases in crack trace lengths through the nondestructive measurement of ε should be compared to measurements from microscopic image analysis.
- Further research on the magnesium phosphate cement based mixtures is needed, since design considerations used for portland cement based materials might not be appropriate.
- Research on autogenous healing capabilities with more than one exposure is needed, especially for the magnesium phosphate cement based mixtures made with Grancrete™. Deterioration by exposure to other damaging mechanisms also needs to be investigated.

CHAPTER 7. CONCLUSIONS AND RECOMMENDATIONS

7.1 Conclusions

7.1.1 Phase I Conclusions

From results of Phase I, the following were concluded:

- Water held in large capillaries in concrete has a stiffening effect on the measured dynamic moduli of elasticity; higher values of both shear and Young's modulus were obtained when the concrete disk was soaked or saturated with water than when dry (or with slight moisture content). Therefore, E_d measured in a dry condition provides a more representative measure of the mechanical properties of the concrete structure without the compounding effects of moisture. The differences in modulus between dry and soaked disks could, however, provide useful information on the microstructure of the concrete.
- Damping ratios were strongly related to moisture content.
- Damping ratios were not found to be useful in assessing differences in damage due to thermal exposure.
- Initial Rates of Absorption of Water (S_i) for 25 mm (1 in.) disks were similar to those measured using standard 50 mm (2 in.) disks. Secondary Rates of Absorption of Water were different, and often it was difficult to obtain useful data with damaged concrete.
- A strong linear relationship between log(API) and E_d was not found in Phase I, probably due to testing methods that were then modified for the remaining tests.

- The relationship between changes in API and S_i with damage was different by mixture and specimen thickness, whereas the inverse relationship between changes in E_d and S_i were different by mixture only, regardless of disk geometry. Since E_d is is a property of the entire specimen and S_i is is a property of the surface, this finding indicates damage gradients in the 50 mm (2 in.) thick disks.

7.1.2 Phase II Conclusions

From results of Phase II, the following were concluded:

- The relations developed by O'Connell and Budiansky (1974; 1977), based on the effective moduli of dry and saturated cracked media were used to obtain a value for the crack density parameter (ε) of conventional concrete.
- Comparison of test results using dry and saturated media provided more reliable estimates of ε than comparison of dry to partially saturated media.
- The sensitivity of ε was ±0.01 for values of υ_0 between 0.15 to 0.30 (typical for concrete), however, changes in crack density parameter ($\Delta\varepsilon$) were practically insensitive to the value of υ_0.
- Ratios of ε before and after damage can be used to develop estimates of increases of crack trace lengths that appeared to be reasonable based on prior studies.
- The technique was applied to three different conventional concrete mixtures to obtain values of the crack density parameter of concrete disks before and after high temperature damage, and to identify and quantify recovery in ε by autogenous healing after damage.

- The values of ε determined were generally consistent with expectations based on previous studies and indicated the potential utility of this parameter in research and forensic applications.

7.1.3 Phase III Conclusions

From results of Phase III, the following were concluded:

- Similar values of S_i for the 25 mm (1 in.) thick disks, compared to the 50 mm (2 in.) thick disks, confirmed that 25 mm (1 in.) thick disks can be used to determine S_i.
- The three sustainable concrete mixtures analyzed had a lower undamaged mean G_d than the control concrete mixture C, consistent with the strength of mixture F, but not of mixtures M and G.
- Decreases between 4 and 5 GPa were observed after an exposure of 60±1 minutes to 300 °C for all mixtures, reducing the G_d of the enhanced sustainability concrete mixtures to about half their original undamaged conditions, compared to about ¾ of the original undamaged condition of mixture C. These relative residual characteristics were within the expected ranges, although they were close to the range limits.
- Autogenous healing occurred in all mixtures after soaking in water. Mixtures based on magnesium phosphate cement (Grancrete™) exhibited significant autogenous healing, with mortar (Mixture M) recovering to its original undamaged state. The very high fly ash concrete mixture (Mixutre F) exhibited autogenous healing, but to a lesser extent.
- Water held in the capillaries produced the stiffening effect observed in Phase I for mixtures C and F during resonant testing, resulting in higher G_d for wet concrete than

for dry concrete. The magnesium phosphate based cements behaved differently, with minor water interaction in the resonant behavior.

- Values for crack density parameter using the analytical technique developed in Phase II of this investigation, could be determined for specimens of portland cement based mixtures. For mixtures M and G, only changes in ε could be determined.
- Higher crack density parameters obtained for mixture F than for mixture C are consistent with expected microstructure and fluid penetrability results. The potential utility of using ε as an analytical tool for research and forensic investigations on conventional concrete mixtures was confirmed.
- Mixtures M and G had high fluid penetrability properties, and similar increases in log(API) with high temperature damage. The significant healing with water saturation after damage by high temperature exposure is consistent with the presence of substantial unreacted product available for later reaction.
- Strong correlations were found between G_d and log(API), and between ΔG_d and Δlog(API), with slight differences observed between mixtures.
- Values for crack density parameter were correlated to values of API for the portland cement based mixtures. Correlations of log(API) with crack density parameter were higher than between log(API) and dynamic shear modulus. Correlations between changes in crack density parameter and changes in API were also high.
- The method to determine the crack density parameter was found useful as a screening tool with utility for research and forensic applications. Differences between magnesium phosphate based cementitious systems and portland cement based

concretes were observed; further research with magnesium phosphate cement based materials is recommended since design considerations for portland cement concretes might not be adequate.

- Variability in API testing suggests using care when sealing the specimen. Use of impervious clay is recommended instead of duct tape.

7.2 Recommendations

The following is a list of recommendations obtained from this investigation:

- Estimates of increases in crack trace lengths through the nondestructive measurement of ε should be compared to measurements from microscopic image analysis.
- Determining the effect of other types of damage exposures on the measured ε is needed to determine if the technique can be used for damage other than from a 300 °C exposure.
- Applicability of the technique using through-transmission shear wave velocity in dry and wet concrete measured directly on concrete structural members is recommended. Similarly, applicability using combined pulse velocity and shear wave velocity to determine the crack density parameter in situ would be very informative.
- Additional analysis of the inverse relationship between elastic properties and air permeability of concrete disks is recommended, especially for materials of low API and high E_d.
- Research on autogenous healing capabilities with more than one exposure and different damaging mechanisms is strongly recommended, especially for the magnesium phosphate cement based mixtures made with Grancrete™.

LIST OF REFERENCES

ACI Committee 201, "201.1R-08: Guide for Conducting a Visual Inspection of Concrete in Service," American Concrete Institute, Farmington Hills, MI, 2008, 15 p.

ACI Committee 214, "214.4R-03: Guide for Obtaining Cores and Interpreting Compressive Strength Results," American Concrete Institute, Farmington Hills, MI, 2003, 16 p.

ACI Committee 216, "216R-89 (Reapproved 2001): Guide for Determining the Fire Endurance of Concrete Elements," American Concrete Institute, Farmington Hills, MI, 1989, 48 p.

ACI Committee 228, "228.1R-03: In-Place Methods to Estimate Concrete Strength," American Concrete Institute, Farmington Hills, MI, 2003, 44 p.

ACI Committee 228, "228.2R-98 (Reapproved 2004): Nondestructive Test Methods for Evaluation of Concrete in Structures" American Concrete Institute, Farmington Hills, MI, 1998, 62 p.

ACI Committee 318, "318-08: Building Code Requirements for Structural Concrete and Commentary," ACI American Concrete Institute, Farmington Hills, MI, 2008, 468 p.

Anderberg, Y., "Spalling Phenomena of HPC and OC," *Proceedings, Int. Workshop on Fire Performance of High-Strength Concrete, NIST Spec. Publ. 919*, 1997, pp. 69-73.

ASCE, "2009 Report Card for America's Infrastructure," American Society of Civil Engineers, Reston, VA, www.infrastructurereportcard.org, 2009, 153 p.

ASTM-C1064, "C1064-08 Standard Test Method for Temperature of Freshly Mixed Hydraulic-Cement Concrete," ASTM International, West Conshohocken, PA, 2008, 3 p.

ASTM-C1202, "C1202-09 Standard Test Method for Electrical Indication of Concrete's Ability to Resist Chloride Ion Penetration," ASTM International, West Conshohocken, PA, 2009, 7 p.

ASTM-C138, "C138M-09 Standard Test Method for Density (Unit Weight), Yield, and Air Content (Gravimetric) of Concrete," ASTM International, West Conshohocken, PA, 2009, 4 p.

ASTM-C143, "C143-09 Standard Test Method for Slump of Hydraulic-Cement Concrete," ASTM International, West Conshohocken, PA, 2009, 4 p.

ASTM-C1585, "C1585-04e1 Standard Test Method for Measurement of Rate of Absorption of Water by Hydraulic-Cement Concretes," ASTM International, West Conshohocken, PA, 2004, 6 p.

ASTM-C215, "C215-08 Standard Test Method for Fundamental Transverse, Longitudinal, and Torsional Resonant Frequencies of Concrete Specimens," ASTM International, West Conshohocken, PA, 2008, 7 p.

ASTM-C231, "C231-09a Standard Test Method for Air Content of Freshly Mixed Concrete by the Pressure Method," ASTM International, West Conshohocken, PA, 2009, 10 p.

ASTM-C31, "C31-09 Standard Practice for Making and Curing Concrete Test Specimens in the Field," ASTM International, West Conshohocken, PA, 2009, 6 p.

ASTM-C39, "C39-05e2 Standard Test Method for Compressive Strength of Cylindrical Concrete Specimens," ASTM International, West Conshohocken, PA, 2008, 7 p.

ASTM-C42, "ASTM C42 Standard Test Method for Obtaining and Testing Drilled cores and Sawed Beams of Concrete," ASTM International, West Conshohocken, PA, 2004, 6 p.

ASTM-C597, "C597-02 Standard Test Method for Pulse Velocity Through Concrete," ASTM International, West Conshohocken, PA, 2003, 4 p.

Bartlett, F. M., and MacGregor, J. G., "Effect of Moisture Condition on Concrete Core Strengths," *ACI Materials Journal*, V. 91, No. 3, 1994, pp. 227-236.

Berryman, J. G., "Origin of Gassmann's Equations," *Geophysics*, V. 64, No. 5, 1999, pp. 1627-1629.

Berryman, J. G., Berge, P. A., and Bonner, B. P., "Transformation of Seismic Data to Extract Porosity and Saturation Values for Rocks," *The Journal of the Acoustical Society of America*, V. 107, No. 6, 2000, pp. 3018-3027.

Biot, M. A., "Theory of Propagation of Elastic Waves in a Fluid-Saturated Porous Solid. I. Low-Frequency Range," *The Journal of the Acoustical Society of America*, V. 28, No. 2, 1956a, pp. 168-178.

Biot, M. A., "Theory of Propagation of Elastic Waves in a Fluid-Saturated Porous Solid. II. Higher Frequency Range," *The Journal of the Acoustical Society of America*, V. 28, No. 2, 1956b, pp. 179-191.

Box, G. E. P., Hunter, J. S., and Hunter, W. G., "Statistics for Experimenters: an Introduction to Design, Data Analysis, and Model Building," Wiley, New York, NY, 1978, 653 p.

Budiansky, B., and O'Connell, R. J., "Elastic Moduli of a Cracked Solid." *International Journal of Solids and Structures,* V. 12, No. 2, 1976, pp. 81-97.

Bungey, J. H., "The Testing of Concrete in Structures," 2nd ed., Surrey University Press, Chapman and Hall, 1989, 228 p.

Carrasquillo, R. L., Slate, F. O., and Nilson, A. H., "Microcracking and Behavior of High Strength Concrete Subject to Short-Term Loading," *ACI Journal Proceedings,* V. 78, No. 3, 1981, pp. 179-186.

Counto, U. J., "Effect of the Elastic Modulus of the Aggregate on the Elastic Modulus, Creep and Creep Recovery of Concrete," *Magazine of Concrete Research,* V. 16, No. 48, 1964, pp. 129-138.

Cruz, C. R., "Elastic Properties of Concrete at High Temperatures." *PCA Journal,* V. 8, No. 1, 1966, pp. 37-45.

DeSouza, S. J., Hooton, R. D., and Bickley, J. A., "Evaluation of Laboratory Drying Procedures Relevant to Field Conditions for Concrete Sorptivity Measurements," *ASTM Journal of Cement, Concrete and Aggregates,* V. 19, No. 2, 1997, 5 p.

Dias, W. P. S., Khoury, G. A., and Sullivan, P. J. E., "Mechanical Properties of Hardened Cement Paste Exposed to Temperatures up to 700 C (1292 F)," *ACI Materials Journal,* V. 87, No. 2, 1990, pp. 160-166.

Dilek, U., "Assessment of Damage Gradients Using Dynamic Modulus of Thin Concrete Disks," *ACI Materials Journal,* V. 105, No. 5, 2008, pp. 429-437.

Dilek, U., and Leming, M. L., "Elastic Dynamic Young's Modulus and Permeability of Concrete in Fire Damaged Structural Members," *ASCE Journal of Materials in Civil Engineering,* V. 20, No.2, 2008, pp. 102-110.

Dilek, U., and Leming, M. L., "Comparison of Pulse Velocity and Impact-Echo Findings to Properties of Thin Disks from a Fire Damaged Slab," *ASCE Journal of Performance of Constructed Facilities,* V. 21, No. 1, 2007a, pp. 13-21.

Dilek, U., and Leming, M. L., "De-icer Salt Scaling Resistance of Concrete Containing Manufactured Sands," *ASTM Journal of Testing and Evaluation,* V. 32, No. 2, 2007b, 9 p.

Dilek, U., Leming, M. L., and Guth, D., "Relationship Between Elastic Modulus and Permeability of Damaged Concrete," *Journal of the Transportation Research Board,* Concrete TRB(1893), 2004, pp. 53-60.

Dilek, U., Leming, M. L., and Sharpe, E. F., "Assessment of Cryogenic Fluid Spill Damage to Concrete," *Forensic Engineering: Proceedings of the Third Congress*, P.A. Bosela *et al.*, eds., American Society of Civil Engineers, Reston, VA, 2003, pp. 269-279.

Dilek, U., "Nondestructive and Laboratory Evaluation of Damage Gradients in Concrete Structure Exposed to Cryogenic Temperatures," *ASCE Journal of Performance of Constructed Facilities*, V. 20, No. 1, 2006, pp. 37-44.

Dilek, U., "Evaluation of Fire Damage to a Precast Concrete Structure Nondestructive, Laboratory, and Load Testing," *Journal of Performance of Constructed Facilities*, V. 19 No.1, 2005, pp. 42-48.

Dilek, U., Caldwell, T., Sharpe, E. F., and Leming, M. L., "Fire Damage Assessment, Pre-stressed Concrete Double-Tees at Parking Deck," *Forensic Engineering: Proceedings of the Third Congress*, P.A. Bosela *et al.*, eds., American Society of Civil Engineers, Reston, VA, 2003, pp. 247-258.

Dvorkin, J., Mavko, G., and Nur, A., "Squirt Flow in Fully Saturated Rocks." *Geophysics*, V. 60, No. 1, 1995, pp. 97-107.

Dvorkin, J., Nolen-Hoeksema, R., and Nur, A., "The Squirt-Flow Mechanism: Macroscopic Description," *Geophysics*, V. 59, No. 3, 1994, pp. 428-438.

Dvorkin, J., and Nur, A., "Dynamic Poroelasticity: A Unified Model with the Squirt and the Biot Mechanisms," *Geophysics*, V. 58, No. 4, 1993, pp. 524-533.

Feldman, R. F., and Sereda, P. J., "A New Model for Hydrated Portland Cement and Its Practical Implications," *Engineering Journal*, V. 53, No. 8/9, 1970, pp. 53-59.

Fiorato, A. E., Burg, R. G., and Gaynor, R. D., "Effects of Conditioning on Measured Compressive Strength of Concrete Cores," *CT-003 Concrete Technology Today*, V. 21, No. 3, 2000, 3 p.

Galloway, J. W., Harding, H. M., and Raithby, K. D., "Effect of Moisture Changes of Flexural and Fatigue Strength of Concrete." *Report No. 864*, Transport and Road Research Laboratory, 1979, 33 p.

Gassmann, F., "Über Die Elastizität Poröser Medien," *Vierteljahrsschrift Der Naturforschenden Gesellschaft in Zürich*, 1951.

Guo, J. S., and Waldron, P., "An Elastic Model to Quantify the Effect of Moisture on the Mechanical Properties of Concrete at the Time of Test," *Magazine of Concrete Research*, V. 53, No. 3, 2001, pp. 151-162.

Hall, C., "Water Sorptivity of Mortars and Concretes: A Review," *Magazine of Concrete Research,* V. 41, 1989, pp. 51-61.

Hanle, L. J., Jayaraman, K. R., and Smith, J. S., "CO_2 Emissions Profile of the U. S. Cement Industry," Environmental Protection Agency, Washington D. C., 2004, 14 p.

Hannant, D. J., "Effects of Heat on Concrete Strength," *Engineering,* V. 197, No. 21, London, 1964, p. 302.

Hansen, T. C., "Influence of Aggregate and Voids on Modulus of Elasticity of Concrete, Cement Mortar, and Cement Paste," *ACI Journal Proceedings,* V. 62, No. 2, 1965, pp. 193-216.

Hashin, Z., "The Elastic Moduli of Heterogeneous Materials," *Journal of Applied Mechanics,* V. 29, No. 1, 1962, pp. 143-150.

Hashin, Z., and Monteiro, P. J. M., "An Inverse Method to Determine the Elastic Properties of the Interphase Between the Aggregate and the Cement Paste," *Cement and Concrete Research,* V. 32, No. 8, 2002, pp. 1291-1300.

Hill, R., "The Elastic Behaviour of a Crystalline Aggregate," *Proceedings of the Physical Society of London,* A-65, 1952, pp. 349-354.

Hirsch, T. J., "Modulus of Elasticity of Concrete Affected by Elastic Moduli of Cement Paste Matrix and Aggregate," *ACI Journal Proceedings,* V. 59, No. 3, 1962, pp. 427-452.

Hsu, T. T. C., Slate, F. O., Sturman, G. M., and Winter, G., "Microcracking of Plain Concrete and the Shape of the Stress-Strain Curve," *ACI Journal Proceedings,* V. 60, No. 2, 1963, pp. 209-224.

Hutchinson, J. R., "Axisymmetric Flexural Vibrations of a Thick Free Circular Plate," *Journal of Applied Mechanics,* V. 46, 1979, pp. 139-144.

Ichniowsky, T., "The Stimulus Bill, Sector by Sector," *Engineering News-Record,* http://enr.construction.com/business_management/finance/2009/0116-StimulusBillBreakdown.asp (last visit: 12/2009), Jan 2009.

Jornet, A., Guidali, E., and Muhlethaler, U., "Microcracking in High Performance Concrete," Swedish National Testing and Research Institute: Building Technology, 1993, 6 p.

Kenall, M. G., and Moran, P. A. P., "Geometrical Probability," *Griffin's Statistical Monographs and Courses,* No. 5, 1963, pp. 78-74.

Kesner, K., Sansalone, M., and Poston, R. W., "Detection and Quantification of Distributed Damage in Concrete Using Transient Stress Waves," *ACI Materials Journal,* V. 101, No. 4, 2004, pp. 318-328.

Larbi, L. A., "Microstructure of the Interfacial Zone Around Aggregate Particles in Concrete," *Heron,* V. 38, No. 1, 1993, pp. 3-69.

Lea, F. M., "The Chemistry of Cement and Concrete", 3rd ed., Edward Arnold, London, 1970, 727 p.

Leming, M. L., Nau, J. M., and Fukuda, J., "Non-Destructive Determination of the Dynamic Modulus of Concrete Disks," *ACI Materials Journal,* V. 95, No. 1, 1998, pp. 50-57.

Mavko, G., and Jizba, D., "Estimating Grain Scale Fluid Effects on Velocity Dispersion in Rocks," *Geophysics,* V.56, No. 12, 1991, pp. 1940-1949.

Mavko, G., Mukerji, T., Dvorkin, J., and Knovel, "The Rock Physics Handbook: Tools for Seismic Analysis in Porous Media," Cambridge University Press, Cambridge, NY, 2003, 339 p.

Mehta, P. K., and Monteiro, P. J. M., "Concrete : Microstructure, Properties, and Materials," 3rd ed., The Mac-Graw Hill Companies, 2006, 659 p.

Mitchell, J. F., and Leming, M. L., "Quantity of Alkali Silica Gel and Its Effect on Concrete Properties," *ASCE Journal of Materials in Civil Engineering,* V. 10, No. 2, 1998, pp. 106-111.

Montesdeoca, O. F., "Basic Characteristics of Grancrete HFR," M.S. Thesis, Department of Civil, Construction and Environmental Engineering, North Carolina State University, Raleigh, NC, 2008, 188 p.

Mori, T., and Tanaka, K., "Average Stress in Matrix and Average Elastic Energy of Materials with Misfitting Inclusions," *Acta Metallurgica,* V. 21, No. 5, 1973, pp. 1605-1609.

National Instruments, "LabVIEW™ 8.5," version 8.5.1, ni.com/labview, 2008.

Neville, A. M., "Properties of Concrete," 4th ed., Pearson Education, 1995, 844p.

Nilsen, A. U., and Monteiro, P. J. M., "Concrete: A Three Phase Material," *Cement and Concrete Research,* V. 23, No. 1, 1993, pp. 147-151.

Nokken, M. R., and Hooton, R. D., "Dependence of Rate of Absorption on Degree of Saturation of Concrete," *Cement, Concrete and Aggregates,* V. 24, No. 1, 2002, pp. 20-24.

O'Connell, R. J., and Budiansky, B., "Seismic Velocities in Dry and Saturated Cracked Solids," *Journal of Geophysical Research,* Vol. 79, No. 36, 1974, pp. 5412-5426.

O'Connell, R. J., and Budiansky, B., "Viscoelastic Properties of Fluid Saturated Cracked Solids," *Journal of Geophysical Research,* Vol. 82, No. 35, 1977, pp. 5719-5735.

Phan, L. T., and Carino, N. J., "Review of Mechanical Properties of HSC at Elevated Temperature," *ASCE Journal of Materials in Civil Engineering,* V. 10, No. 1, 1998, pp. 58-656.

Phan, L. T., and Carino, N., J., "Effects of Test Conditions and Mixture Proportions on Behavior of High-Strength Concrete Exposed to High Temperatures," *ACI Materials Journal,* V. 99, No. 1, 2002, pp. 54-66.

Philleo, R., "Some Physical Properties of Concrete at High Temperatures," *ACI Journal Proceedings,* V. 54, No. 10, 1958, pp. 857-864.

Popovics, S., "Effect of Curing Method and Final Moisture Condition on Compressive Strength of Concrete," *ACI Journal Proceedings,* V. 83, No. 4, 1986, pp. 650-657.

Powers, T. C., "Structure and Physical Properties of Hardened Portland Cement Paste," *Journal - American Ceramic Society,* V. 41, No. 1, 1958, pp. 1-6.

Qiu, T., and Fox, P. J., "Hydraulic Damping of Saturated Poroelastic Soils During Steady-State Vibration," *ASCE Journal of Engineering Mechanics,* V. 132, No. 8, 2006, pp. 859-870.

R Development Core Team, "R: A Language and Environment for Statistical Computing," R version 2.7.2, 2008.

Recalde, J. J., "Vibration Characteristics and Use in Concrete Damage Assessment," M.S. Thesis, Department of Civil, Construction, and Environmental Engineering, North Carolina State University, Raleigh, NC, 2005, 254 p.

Recalde, J. J., and Leming, M. L., "Changes in Fluid Penetrability and Mechanical Properties of Concrete Due to High Temperature Exposure," *Journal of ASTM International,* V. 6, No. 6, 2009, 13 p.

Ringot, E., and Bascoul, A., "About the Analysis of Microcracking in Concrete," *Cement and Concrete Composites,* V. 23, No. 2-3, 2001, pp. 261-266.

Santamarina, J. C., Klein, K. A., and Fam, M. A., "Soils and Waves: Particulate Materials Behavior, Characterization and Process Monitoring," J. Wiley, Chichester, New York, 2001, 488 p.

Schonlin, K., and Hilsdorf, H. K., "Permeability as a Measure of Potential Durability of Concretes- Development of a Suitable Test Apparatus," *ACI SP-108: Permeability of Concrete*, American Concrete Institute, Detroit, MI, 1988, pp. 99-115.

Scrivener, K. L., and Gartner, E. M., "Microstructural Gradients in Cement Paste Around Aggregate Particles," *Materials Research Society Symposium Proceedings*, V. 114, 1988, pp. 77-86.

Slate, F. O., and Hover, K. C., "Microcracking in Concrete," in *Fracture Mechanics of Concrete: Characterization and Testing*, Carpinteri and Ingraffea Eds., 1984, pp. 137-58.

Slate, F. O., and Olsefski, S., "X-Rays for Study of Internal Structure and Microcracking of Concrete," *ACI Journal Proceedings*, V. 60, No. 5, 1963, pp. 575-588.

U. S. Census Bureau, "2008 Value of Construction Put in Place - Seasonally Adjusted Annual Rate," Manufacturing, Mining and Construction Statistics, http://www.census.gov/const/C30/totsa2008.pdf, 2009a.

U. S. Census Bureau, "2009 Value of Construction Put in Place - Seasonally Adjusted Annual Rate," Manufacturing, Mining, and Construction Statistics, http://www.census.gov/const/C30/totsahist.pdf, 2009b.

U. S. Census Bureau, "Annual Value of Construction Put in Place 2002-2008." Manufacturing, Mining, and Construction Statistics, http://www.census.gov/const/C30/total.pdf, 2009c.

U. S. Census Bureau, "C30 Value of Construction Put in Place Index - Table 1. Annual Value of Construction, Constant Dollars," Manufacturing, Mining and Construction Statistics, http://www.census.gov/const/C30/oldtc.html, 2008.

U. S. Green Building Council, "LEED 2009 for New Construction and Major Renovations Rating System," http://www.usgbc.org/ShowFile.aspx?DocumentID=5546, Washington D.C., 2008.

Ulm, F., Constantinides, G., and Heukamp, F., "Is Concrete a Poromechanics Materials?—A Multiscale Investigation of Poroelastic Properties," *Materials and Structures*, V. 37, No. 1, 2004, pp. 43-58.

Walsh, J. B., "The Effect of Cracks on the Compressibility of Rocks," *Journal of Geophysical Research*, V. 70, No. 2, 1965, pp. 381-389.

Weiss, J., "Chapter 19: Elastic Properties, Creep, and Relaxation," in *Significance of Tests and Properties of Concrete & Concrete-Making Materials*, ASTM International, West Conshohocken, PA, 2006, pp. 194-206.

Zia, P., Ahmad, S. H., Leming, M. L., Schemmel, J. J., and Elliot, R. P., "Mechanical Behavior of High Performance Concretes, Volume 5, Very High Strength Concrete," *Report No. SHRP-C-365,* Strategic Highway Research Program, National Research Council, Washington, D. C., 1993.

Zoldners, N. G., "Effect of High Temperatures on Concretes Incorporating Different Aggregates," *Mines Branch Research Report R.64,* Department of Mines and Technical Surveys, Ottawa, Canada, 1960.

.

APPENDICES

APPENDIX A -

HUTCHINSON'S THICK CIRCULAR PLATE THEORY SOLUTION

An approximate solution for the axisymmetric flexural vibration of a thick circular plate in free-free conditions was developed by Hutchinson (1979), and its application to concrete disks is discussed in detail by Leming, Nau and Fukuda (1998). This appendix provides the governing equations and its solution.

Hutchinson's approximate thick plate theory assumes that the axial displacement is independent of the axial coordinate *z* and that the radial displacement is a linear function of *z*. This assumption implies that the linearly weighted average effect of the axial stress is zero and that there is a constant shear stress through the thickness of the disk. These assumptions are not necessarily true, but the use of a shear coefficient to account for the shear distribution provides a solution that is accurate for the first mode and for higher order modes depending on the disk thickness-to-diameter ratio (see Hutchinson, 1979). The two governing equations for free-free vibration of a thick circular plate, in dimensionless notation, are:

$$K\left(\psi' + \frac{\psi}{r} + w'' + \frac{w'}{r}\right) + \Omega^2 w = 0 \tag{A.1}$$

$$\frac{2}{1-\upsilon}\left(\psi'' + \frac{\psi'}{r} - \frac{\psi}{r^2}\right) - \frac{3K}{h^2}\left(\psi + w'\right) + \Omega^2 \psi = 0 \tag{A.2}$$

where

r = dimensionless radial coordinate,

w = dimensionless axial displacement of the disk,

ψ = dimensionless radial displacement of the disk,

h = dimensionless half-height of the disk (the thickness-to-diameter ratio),

υ = Poisson's ratio,

K = shear coefficient,

Ω = dimensionless resonant frequency,

and prime denotes differentiation with respect to r. Parameters r, h, w and ψ are made dimensionless by dividing by the disk radius, and Ω is made dimensionless by multiplying the resonant frequency (rad/s) by the disk radius and dividing by the shear wave speed. The shear coefficient K accounts for the shear distribution through the disk thickness, for which the constant value of $\pi^2/12$ provides matching thickness shear modes with the infinite plate theory (Mindlin, 1951), and was used by Hutchinson (1979) for his analysis examples and by Leming, Nau and Fukuda (1998) in their application to concrete disks. As discussed by Hutchinson (1979), Ω becomes less dependent on K for small values of h and virtually independent of K for very thin disks.

A solution to Equations (1) and (2) are:

$$\psi = J_1(\delta r) \tag{A.3}$$

$$w = AJ_0(\delta r) \tag{A.4}$$

where

A = an arbitrary constant, and

J_1 and J_0 are Bessel functions of the first kind.

Applying this solution to Equations 1 and 2, results in the following system:

$$\begin{bmatrix} K\delta & \Omega^2 - K\delta^2 \\ \Omega^2 - \dfrac{2\delta^2}{1-\upsilon} - \dfrac{3K}{h^2} & \dfrac{3K\delta}{h^2} \end{bmatrix} \begin{Bmatrix} 1 \\ A \end{Bmatrix} = \begin{Bmatrix} 0 \\ 0 \end{Bmatrix} \tag{A.5}$$

Setting the determinant of the coefficients in Eq. A.5 to zero gives

$$\delta^4 + a_1\delta^2 + a_2 = 0 \tag{A.6}$$

where

$$a_1 = -\Omega^2\left(\frac{1}{K} + \frac{1-\upsilon}{2}\right) \tag{A.7}$$

$$a_2 = \Omega^2\left(\frac{\Omega^2}{K} - \frac{3}{h^2}\right)\frac{1-\upsilon}{2} \tag{A.8}$$

Equation (6) yields two roots for δ^2, both of which are real and at least one of them is positive. If one of the roots is negative, then the solution in Equations (3) and (4) use the modified Bessel functions *I* instead of the Bessel functions *J*. There are two values of A (A_1 and A_2), corresponding to the two roots δ_1^2 and δ_2^2, therefore the solution may be rewritten as:

$$\psi = B_1 J_1(\delta_1 r) + B_2 J_1(\delta_2 r) \tag{A.9}$$

$$w = B_1 A_1 J_0(\delta_1 r) + B_2 A_2 J_0(\delta_2 r) \tag{A.10}$$

where B_1 and B_2 are arbitrary constants.

Applying boundary conditions for the free-free plate at the outer edge gives

$$\begin{bmatrix} (1 - S_1 \delta_1 A_1) J_1(\delta_1) & (1 - S_2 \delta_2 A_2) J_1(\delta_2) \\ \delta_1 J_1'(\delta_1) + \upsilon J_1(\delta_1) & \delta_2 J_1'(\delta_2) + \upsilon J_1(\delta_2) \end{bmatrix} \begin{Bmatrix} B_1 \\ B_2 \end{Bmatrix} = \begin{Bmatrix} 0 \\ 0 \end{Bmatrix} \tag{A.11}$$

where S_n is the sign of δ_n^2. If δ_n^2 is negative, then the Bessel functions *J* in Eq. A.11 must be replaced by the modified Bessel functions *I*, and δ_n is the square root of the absolute value of δ_n^2.

The solution process is to assume a value of Ω, find δ_1 and δ_2 from Eq. A.6 and A_1 and A_2 from Eq. A.5. The determinant of the coefficients in Eq. A.11 is then evaluated. If this determinant is not zero, then a new value of Ω is tried and the process repeated until a value of Ω is found such that the determinant of the coefficients in Eq. A.11 is zero within some tolerance. The lowest value of Ω at which the determinant is zero is the natural frequency Ω_0 of the circular plate.

APPENDIX B-

STRESS WAVE PROPAGATION IN CONTINUOUS MEDIA

The wave equation in the continuum in direction x_i, as presented by Santamarina, Klein and Fam (2001), is given in Eq. 2.1, where ρ is the solid density, u_i is the displacement in direction x_i, t is time, M is the constraint modulus, G is the shear modulus, and ε_{vol} is the volumetric strain. This governing equation predicts two modes of propagation: compression waves (P-waves) and shear waves (S-waves). A solution to the wave equation for plane waves propagating in a single direction is given by Eq. 4.2 where A is the maximum amplitude, $\omega = 2\pi/T$ is the temporal angular frequency, $\kappa = 2\pi/\lambda$ is the spatial frequency (wave number), T is the period, λ is the wavelength, t is time and $j = \sqrt{-1}$. The phase velocity ω/κ for P-waves is $\sqrt{M/\rho}$, and for S-waves is $\sqrt{G/\rho}$.

$$\rho \frac{\partial u_i}{\partial t^2} = \left(M - G\right)\frac{\partial \varepsilon_{vol}}{\partial x_i} + G\nabla^2 u_i$$

$$u_i = Ae^{j\left(\omega t \pm \kappa x_i\right)} \quad (2.2)$$

For low-loss phenomena such as small-strain waves in cracked or particulate materials, and assuming harmonic motion, the elastic modulus can be replaced by a complex modulus (Santamarina, Klein, & Fam, 2001). For P-waves, the wave equation becomes

$$\rho \frac{\partial u_x}{\partial t^2} = \frac{M^*}{\rho}\frac{\partial^2 u_x}{\partial x^2}$$

where the complex constraint modulus is $M^* = M' + jM''$, and a solution is

$$u = Ae^{j\left(\omega t - \gamma^* x\right)} = Ae^{-\alpha x}e^{j(\omega t - \kappa x)}$$

where $\gamma^* = \kappa - j\alpha$ is the complex propagation constant and the attenuation coefficient $\alpha = -\mathrm{Im}(\gamma^*)$ is the decay in amplitude with distance. Incorporating the solution into the wave equation provides the complex phase velocity:

$$V_p^* = \frac{\omega}{\gamma^*} = \frac{\omega}{\kappa - j\alpha} = \sqrt{\frac{M^*}{\rho}}$$

The real phase velocity is computed by

$$V_p = \frac{\omega}{\kappa} = \sqrt{\frac{M'}{\rho}} \sqrt{\frac{2\left[1+\left(\tan\delta\right)^2\right]}{\sqrt{1+\left(\tan\delta\right)^2}+1}} \approx \sqrt{\frac{M'}{\rho}}$$

and attenuation by

$$\alpha = \frac{\omega}{\sqrt{\frac{M'}{\rho}}} \sqrt{\frac{\sqrt{1+\left(\tan\delta\right)^2}-1}{2\left[1+\left(\tan\delta\right)^2\right]}} \approx \frac{\omega \tan\delta}{2V_p}$$

The quality factor Q is defined as

$$\frac{1}{Q} = \frac{M''}{M'} = \tan\delta = 2D = \frac{2V_p\alpha}{\omega} = \frac{V_p\alpha}{\pi f}$$

where the loss angle δ is the phase angle between the stress and the strain and D is the damping ratio. Total material attenuation in space is caused by three phenomena: geometric attenuation, material loss or intrinsic attenuation, and apparent attenuation due to scattering and partial transmission of inclusions in the material.

APPENDIX C -

METHOD TO DETERMINE THE CRACK DENSITY PARAMETER OF CONCRETE DISKS

Introduction

The following procedures describe the method to determine the crack density parameter (ε) of concrete disks, with recommendations. The purpose is to provide a guide for future research and forensic investigations. The analysis is based on results by O'Connell and Budiansky (1974) on cracked media, applied to differences in dynamic shear modulus (G_d) of dry and wet concrete disks. The dynamic shear modulus can be obtained using the method developed by Leming, Nau and Fukuda (1997), which is based on Hutchinson's (1979) solution for the axisymmetric vibration of thick free circular plates. A value of ε can be determined if the shear modulus of wet concrete (G_{wet}) is higher than the shear modulus of dry concrete (G_{dry}), as observed in high frequency testing of concrete disks in free resonance.

Testing Procedure

1. Obtain an average thickness and average diameter of the specimen from at least four thickness measurements and at least three diameter measurements, at locations equally spaced around the perimeter of the disk. Measure dimensions to the nearest 0.1 mm.

2. Soaking Procedure

2.a. For disk specimens that are dry, soak specimens by allowing sorption of water through one face for at least 18 hours, followed by complete submersion in water for at least 18 hours. The sorption procedure is intended to absorb water through

capillary suction through a face and the sides of the specimen, with the other face exposed to ambient air or covered with a plastic sheet as in ASTM C 1585 (2004), so that air can be expelled by the ingress of water. In this investigation, specimens were submerged in water so that the water level was 2 to 5 mm below the top face of the specimen for the first 18 hours, then water was added for complete submersion.

2.b. For disk specimens obtained by saw-cutting wet cylinders that were cured in water or in a moist room at 100% relative humidity, soak specimens by submerging disks in water immediately after saw-cutting.

Notes: Vacuum saturation is not recommended since pore fluid may deteriorate the concrete microstructure at low pressures. For forensic investigations, autogenous healing may occur with water ingress after core-drilling or after the soaking procedure, therefore measuring G_d prior to soaking might be advantageous. For resonant frequency measurement, the investigator needs to ensure proper attachment of the accelerometer to the specimen, therefore specimen preparation prior to soaking might be needed in case that a coupling device needs to be attached to the specimen.

3. Obtain a value for the dynamic shear modulus of the wet concrete disk (G_{wet}), using the relationship given in Eq. D.1 (see also Eq. 5.3), where ρ is density (kg/m^3), f is frequency (Hz), d is diameter (m), and Ω_0 is the dimensionless frequency parameter. The resonant frequency of the wet concrete disk (f_{wet}) may be obtained using the procedure described in section 3.4.2; frequency obtained using Fast Fourier Transform techniques is adequate if the resolution allows reporting the frequency to the nearest 0.01 kHz. A value of Ω_0 may be obtained using the method described by

Leming, Nau and Fukuda (1998), which is also given in Appendix A of this dissertation.

$$G_{wet} = \rho_{wet}\left(\frac{\pi f_{wet} d}{\Omega_{0,wet}}\right)^2 \quad \text{(D.1)}$$

Notes: If the value of the dynamic Poisson's ratio (υ_d) will be estimated from stress wave velocity measurements, instead of being assumed, measure the ultrasonic pulse velocity along the disk diameter at least at three different locations according to ASTM C 597 (2003) immediately after measuring the resonant frequency. Since Ω_0 depends on υ, a numerical optimization procedure may be used to solve for values of Ω_0 and υ_d simultaneously incorporating Eq. 3.7 and Eq. 3.8 into the solution.

4. Drying Procedure: Dry the specimen at 40 °C in an oven at a relative humidity below 50% until the specimen reaches a constant mass with no further loss of water. In this investigation, 25 mm (1 in.) thick specimens were dried for at least 48 hours prior to testing, thicker specimens might require longer times.

5. Obtain a value for the dynamic shear modulus of the dry concrete disk (G_{dry}), using the same procedure used in step 3, applied for dry concrete as given in Eq. D.2.

$$G_{dry} = \rho_{dry}\left(\frac{\pi f_{dry} d}{\Omega_{0,dry}}\right)^2 \quad \text{(D.2)}$$

Analytical Procedure to Determine the Crack Density Parameter

The relationship between shear modulus, crack density parameter (ε) and degree of saturation of cracked media, as developed by O'Connell and Budiansky (1974), are given by

Eq. 5.14, Eq. 5.15 and Eq. 5.18, which applied to wet and dry concrete are given by Eq. 5.19 to Eq. 5.22. Assuming wet concrete behaves similar to a saturated cracked media, and that air dried concrete behaves like dry cracked media, then ξ_{OB}=1 for wet conditions and ξ_{OB}=0 for dry conditions. The resulting equations are given by Eq. D.3 to Eq. D.6.

$$\frac{G_{dry}}{G_0} = 1 - \frac{32}{45}\left(1-\upsilon_{dry}\right)\left[1+\frac{3}{\left(2-\upsilon_{dry}\right)}\right]\varepsilon \tag{D.3}$$

$$\frac{G_{wet}}{G_0} = 1 - \frac{32}{45}\left(1-\upsilon_{wet}\right)\left[\frac{3}{\left(2-\upsilon_{wet}\right)}\right]\varepsilon \tag{D.4}$$

$$\varepsilon = \varepsilon_{dry} = \frac{45}{16}\frac{\left(\upsilon_0-\upsilon_{dry}\right)}{\left(1-\upsilon_{dry}{}^2\right)}\frac{\left(2-\upsilon_{dry}\right)}{\left[\left(1+3\upsilon_0\right)\left(2-\upsilon_{dry}\right)-2\left(1-2\upsilon_0\right)\right]} \tag{D.5}$$

$$\varepsilon = \varepsilon_{wet} = \frac{45}{16}\frac{\left(\upsilon_0-\upsilon_{wet}\right)}{\left(1-\upsilon_{wet}{}^2\right)}\frac{\left(2-\upsilon_{wet}\right)}{\left(2\upsilon_0-1\right)} \tag{D.6}$$

Values for υ_{dry} and υ_{wet} are found by obtaining a system of two equations and two unknowns by dividing Eq. D.3 by Eq. D.4, and equating ε_{dry}=ε_{wet} with Eq. D.5 and Eq. D.6. The resulting system of equations is given by Eq. D.7 and D.8, respectively. A value of υ_0 needs to be assumed; in this investigation υ_0 was estimated from the average dynamic Poisson's ratio of wet and dry concrete, as measured on the same specimen before and after damage (see section 5.4). If the dynamic Poisson's ratio will not be measured, the value assumed to determine Ω_0 should be used. A valid solution requires that $0 < \upsilon_{dry} < \upsilon_{wet} < 0.5$, as more than one solution may exist.

$$\frac{G_{dry}}{G_{wet}} = \frac{1-\frac{32}{45}\left(1-\upsilon_{dry}\right)\left[1+\frac{3}{\left(2-\upsilon_{dry}\right)}\right]}{1-\frac{32}{45}\left(1-\upsilon_{wet}\right)\left[\frac{3}{\left(2-\upsilon_{dry}\right)}\right]} \tag{D.7}$$

$$\frac{\left(\upsilon_0-\upsilon_{dry}\right)}{\left(1-\upsilon_{dry}{}^2\right)}\frac{\left(2-\upsilon_{dry}\right)}{\left[\left(1+3\upsilon_0\right)\left(2-\upsilon_{dry}\right)-2\left(1-2\upsilon_0\right)\right]} = \frac{\left(\upsilon_0-\upsilon_{wet}\right)}{\left(1-\upsilon_{wet}{}^2\right)}\frac{\left(2-\upsilon_{wet}\right)}{\left[2\left(2\upsilon_0-1\right)\right]} \tag{D.8}$$

The crack density parameter can evaluated using either Eq. D.5 or Eq. D.6 with the values found for υ_{dry} or υ_{wet}, respectively. A value of G_0 can then be obtained from either Eq. D.3 or Eq. D.4. In this dissertation, a solution was found by implementing a numerical optimization procedure to find the values of υ_{dry}, υ_{wet} and G_0, such that $\varepsilon_{dry}=\varepsilon_{wet}$ and $0< \upsilon_{dry} < \upsilon_{wet}<0.5$.

Note: If specimens will be subject to microstructural changes (i.e.: damage or healing), once a value for G_0 is known, ε after changes (ε_i) can be determined by calculating $\upsilon_{dry,i}$ by combining Eq. D.3 and Eq. D.4, and evaluating ε_i using Eq. D.4 only. This method has the convenience of using dry measurement to determine values of ε_i after changes.

APPENDIX D -

PHASE III, COMPLEMENTARY DATA

Table C.1 - Damping Ratio of Sustainability Enhanced Cementitious Materials at Different Moisture Conditions

Group	Spe-cimen	Damping Ratio, %								
		SKD	**CND**	**DRY1**	**DMG**	**CND'**	**SKD'**	**SAT**	**ALC**	**DRY2**
C1T	C11	3.6	2.4	2.5	*0.5*	*0.7*	*2.9*	*1.5*	*3.2*	*2.0*
	C12	1.8	2.8	1.9	*0.4*	*1.6*	*2.5*	*2.1*	*2.1*	*2.7*
	C13	1.8	2.0	3.2	*0.5*	*1.5*	*3.1*	*1.9*	*2.7*	*1.0*
C1U	C14	1.5	2.5	0.6	—	0.7	3.0	2.2	1.5	1.3
	C15	1.5	2.2	1.1	—	1.8	3.2	1.8	1.6	1.0
	C16	1.8	1.3	2.6	—	1.1	2.2	2.3	2.3	2.4
F1T	F11	2.2	2.3	2.1	*0.4*	*1.5*	*4.5*	*3.1*	*2.4*	*1.3*
	F12	2.1	2.8	0.9	*3.5*	*1.6*	*4.4*	*3.2*	*2.7*	*0.7*
	F13	1.6	2.2	3.2	*1.4*	*1.4*	*3.1*	*4.0*	*2.5*	*1.2*
F1U	F14	1.7	1.4	2.9	—	1.0	2.6	1.9	2.4	1.0
	F15	1.3	1.8	2.1	—	2.0	1.5	2.3	1.9	0.8
	F16	3.3	1.6	1.6	—	0.9	3.3	2.3	2.7	1.3
M1T	M11	0.8	0.6	0.5	*0.6*	*0.7*	*1.4*	*1.9*	*2.2*	*0.7*
	M12	0.7	0.6	0.5	*0.7*	*0.6*	*2.5*	*2.0*	*2.2*	*0.6*
	M13	0.7	0.7	0.3	*0.8*	*0.6*	*1.5*	*2.6*	*1.8*	*1.8*
M1U	M14	0.9	0.7	0.3	—	0.3	0.8	1.9	3.2	1.8
	M15	0.8	0.6	0.5	—	0.3	0.6	1.1	1.6	1.2
	M16	1.8	0.9	0.3	—	0.3	0.6	1.1	1.6	0.9
G1T	G11	4.2	—	0.5	*1.3*	—	—	*3.4*	—	*0.4*
	G12	3.6	—	0.6	*1.3*	—	—	*3.1*	—	*0.5*
	G13	3.8	—	0.5	*1.3*	—	—	*2.6*	—	*0.5*
G1U	G14	3.7	—	0.5	—	—	—	2.7	—	0.5
	G15	3.4	—	0.5	—	—	—	3.2	—	0.5
	G16	3.5	—	0.5	—	—	—	2.8	—	0.6
F1T*	F11*	—	—	—	*0.7*	—	—	*2.8*	—	*0.8*
	F12*	—	—	—	*0.8*	—	—	*3.0*	—	*0.8*
	F13*	—	—	—	*0.7*	—	—	*3.6*	—	*0.8*
F1U*	F14*	—	—	—	—	—	—	2.6	—	0.7
	F15*	—	—	—	—	—	—	2.3	—	0.6
	F16*	—	—	—	—	—	—	2.7	—	0.6

"C" is conventional concrete, "F" is very high fly ash concrete, "M" is Grancrete™ mortar, "G" is Grancrete™ concrete, "*" indicates specimens that were re-tested at a later age. "T" is high temperature exposure (300°C) group, "U" is unexposed/undamaged group. "SKD" and "SKD'": in water for 1 day with one face exposed to ambient air, then at least 1 day submerged in water or moist room at 100 % RH and tested immediately after removal from water; "CND" and "CND'": 3 days at 50±2 °C and 80% RH, then at least 1 day sealed at 23±2 °C; "DRY1" and "DRY2": oven dried at 40±2 °C (RH = 25±5 %) for 2 days then sealed and tested within 18 hours; "DMG": air dried specimens at 23 ± 2 °C exposed to 300 ± 20 °C for 60 ± 1 min, then sealed and tested at 23 ± 2 °C within 24 hours; "SAT": oven dried at 40 ± 2 °C for 2 days, then vacuum saturated in general accordance with ASTM Standard C1202-09; "ALC": 1 day standing in 70% isopropyl alcohol (one face immersed, one face exposed to the atmosphere), then at least 1 day submerged. "—" is data not taken.

Table C.2 - Dynamic Poisson's Ratio of Sustainability Enhanced Cementitious Materials at Different Moisture Conditions

Group	Spe-cimen	Poisson's Ratio								
		SKD	CND	DRY1	DMG	CND'	SKD'	SAT	ALC	DRY2
C1T	C11	0.301	0.296	0.275	*0.274*	*0.308*	*0.324*	*0.329*	*0.301*	*0.292*
	C12	0.325	0.316	0.288	*0.326*	*0.324*	*0.326*	*0.343*	*0.325*	*0.335*
	C13	0.305	0.304	0.285	*0.327*	*0.309*	*0.335*	*0.307*	*0.319*	*0.299*
C1U	C14	0.313	0.329	0.291	—	0.296	0.291	0.315	0.313	0.313
	C15	0.311	0.323	0.295	—	0.304	0.279	0.337	0.300	0.320
	C16	0.299	0.285	0.286	—	0.260	0.287	0.302	0.235	0.316
F1T	F11	0.307	0.340	0.239	*0.370*	*0.313*	*0.347*	*0.337*	*0.357*	*0.334*
	F12	0.332	0.313	0.353	*0.360*	*0.364*	*0.362*	*0.343*	*0.352*	*0.335*
	F13	0.310	0.310	0.271	*0.256*	*0.298*	*0.349*	*0.291*	*0.339*	*0.328*
F1U	F14	0.347	0.332	0.350	—	0.326	0.318	0.324	0.356	0.350
	F15	0.323	0.315	0.357	—	0.329	0.325	0.318	0.360	0.363
	F16	0.315	0.297	0.326	—	0.278	0.260	0.254	0.293	0.344
M1T	M11	0.298	0.289	0.283	*0.351*	*0.346*	*0.323*	*0.333*	*0.282*	*0.298*
	M12	0.295	0.286	0.294	*0.380*	*0.348*	*0.312*	*0.334*	*0.271*	*0.295*
	M13	0.291	0.276	0.281	*0.334*	*0.321*	*0.312*	*0.329*	*0.257*	*0.271*
M1U	M14	0.299	0.277	0.282	—	0.280	0.300	0.315	0.213	0.295
	M15	0.301	0.282	0.286	—	0.284	0.290	0.313	0.218	0.275
	M16	0.302	0.280	0.279	—	0.277	0.294	0.324	0.186	0.279
G1T	G11	0.338	—	0.287	*0.356*	—	—	*0.364*	—	*0.320*
	G12	0.347	—	0.245	*0.306*	—	—	*0.374*	—	*0.300*
	G13	0.343	—	0.282	*0.351*	—	—	*0.367*	—	*0.328*
G1U	G14	0.342	—	0.252	—	—	—	0.367	—	0.301
	G15	0.354	—	0.280	—	—	—	0.373	—	0.306
	G16	0.347	—	0.288	—	—	—	0.368	—	0.297
F1T*	F11*	—	—		*0.370*	—	—	*0.359*	—	*0.389*
	F12*	—	—		*0.361*	—	—	*0.366*	—	*0.384*
	F13*	—	—		*0.330*	—	—	*0.352*	—	*0.381*
F1U*	F14*	—	—		—	—	—	0.344	—	0.387
	F15*	—	—		—	—	—	0.356	—	0.386
	F16*	—	—		—	—	—	0.323	—	0.363

"C" is conventional concrete, "F" is very high fly ash concrete, "M" is Grancrete™ mortar, "G" is Grancrete™ concrete, "*" indicates specimens that were re-tested at a later age. "T" is high temperature exposure (300°C) group, "U" is unexposed/undamaged group. "SKD" and "SKD'": in water for 1 day with one face exposed to ambient air, then at least 1 day submerged in water or moist room at 100 % RH and tested immediately after removal from water; "CND" and "CND'": 3 days at 50±2 °C and 80% RH, then at least 1 day sealed at 23±2 °C; "DRY1" and "DRY2": oven dried at 40±2 °C (RH = 25±5 %) for 2 days then sealed and tested within 18 hours; "DMG": air dried specimens at 23 ± 2 °C exposed to 300 ± 20 °C for 60 ± 1 min, then sealed and tested at 23 ± 2 °C within 24 hours; "SAT": oven dried at 40 ± 2 °C for 2 days, then vacuum saturated in general accordance with ASTM Standard C1202-09; "ALC": 1 day standing in 70% isopropyl alcohol (one face immersed, one face exposed to the atmosphere), then at least 1 day submerged. "—" is data not taken.

Table C.3 - Mechanical Properties of Specimens Soaked in 70% Isopropyl Alcohol

Specimen	SOAKED IN ALCOHOL							
	density	Vp	Vs	ξ	ν	G	K	E
	kg/m^3	km/s	km/s	%		GPa	GPa	GPa
C11	2341	4.477	2.390	3.2%	0.301	13.4	29.1	34.8
C12	2352	4.480	2.280	2.1%	0.325	12.2	30.9	32.4
C13	2338	4.429	2.285	2.7%	0.319	12.2	29.6	32.2
C14	2351	4.587	2.391	1.5%	0.313	13.4	31.5	35.3
C15	2345	4.535	2.425	1.6%	0.300	13.8	29.8	35.8
C16	2364	4.366	2.571	2.3%	0.235	15.6	24.2	38.6
F11	2272	3.928	1.852	2.4%	0.357	7.8	24.7	21.2
F12	2298	3.847	1.838	2.7%	0.352	7.8	23.7	21.0
F13	2275	3.780	1.865	2.5%	0.339	7.9	22.0	21.2
F14	2297	4.169	1.969	2.4%	0.356	8.9	28.0	24.2
F15	2268	4.165	1.950	1.9%	0.360	8.6	27.8	23.5
F16	2295	4.035	2.184	2.7%	0.293	10.9	22.8	28.3
M11	2096	3.815	2.103	2.2%	0.282	9.3	18.1	23.8
M12	2072	3.834	2.148	2.2%	0.271	9.6	17.7	24.3
M13	2106	3.839	2.196	1.8%	0.257	10.2	17.5	25.5
M14	2108	3.691	2.230	3.2%	0.213	10.5	14.7	25.4
M15	2092	3.768	2.262	1.6%	0.218	10.7	15.4	26.1
M16	2104	3.729	2.317	1.6%	0.186	11.3	14.2	26.8

Table C.4 – Sorptivity Measurements of 25 mm Thick Specimens

$t^{1/2}$, $sec^{0.5}$	I, mm							
	C11	C12	C13	C14	M11	C16	C15	M12
0.0	0.00	0.00	0.00	0.00	0.00	0.00	0.00	0.00
7.7	0.13	0.10	0.11	0.11	0.12	0.13	0.12	0.13
17.3	0.29	0.24	0.23	0.20	0.27	0.22	0.21	0.30
24.5	0.44	0.36	0.35	0.27	0.40	0.28	0.27	0.44
34.6	0.65	0.54	0.54	0.35	0.60	0.35	0.35	0.65
42.4	0.80	0.68	0.69	0.40	0.77	0.41	0.40	0.82
60.0	1.15	0.99	1.06	0.51	1.14	0.52	0.53	1.19
84.9	1.65	1.45	1.58	0.66	1.66	0.66	0.69	1.72
103.9	2.04	1.80	1.98	0.76	2.06	0.77	0.80	2.12
120.0	2.33	2.10	2.28	0.84	2.20	0.84	0.90	2.26
134.2	2.46	2.33	2.45	0.90	2.22	0.92	0.98	2.30
147.0	2.50	2.45	2.50	0.97	2.24	0.99	1.06	2.31
281.4	2.58	2.57	2.58	1.57	2.34	1.59	1.69	2.40
286.7	2.59	2.57	2.58	1.60	2.34	1.61	1.71	2.40
Initial Mass, g (sealed)	491.00	501.63	474.59	479.21	430.53	489.52	470.29	427.37

Table C.4 (continued) – Sorptivity Measurements of 25 mm Thick Specimens

$t^{1/2}$, $sec^{0.5}$	I, mm							
	F11	F12	F13	F14	F15	F16	M13	M14
0.0	0.00	0.00	0.00	0.00	0.00	0.00	0.00	0.00
7.7	0.22	0.23	0.18	0.19	0.18	0.19	0.23	0.09
17.3	0.40	0.43	0.35	0.34	0.31	0.31	0.40	0.19
24.5	0.53	0.55	0.46	0.42	0.39	0.39	0.51	0.28
34.6	0.71	0.73	0.61	0.53	0.49	0.48	0.66	0.40
42.4	0.85	0.86	0.72	0.60	0.56	0.56	0.78	0.50
60.0	1.16	1.16	1.00	0.77	0.69	0.69	1.07	0.73
84.9	1.62	1.58	1.38	0.97	0.87	0.88	1.51	1.07
103.9	1.97	1.91	1.69	1.11	1.00	1.00	1.85	1.35
120.0	2.25	2.18	1.93	1.23	1.09	1.13	2.15	1.57
134.2	2.43	2.38	2.14	1.33	1.18	1.21	2.32	1.71
147.0	2.52	2.50	2.32	1.42	1.25	1.29	2.37	1.76
277.8	2.63	2.63	2.61	1.94	1.78	1.79	2.47	1.85
283.1	2.64	2.65	2.62	1.95	1.79	1.81	2.47	1.85
Initial Mass, g (sealed)	462.28	474.89	475.78	510.62	455.99	498.30	468.28	434.45

Table C.4 (continued) – Sorptivity Measurements of 25 mm Thick Specimens

$t^{1/2}$, $sec^{0.5}$	I, mm	
	M15	M16
0.0	0.00	0.00
7.7	0.10	0.09
17.3	0.20	0.18
24.5	0.27	0.27
34.6	0.41	0.40
42.4	0.50	0.49
60.0	0.73	0.72
84.9	1.08	1.04
103.9	1.36	1.29
120.0	1.57	1.52
134.2	1.65	1.71
147.0	1.68	1.81
270.8	1.74	1.92
276.3	1.75	1.93
Initial Mass, g (sealed)	431.32	490.93

Table C.5 – Sorptivity Measurements of 50 mm Thick Specimens

$t^{1/2}$, $sec^{0.5}$	I, mm							
	C21	C22	C24	C25	F21	F22	F24	F25
0.0	0.00	0.00	0.00	0.00	0.00	0.00	0.00	0.00
7.7	0.16	0.17	0.12	0.11	0.27	0.24	0.19	0.15
17.3	0.32	0.31	0.20	0.17	0.46	0.42	0.31	0.28
24.5	0.43	0.41	0.24	0.20	0.60	0.53	0.39	0.34
34.6	0.64	0.58	0.31	0.26	0.81	0.70	0.50	0.45
42.4	0.79	0.71	0.34	0.29	0.94	0.81	0.60	0.52
60.0	1.12	1.01	0.42	0.36	1.25	1.04	0.74	0.64
84.9	1.57	1.42	0.53	0.44	1.66	1.35	0.93	0.81
103.9	1.90	1.71	0.59	0.50	2.00	1.60	1.07	0.94
120.0	2.17	1.95	0.65	0.54	2.29	1.82	1.20	1.04
134.2	2.39	2.14	0.70	0.57	2.54	2.02	1.31	1.12
147.0	2.57	2.31	0.72	0.61	2.75	2.20	1.39	1.21
210.3	3.48	3.09	0.93	0.72	3.86	3.10	1.82	1.57
352.4	4.40	4.06	1.32	0.98	4.60	4.20	2.59	2.37
454.6	4.42	4.09	1.56	1.13	4.65	4.24	2.85	2.81
542.5	4.47	4.13	1.76	1.27	4.69	4.28	2.97	3.06
617.5	4.48	4.15	1.93	1.37	4.71	4.30	3.02	3.16
676.6	4.51	4.18	2.07	1.45	4.74	4.33	3.05	3.21
749.8	4.54	4.21	2.22	1.54	4.76	4.35	3.08	3.25
796.7	4.56	4.22	2.31	1.60	4.77	4.37	3.09	3.27
854.9	4.57	4.24	2.41	1.66	4.80	4.38	3.11	3.28
Initial Mass, g (sealed)	775.68	763.01	769.4	771.05	725.21	726.47	732.07	734.58

Table C.5 (continued) – Sorptivity Measurements of 50 mm Thick Specimens

$t^{1/2}$, $sec^{0.5}$	I, mm			
	M21	M22	M24	M25
0.0	0.00	0.00	0.00	0.00
7.7	0.19	0.25	0.08	0.09
17.3	0.35	0.42	0.17	0.22
24.5	0.47	0.53	0.25	0.30
34.6	0.62	0.69	0.36	0.43
42.4	0.74	0.82	0.46	0.53
60.0	0.99	1.09	0.67	0.75
84.9	1.39	1.48	0.99	1.06
103.9	1.67	1.79	1.23	1.30
120.0	1.91	2.06	1.44	1.50
134.2	2.13	2.30	1.62	1.68
147.0	2.33	2.51	1.78	1.85
201.5	3.17	3.48	2.52	2.59
347.3	4.08	4.05	3.07	3.37
450.7	4.13	4.08	3.10	3.40
539.2	4.16	4.13	3.13	3.42
614.6	4.19	4.14	3.14	3.44
673.9	4.22	4.18	3.16	–
747.4	4.23	4.19	3.18	–
794.5	4.26	4.21	3.20	3.50
852.8	4.27	4.21	3.20	3.51
Initial Mass, g (sealed)	665.39	639.76	624.98	696.85

Table C.5 (continued) – Sorptivity Measurements of 50 mm Thick Specimens

$t^{1/2}$, $sec^{0.5}$	I, mm			
	G21	G22	G21*	G22*
0.0	0.00	0.00	0.00	0.00
7.7	0.03	0.04	0.06	0.08
17.3	0.04	0.06	0.11	0.12
24.5	0.05	0.06	0.13	0.15
34.6	0.07	0.08	0.17	0.21
42.4	0.08	0.09	0.21	0.24
60.0	0.09	0.10	0.28	0.30
84.9	0.11	0.13	0.35	0.38
103.9	0.11	0.16	0.38	0.43
120.0	0.14	0.17	0.41	0.47
134.2	0.14	0.18	0.46	0.50
147.0	0.15	0.19	0.50	0.55
158.7	0.16	0.21	–	–
290.9	0.26	0.34	–	–
412.6	0.34	0.46	–	–
542.5	0.44	0.59	–	–
598.0	0.48	0.62	–	–
674.5	0.53	0.67	–	–
721.9	0.55	0.68	–	–
775.8	0.56	0.69	–	–
839.0	0.58	0.72	–	–
Initial Mass, g (sealed)	403.87	434.45	396.71	427.13